

# 2021 ANNUAL REPORT

HP-HT laboratory

EXPERIMENTAL VOLCANOLOGY  
AND GEOPHYSICS

LNTS

NEW TECHNOLOGIES  
AND INSTRUMENTS  
LABORATORY

Department of Seismology and Tectonophysics  
Istituto Nazionale di Geofisica e Vulcanologia

Via di Vigna Murata 605 | 00143 Roma Italia | Tel +39-0651860437 | Fax +39-0651860507  
[www.ingv.it](http://www.ingv.it)

Follow us on





About the cover | Very high resolution Digital Surface Model of Cumbre Vieja's new volcanic edifice (January 2022)

Credits | HPHT Lab, Riccardo Civico, Tullio Ricci

Follow us on



HPHTlab - Science, Technology & Engineering




HPHTlab (@hphtlab) | Twitter



# Contents

1  ABSTRACT	5
2  PERSONNEL	7
3  INSTRUMENTS and FACILITIES	9
4  LABORATORY ACTIVITIES	13
5  RESEARCH PROJECTS	17
6  PARTNER LABORATORIES	19
7  PARTNER INSTITUTIONS	20
8  RESEARCH ACTIVITY and RESULTS	21
9  SEMINARS and TEACHING	99
10  VISITING SCIENTISTS	103
11  MEETINGS, WORKSHOP and SYMPOSIA	103
12  PUBLICATIONS	107





HP-HT Laboratory of Experimental Volcanology  
and Geophysics LNT Laboratory of New Technologies  
**2021 Annual Report**

## 11 ABSTRACT

This report summarizes the facilities, activities, collaborations, scientific and technological products of the High Pressure High Temperature Laboratory of Experimental Volcanology and Geophysics (HPHT Lab) and of the Laboratory of New Technologies (LNTS) updated to the year 2021. The two laboratories are an active part of all the three main Departments of INGV: Earthquake, Volcano and Environment. Research activities were framed within 16 national and international research projects and involved 19 proposals. In collaboration with Italian and foreigner universities, the laboratories hosted 9 Master students and 11 PhD students.

Scientific production for 2021 amounts to 40 publications.

In 2021 the HPHT Lab continued its activities under several research projects, most notably the four EU-funded projects: 1) IMPROVE - Innovative Multi-disciplinary European Research training network on VolcanoEs; 2) FEAR - Fault activation and Earthquake Rupture; 3) EXCITE-Electron and X-ray microscopy Community for structural and chemical Imaging Techniques for Earth materials; and 4) EUROVOLC - European Network of Observatories and Research Infrastructures for Volcanology.

Instrumental upgrades involved mainly the installation of two new experimental apparatus: a novel biaxial cell designed to investigate earthquake mechanics by simulating a the stress field in a prescribed tectonic regime (MEERA), and a new high temperature furnace (GHIRO) to study the crystallization dynamics in magmas. To investigate different aspects of the interaction between magmatic flow and conduit morphology, we developed an experimental setup (Fractal Burster) capable of generating scaled volcanic ject in a geometrically complex conduit and measuring the related seismic and acoustic radiation.

Worth of note, in 2021 several field campaigns were performed to document the volcanic activity of Mt. Etna and Cumbre Vieja volcano (La Palma, Spain), providing an exceptional chance to further understand the dynamics of basaltic explosive eruptions.

The **New Technologies and Instruments Laboratory** (LNTS) represents a “transversal” research infrastructure and belongs to the experimental laboratories group of the INGV infrastructure park. It is located in the Roma1 section and basically deals with the development, construction and engineering of measuring instruments, electro-mechanical systems and technological equipment for scientific research, in which specific characteristics are required, not found on the market.



The LNTS consists of an electronic laboratory and a mechanical workshop, with the ability to design, build prototypes and fine-tune measurement methods. The mechanical workshop is the reference workshop of the Rome office, while the electronic laboratory, in addition to following its own projects, approved and financed or simply ideas to be realized with an innovative spirit and with internal resources, offers a transversal support for technical consultancy on technological issues both with other INGV offices and with external institutions.

The LNTS works closely with the HPHT laboratory, taking care of its laboratory facilities. Together with the laboratories of section Roma2 of INGV, the LNTS collaborates with the G31 experimental cosmology group, with Roma3 University and the new Rock Mechanics laboratory of the Geology department of the University "La Sapienza". From 2021 the LNTS joined the COS, Center for the Observation of the Earth from Space, setting up a "Technological Development" module which involves other colleagues from other sections of INGV.





## 21 PERSONNEL

### HPHT Laboratory

**Piergiorgio Scarlato** | Senior Researcher

Responsible of the HP-HT Laboratory

**Stefano Aretusini** | Contract Researcher

**Emanuela Bagnato** | Researcher

**Riccardo Civico** | Researcher

**Chiara Cornelio** | Contract Researcher

**Gianfilippo De Astis** | Senior Researcher

**Elisabetta Del Bello** | Researcher

**Danilo Di Genova** | Researcher

**Valeria Misiti** | Technologist

**Manuela Nazzari** | Researcher

**Alessio Pontesilli** | Contract Researcher

**Giacomo Pozzi** | Contract Researcher

**Tullio Ricci** | Researcher

**Elena Spagnuolo** | Researcher

**Laura Spina** | Researcher

**Jacopo Taddeucci** | Senior Researcher

**Giancarlo Tamburello** | Researcher

### Laboratory of New Technologies

**Giuseppe Di Stefano** | Senior Technologist

Responsible of the Laboratory of New Technologies

**Alessandro Iarocci** | Engineer Technologist

**Massimo Mari** | Technician

**Marcello Silvestri** | Technician

**Francesco Pongetti** | Engineer Technician

**Giuseppe Spinelli** | Engineer Technologist

**Massimiliano Vallocchia** | Engineer Technician

**Giovanni Romeo** | Associated



## Associated researchers

**Cristiano Collettini** | Sapienza University of Rome, Italy | Associated Professor in Structural Geology

**Frances M. Deegan** | Uppsala University, Sweden | Researcher

**Giancarlo Della Ventura** | University of Roma Tre, Italy | Full Professor in Mineralogy

**Giulio Di Toro** | University of Padua, Italy | Full Professor in Structural Geology

**Gianluca Iezzi** | University of Chieti, Italy | Associated Professor

**Silvio Mollo** | Sapienza University of Rome, Italy | Associated Professor in Petrology

**Vincenzo Stagno** | Sapienza University of Rome, Italy | Associated Professor in Petrology

**Valentin R. Troll** | Uppsala University, Sweden | Chair of Petrology

## Collaborators

**Matteo Masotta** | University of Pisa, Italy | Researcher

**Marco M. Scuderi** | Sapienza University of Rome, Italy | RTDB Geophysics





## 3I INSTRUMENTS and FACILITIES

### HPHT Laboratory

- Multiple press 840 ton | [Voggenreiter](#)
- Piston cylinder - 3/4" and 1" pressure plates | [Voggenreiter](#)
- Multianvil - Walker type 6/8 | [Voggenreiter](#)
- Quick Press - Piston Cylinder 3/4" and 1" pressure plates | [Depth of the Earth](#)
- Bi-Tri-Axial Press 1/2" (BRAVA) | [RMP - INGV](#)
- Low to High Velocity Apparatus (SHIVA) | [RMP - INGV](#)
- Electron microprobe equipped with 5 WDS and 1 EDS | [JEOL JXA-8200](#)
- Field Emission Scanning Electron Microscope equipped with EDS and BSE detectors | [JEOL JSM-6500F](#)
- Auto Carbon coater | [JEOL JEC-530](#)
- Fine coater | [JEOL JFC-2300HR](#)
- High and low temperature furnaces | [Lenton](#)
- Impedance analyser | [Solartron SI1260](#)
- Digital oscilloscope | [Tektronix DPO4032](#)
- Wave generator | [Agilent 33250A](#)
- H-Frame presses 10 ton | [Enerpac](#)
- Uniaxial testing machine with double load cell (15 and 250 kN) and LVDT controller | [Tecnotest](#)
- Precision balance | [Sartorius](#)
- Optical and stereo microscopes | [Leica DMRXP](#) and [Euromex](#)
- Ultra-high velocity, intensified, gated digital camera | [Cordin 204-2](#)
- Stereomicroscopes | [Leica MZ 9.5](#)
- Semiautomatic polisher | [Buehler Minimet 1000](#)
- Power Supply | [Agilent 6575A](#)
- Helium Picnometer | [AccuPyc II 1340](#)
- Permeameter with double intensifier | [Rock Physics](#)
- Rheometer MCR 301 Physica | [Anton Paar](#)
- Vertical Furnace RHTV 120-300/18 | [Nabertherm](#)
- High Temperature Furnace LHT 04/18 | [Nabertherm](#)
- Cecchi data acquisition system | [Applied Seismology](#)
- Rock drilling, cutting, and grinding equipment for samples preparation
- Thermal High speed camera | [FLIR SC 645](#)
- Welder PUK U3 | [Lampert](#)
- Laser line generator | [Edmund optics](#)
- Precision test sieves | [Endecotts](#)
- Laser MGL-III, 532nm 200mW, PSU-III-LED/Unit | [Changchun New Industries](#)
- Multi-Wavelength Analyser LUMiReader® PSA with Particle sizing according to ISO 13317



- 2 Polarized Free-field Microphones 40AN 1/2", Low Frequency (0.5Hz - 20kHz) | G.R.A.S.
- Ext. Polarized Pressure Microphone 46DP-1 1/8", High Frequency (6.5Hz -140kHz) | G.R.A.S.
- Vacuometro | Pirani PVG-500
- Petrographic microscope ECLIPSE E-50i POL | Nikon
- Drying oven UF 75 | Memmert
- 4K digital camcorders | Sony
- High Speed digital camcorder | NAC Memrecam - HX6
- Shock-tube apparatus (Jet-Buster) | INGV
- High speed digital camcorders | NAC 512 SC, Optronis CR600x2, NAC HX6, NAC HX3
- Laser range finder | Vectronix VECTOR 21
- Time Lapse Camera with 24-70 lens | Brinno TLC200 Pro
- Precision Syringe Pumps | ISCO
- Ash dispersal/settling apparatus (Ash-Buster) | INGV
- Drone Mavic 2 Pro | DJI
- Drone Phantom 4 RTK | DJI
- Drone Mini 2 | DJI
- Dual UV cameras 340 UVGE | Thorlabs
- Laboratory sieve shaker Octagon 200 | Endecotts
- Optical Profilometer Modus6ZS-3D | DeltaPIX
- Triaxial ICP accelerometer | PCB Piezotronics
- Two high frequency ICP pressure sensors | PCB Piezotronics
- Three ceramic shear ICP accelerometers | PCB Piezotronics
- Two 4-channel ICP sensor signal conditioners | PCB Piezotronics
- MEERA biaxial direct shear apparatus
- High-temperature, vacuum, inert, and reactive gas furnace
- Microdriller for experimental glasses | ARNOLD 561/01
- Mortar grinder for experimental glasses | PULVERISETTE 23 FRITSCH
- SKO-D XL Orbital Shaker | SKO
- Centrifuge Neya 8 Basic | NEYA
- DANTE: Dynamic sample transfer system for high temperature, gas mixing, and vacuum experiments | Carbolite Gero | Verder Scientific



## Laboratory of New Technologies

- Analog Oscilloscope | HP
- Analog Oscilloscope | Iwatsu SS5710
- Analog Oscilloscope | Tektronix TDS220
- Analog Oscilloscope | Tektronix
- Oscilloscope | HP54201
- Oscilloscope | HP54602b
- Power supply | Elind HL series
- Power supply | Elind 6TD20
- Power supply | DC DF1731SB
- Signal generator | HP8656A
- Function generator | HP3325A
- Multimeter | HP3478A
- Milling machine for printed circuit boards | T-Tech
- Logic state analyzer | HP16500A
- Superheterodyne spectrum analyzer | Tektronix
- Soldering-reworking station | JBC advanced AM6500
- Oscilloscope | FLUKE 199C
- Oscilloscope | Tektronix DPO4000
- Oscilloscope | Tektronix MSO4034
- Calibrator | FLUKE 5700 (series II)
- Function generator | HP33120
- Function generator | AGILENT 33250 A
- PXI Industrial computer with I/O boards | National Instruments
- Universal counter | HP53131A
- Waveform generator | Agilent 33210 A
- Oscilloscope W wave surfer | LeCroy 44MXs-A
- Drone Phantom 3 pro with termination system
- Power supply (4 items) | -3005D



## Machine shop

- Lathe | Grazioli Fortuna
- Small lathe | Ceriani
- Small milling machine | Schaublin
- Cutting machine | Ercoletta
- Bending machine | Ercoletta
- Drill press | Serrmac
- Small drill press | Webo
- Bandsaw | Femi
- Grinder | Femi
- Extractor hood | Filcar
- Inverter welding machine | Tecnica
- TIG welding machine | Cebora
- Miter saw
- Numerically controlled milling machine



## 41 LABORATORY ACTIVITIES

### Experimental laboratory

#### Quick press | Piston cylinder

20 days of experiments in the frame of 3 research proposals.

#### BRAVA

BRAVA performed 134 experiments during 2021 including: room pressure friction experiments (double-direct and double-direct configuration) and in-vessel experiments up to 35 MPa of confining pressure.

#### Slow to HIgh Velocity Apparatus (SHIVA)

SHIVA performed 44 experiments during 2021 including two challenging novel experiments:

1. performed on gouges under fluid pressure confinement and 2. with in-situ, close to the surface, temperature measurements using optical fibers.

### Analog modeling laboratory

The Jet Burster laboratory device for the study of volcanic jets was implemented with the following systems: 1) four epoxy analogue conduit characterized by different degrees of internal surface roughness quantified by fractal dimensions of 2, 2.18, 2.7, 2.9) two pressure sensors to be placed at the inlet and outlet of the analogue conduits. The newly improved experimental device will allow to investigate the effects of conduit geometry on the dynamics of explosive volcanic eruptions and the related elastic radiation. We conducted so far different series of experiments to characterize the seismo-acoustic response of different setups and the related ejection at the tube outlet.

#### FaMoUS (Fast Multiparametric Setup)

We carried out two field campaigns at Mt. Etna (February-March) to observe the lava fountaining paroxysmal episodes. We performed five data acquisition campaigns at Stromboli (May-June, September, October), in the framework of the projects UnO and PRIN 2017, to collect multi-sensor data on the ordinary explosive activity. Finally two field campaigns were conducted (September-November) during the 2021 Cumbre Vieja eruption (Canary Islands, Spain).

Visible High Speed cameras (NAC and Optronis): i) about 30 Strombolian explosion events were filmed at 500 fps and at 1280x1024 pixel resolution during the period 9-16 May.

Infrared Camera: about 1 to 5 hours of continuous recording per day of the volcanic activity at the crater terrace of Stromboli were acquired at 50 Hz and at 640x480 pixel resolution during the periods 9-16 and 25-26 May, 12-17 June, 6 September, and 10-14 October.

UV Camera: about 1 to 5 hours of continuous recording of the volcanic activity at the crater terrace of Stromboli were acquired at a 50 Hz and at 640x480 pixel resolution during the period 9-16 May. Other acquisitions at 5 Hz were carried out at Etna (March) and Stromboli (July).



## Unmanned Aircraft System (UAS)

We performed UASs surveys at Stromboli (February, May, July, October, December), Etna (March), La Palma (September), and Vulcano (October-November). At Stromboli and La Palma we characterized the surface topography using Structure from Motion (SfM) photogrammetry that allowed us to produce very high resolution (10-50 cm pixel) digital Surface Models (DSMs) and orthophotomosaics and detect elevation, volumetric, and areal variations. At Etna and Vulcano, UASs were used to observe and characterise the volcanic activity. At Vulcano, in addition, we carried out measurements of CO<sub>2</sub>, H<sub>2</sub>S, and SO<sub>2</sub> concentrations in the plume using a drone equipped with miniaturized diffusive gas sensors.

## Microanalytical laboratory

FE-SEM and EMP performed 109 days of analysis in the frame of 19 research proposals

### Proposals

- 1. Geochemical characterization of tephra layers**  
I. Arienzo – M. Nazzari | INGV OV - INGV Roma1
- 2. Structure, evolution and deformation mechanisms of large displacement seismogenic faults in the continental crust**  
S. Masoch – E. Spagnuolo | University of Padua - INGV Roma 1
- 3. Viscosity and mobility of Ti-rich volatile-bearing melts representative of metasomatic fluids in the Earth's upper mantle**  
V. Stagno – P. Scarlato | Sapienza University of Rome - INGV Roma1
- 4. Reconstruction of the intensive variables and magmatic architecture of Vulcano island**  
F. Palummo – M. Nazzari – G. De Astis | Sapienza University of Rome - INGV Roma1
- 5. Understanding the ordinary to forecast the extraordinary: an integrated approach for studying and interpreting the explosive activity at Stromboli volcano**  
P. Landi | INGV PI
- 6. Volcanic hazard assessment at Mt. Etna: a time-integrated, polybaric and polythermal perspective**  
P. Moschini – P. Scarlato | Sapienza University of Rome - INGV Roma1
- 7. The 3 July 2019 paroxysm at Stromboli volcano (Italy): is Stromboli playing by new rules?**  
P. Scarlato – M. Nazzari | INGV Roma 1



8. COupling of Rheology and Textures in Experimental Seismic faults (CORTES)  
G. Pozzi | INGV Roma1
9. Fractured microlites  
J. Taddeucci | INGV Roma1
10. Time scales of solidification in magmas (Applications to Volcanic Eruptions, Silicate Melts, Glasses, Glass-Ceramics)  
P. Landi | INGV PI
11. Crystal-chemical and textural variations along a dyke of the Somma-Vesuvius volcano: insights on its solidification and emplacement processes  
G. Iezzi – M. Nazzari | University of Chieti - INGV Roma1
12. Tephrochronological study of the lacustrine succession of the maar of Castiglione (Central Italy) and evaluation of the possible impact on the climate of the explosive eruptions of the perithyrrenic volcanoes  
A. Di Roberto | INGV PI
13. CHIMERA - Cryptotephra In Marine sEquences of the Ross sea, Antarctica: implications and potential applications  
P. Del Carlo | INGV PI
14. Tracking alkaline magma evolution through cumulate rocks  
A. Pontesilli – P. Scarlato | University of Otago (New Zealand) - INGV Roma1
15. The role of the basement within the seismicity of the Apennines  
C. Collettini – G. Pozzi | Sapienza University of Rome - INGV Roma1
16. Alpine subduction zone metamorphism in the Paleozoic successions of the Monti Romani (Northern Apennines, Italy)  
F. Rossetti – A. Pontesilli | University of Roma Tre - INGV Roma1
17. Research Project: Unravelling the early crystallization pressure temperature domain of the Jersey minette lamprophyre (Channel Islands, UK): insights from Ti-zoning in phlogopite  
F. Lucci – M. Nazzari | University of Roma Tre - INGV Roma1





**18. Mineral chemistry (major and trace elements) of titanite and other silicates within meta-carbonate from amphibolite to granulite facies conditions: an example from Valle Strona d'Omegna (Ivrea-Verbano Zone, Italy)**

**A. Langone - M. Nazzari | University of Pavia - INGV Roma1**

**19. Messinian tephra in central and northern Apennines: distribution, texture and mineralogy of a large eruption(Northern Apennines, Italy)**

**G. Iezzi - P. Scarlato | University of Chieti - INGV Roma1**



## 51 RESEARCH PROJECTS

### 1. MIUR Progetto PRIN 2017

Scales of solidification in magmas: applications to volcanic eruptions, silicate melts, glasses, glass-ceramics | **P.I. M. Carroll**

### 2. MIUR PON-GRINT

Infrastruttura di Ricerca Italiana per le Geoscienze: GRINT | **P.I. G. Puglisi**

### 3. European research project

EXCITE 'Electron and X-ray microscopy Community for structural and chemical Imaging Techniques for Earth materials' | **P.I. V. Cnudde**

### 4. European research project

EUROVOLC 'European Network of Observatories and Research Infrastructures for Volcanology' | **P.I. K. VogFjord**

### 5. European research project

EPOS 'European Plate Observing System' Sustainability Phase, WP 16 Multi-scale Laboratories | **P.I. M. Cocco**

### 6. Petrobras3 - Petroleo Brasileiro S.A.

Igneous rocks as source and sink of abiotic hydrocarbons and CO<sub>2</sub> | **P.I. G. Etiope**

### 7. INGV "Ricerca libera" Project

Magma dynamics triggering the 3 July and 28 August 2019 paroxysms at Stromboli volcano: A comparative approach based on the ascent rates, timescales and P-T-H<sub>2</sub>O paths of magma | **P.I. P. Scarlato**

### 8. INGV "Ricerca libera" Project

PoWAR, a Portable Wind-tunnel for volcanic Ash Resuspension | **P.I. J. Taddeucci - E. Del Bello**

### 9. INGV "Ricerca libera" Project

ROUGHER, experimeNtal Observations aboUt irReGular cHannel gEometRies | **P.I. L. Spina**

### 10. INGV Departmental Strategic Projects

UNO - UNderstanding the Ordinary to forecast the extraordinary: An integrated approach for studying and interpreting the explosive activity at Stromboli volcano | **P.I. P. Scarlato**



#### 11. INGV “Pianeta Dinamico” Project

Task V1: Studio 3D-4D della struttura dei vulcani tramite tecniche di geofisica di esplorazione e confronto, integrazione e modellazione di dati geofisici, geochimici e geodetici | **P.I. C. Doglioni**

#### 12. INGV “Pianeta Dinamico” Project

Task S1: Studio teorico e sperimentale del processo di nucleazione e arresto dei terremoti, complessità della sorgente sismica | **P.I. C. Doglioni**

#### 13. INGV “Pianeta Dinamico” Project

Task S2: Struttura 3D dell’Italia da analisi multidata. Sismica passiva/attiva, Prospezioni magnetiche, magnetotelluriche, elettriche, gravimetriche | **P.I. C. Doglioni**

#### 14. ASI-INAF Project

“Esopianeti” | **P.I. G. De Astis**

#### 15. ERC Synergy Grant Fear

Fault activation and Earthquake Rupture | **P.I. D. Giardini, F. Amman, M. Cocco, S. Wiemer**

#### 16. European Training Network

IMPROVE Innovative Multi-disciplinary European Research training network on VolcanoEs  
**P.I. P. Papale**



## 61 PARTNER LABORATORIES

1. Planetary Environmental Facilities | Aarhus University | Denmark
2. Experimental & Physical Volcanology | Ludwig Maximillians Universitat | Germany
3. Dipartimento di Scienze | University of Roma Tre | Italy
4. Geoscience Department | Utrecht University | Netherlands
5. Institute of Geochemistry and Petrology | ETH Zurich | Switzerland
6. Dipartimento di Scienze Biologiche, Geologiche e Ambientali | University of Catania | Italy
7. Dipartimento di Fisica e Scienze della Terra | University of Ferrara | Italy
8. Petro-Volcanology Research Group (PVRG) Department of Physics and Geology  
University of Perugia | Italy
9. School of Earth and Environmental Sciences | University of Queensland | Australia
10. Department of Geology | University of Otago | New Zealand
11. Dipartimento di Geoscienze | University of Padua | Italy
12. LEMR | EPFL | Lausanne | Switzerland
13. Rock Mechanics Laboratory | Durham University | UK
14. Jackson School of Geosciences | Texas University at Austin | USA
15. The Rocks Physics and Mechanics Laboratory (RPML) | ETH | Switzerland
16. Rock Mechanics Laboratory | UCL Earth Sciences | UK
17. Laboratoire Aleas géologiques et Dynamique sédimentaire | IFREMER | France
18. RMP LAB | ETH | Switzerland
19. Geotechnical lab | RWTH Aachen University | Germany



## 71 PARTNER INSTITUTIONS

1. Ludwig Maximillians Universitat Munchen | Munich | Germany
2. Department of Geology and Geophysics, SOEST | University of Hawaii | USA
3. Department of Physics and Astronomy | Aarhus University | Denmark
4. HVO Hawaiian Volcano Observatory | USGS | USA
5. School of Earth and Environmental Sciences | University of Queensland | Australia
6. Department of Earth Science | University of Durham | UK
7. Instituto Volcanologico de Canarias | INVOLCAN | Spain
8. Dipartimento di Geoscienze | University of Padua | Italy
9. Departamento Tecnología Electrónica | Universidad Carlos III Madrid | Spain
10. Department of Geology | University of Otago | New Zealand
11. Dipartimento di Scienze della Terra | Sapienza University of Rome | Italy



## 8 | RESEARCH ACTIVITY and RESULTS

### 8.1 PETROLOGY, MINERALOGY, VOLCANOLOGY

#### Preliminary ash-leachates analysis from some recent eruptions at Stromboli volcano

Bagnato E., Andronico D., Cinti D., Del Bello E., Nazzari M., Scarlato P., Taddeucci J.

As volcanic gases leave the vent upon surface eruption, they mix with air and become oxidized. In response to these changes, condensation reactions occur, with fine-grained tephra often serving as catalysts for the formation of water-soluble minerals on their surfaces, thus rapidly scavenging volatile elements such as sulfur, halogens, and metal species (up to 30%). The analysis of water-soluble materials adhering to ash surfaces by leaching experiments ('ash leachates') was performed to obtain a time-resolved concentration of volcanic gas species adsorbed on ash surfaces as S-, Cl-, F-bearing soluble salts, whose composition may reflect, at least to some extent, plume chemistry and changes in the activity state of the volcano. In this study, forty-four ash samples for leaching experiments have been collected at Stromboli volcano from different types of activity (Strombolian explosions, ash emissions, landslides episodes and paroxysm) in 2019, 2020 and 2021, respectively. Accurate criteria were followed for selecting the samples: these were unexposed to rain prior to collection (thus preventing possible "natural" leaching of the soluble salts onto ash particles) and, when possible, collected during real-time observation of ordinary explosions or sporadic ash emissions on the volcano's

summit, as well as after landslides episodes. We therefore consider the selected samples representative of fresh-fallen ash, and overall uncontaminated/unaltered by post-deposition processes. A centrifuge and an orbital shaker have been implemented and installed at INGV-Roma 1, in order to perform leaching experiments. For the leachate analysis, 1 g ash will be eluted with 25 ml of  $\alpha Q$  grade Millipore water for 2 h with constant agitation. The solution will be subsequently centrifuged at 3,500 rpm for 15 min and filtered, to remove fine suspended materials. The extracted solutions were analyzed for F, Cl,  $SO_4$ , Na, K, Mg and Ca contents by ion chromatography. Few selected ash samples have also been observed by Scanning Electron Microscope (SEM), in order to identify and characterize the principal water-soluble materials adhering to the particles' surfaces. Among the soluble salts,  $CaSO_4$  (Anhydrite and/or Gypsum) and NaCl (Halite) were repeatedly observed by SEM analysis on Stromboli's ash surfaces (Figure 1) and both mineral phases have commonly been reported as incrustations on ash particles at many active volcanoes. The most abundant elements in ash leachates are sulphate (among anions) and calcium (among cations), with mean concentrations of 5744 and 1961  $\mu g/g$  ash, respectively.



The highly heterogeneous composition we found in the Stromboli's ash leachates is a hint for the complexity (and time variability) of factors governing the formation of water-soluble materials adhering onto volcanic ash surfaces (i.e. the availability of acid gases in the eruptive plume, tephra composition and origin, in-plume residence time of ash, meteorological factors). The relationship between the chemical composition of water-soluble components and the state of activity of Stromboli allowed obtaining marked temporal variations in the composition of the ash-leachate (Figure 1). Despite the compositional heterogeneity exhibited by our results, S/Cl and S/F molar ratios measured in ash-leachates are consistent with the Stromboli's bulk plume signature (mean S/Cl ratio: 2, range 0,4-8,8); while Cl/F ratios fall within the accepted volcanic arc (and Stromboli's) gas range. This suggests a prevalent volcanogenic

origin of  $\text{SO}_4$ , Cl and F, confirming that the adsorption of plume acidic gas species onto volcanic ash is among the key controlling factors on ash leachate chemistry. The relationships between the leached ratios of S/F and S/Cl increased significantly before and during the paroxysm started on 3 July 2019 (Figure 2). These values agree well with a greater volume of ash and volatiles produced within the eruptive cloud. As expected, the ratios turned to decrease after the paroxysm had come to an end. We speculate that more gas condensation on ash surfaces, and more extensive gas-ash interaction, may also have been favoured by the usually fine nature of ash emitted during the July 3 paroxysm as well as the more recent major explosion occurred on October 6 (2021), contributing to an increased surface area for water-aerosol adsorption, and consequently the occurrence of gas-ash reactions.

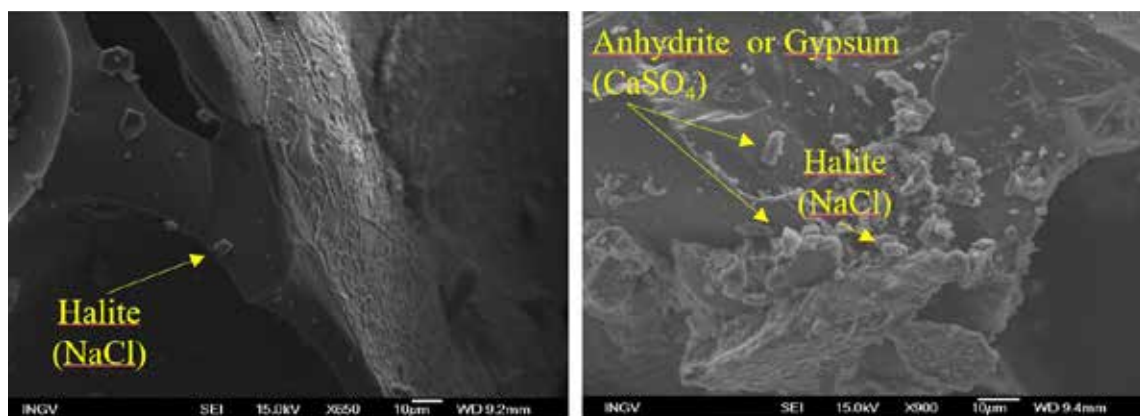
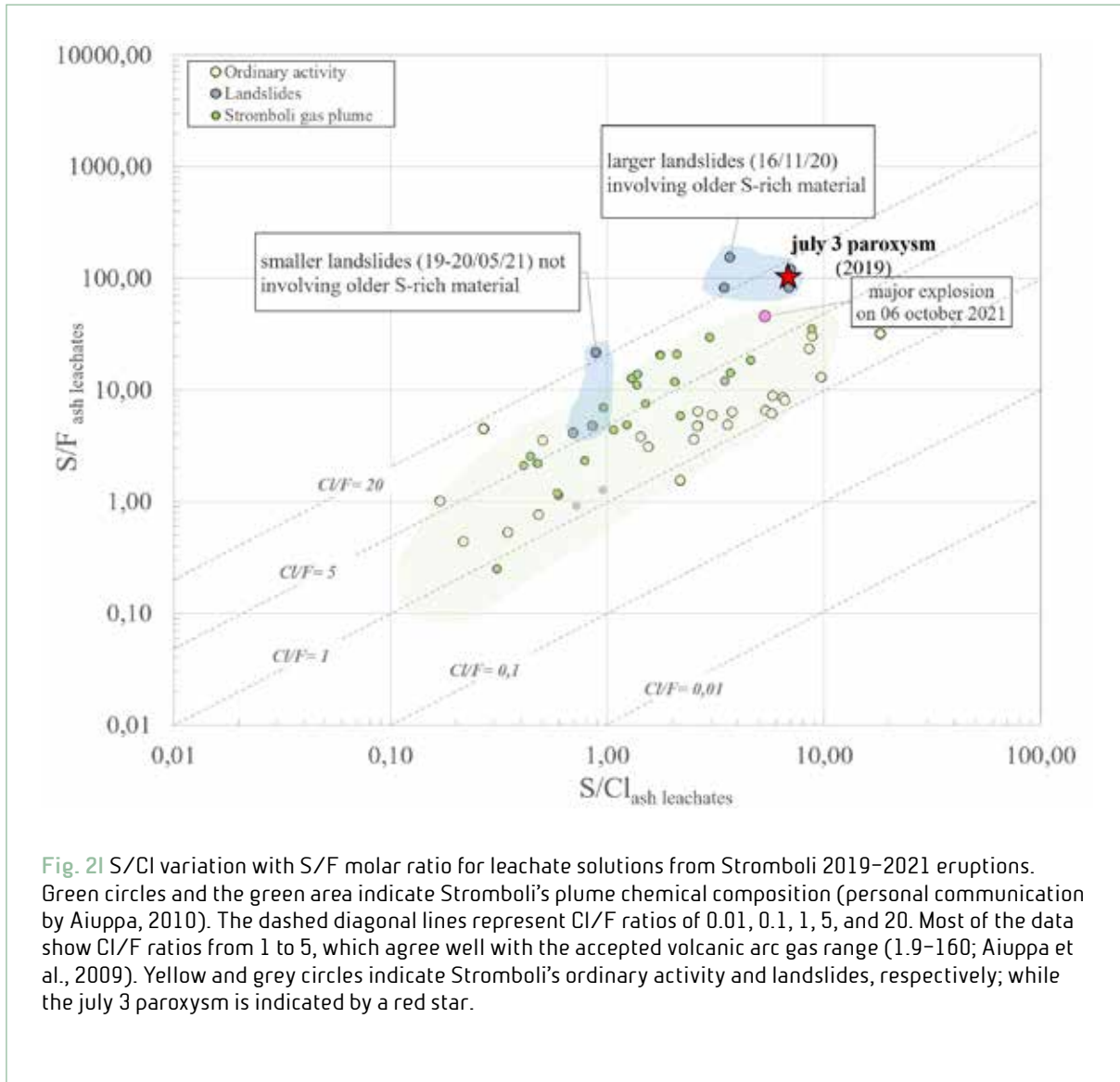


**Fig. 11**  $\text{CaSO}_4$  (Anhydrite or Gypsum) and Halite crystals observed by SEM analysis on Stromboli's ash surfaces.







## High-frequency parameterization of the changes in ordinary explosive activity at Stromboli volcano

**Del Bello E., Falcone E., Taddeucci J., Palladino D., Scarlato P., Andronico D.**

In the framework of the Progetto Dipartimentale PROJECT: UNO - UNderstanding the Ordinary to forecast the extraordinary: An integrated approach for studying and interpreting the explosive activity at Stromboli volcano, WI we applied high-speed- high-definition imaging techniques to ordinary explosive activity at Stromboli to capture eruptive processes and their variation in style, intensity and frequency at a high spatial and temporal resolution. Visible and thermal HS-HD imaging data were collected during four and twelve field campaigns respectively, in the period 2019-2021. The period covered was characterized by a widely varied volcanic activity, in which various non-ordinary events occurred. More specifically, two 'paroxysms', eleven 'major' explosions, and several spattering and lava flows episodes, which lasted up to weeks in time. As for the thermal time series acquired at 50 Hz, all the 12 datasets were processed to obtain quantitative parameters of the explosions. An ad hoc-implemented version of the algorithm of Gaudin et al. (2016) was used to obtain changes in thermal anomalies over time, allowing a quick detection of the explosions and their temporal and spatial evolution, and to distinguish their type through the visualization and recognition of bombs / gas / ash. The analysis of the high frequency thermal time series of 2019-2020 has so far

allowed recognising over 400 events, which were discriminated by explosion type (i.e., type 0, gas-dominated, type 1, bombs-dominated, type 2a-b, bombs-and-ash dominated, type 3, ash-explosions) according to the most recent classification published by Simons et al., (2020). For each type identified the eruption frequency, duration, height are quantified). Total frequency data by crater area were discriminated and compared with bulletin frequencies. The data show that in the days of 28 July and 7 September 2019, not far from the events of the 2019 paroxysms, the activity was characterized not only by high frequencies as known from the bulletins, but also by relatively shorter but more intense explosions, and the almost exclusive predominance of explosion types 1 and 2. On the contrary, in the periods of 9 May 2019 and 2 July 2020, the frequency of occurrence of events was lower, so was the height of the jets, and all explosive types, from 0 to 3, were present. From the results of these first datasets analysed, it seems that not only the mean eruption frequency, but the intensity of the explosions, paired with the variation of eruptive styles, need to be analysed together in order to better identify possible detectable changes in the general state of the volcano (Figure 1).

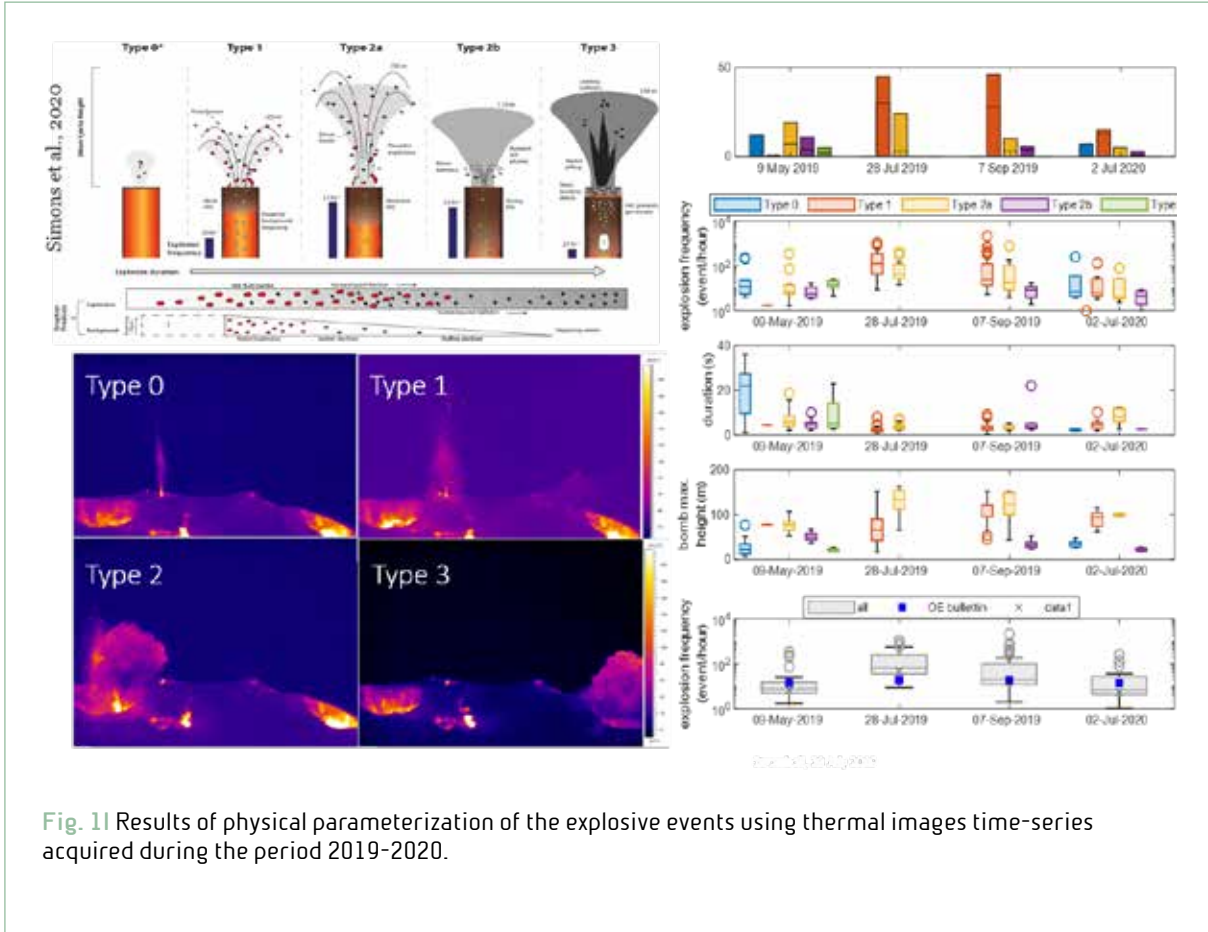


Fig. 11 Results of physical parameterization of the explosive events using thermal images time-series acquired during the period 2019-2020.



## Geochemical characterization of tephra layers from the Pollino Geopark

Di Vito M.A., Nazzari M., Arienzo I., Pelullo C.

In the framework of the Pianeta Dinamico task V1 project, major elements and Cl contents of glass shards from cored sequences from the Pollino Geopark (Calabria region), were determined at the HP-HT Laboratory of Experimental Volcanology and Geophysics of the Istituto Nazionale di Geofisica e Vulcanologia (INGV) in Rome (Italy), using a Jeol-JXA8200 field-emission electron microprobe equipped with five wavelength dispersive spectrometers.

This study is aimed at better defining the dispersion of the products extruded during volcanic eruptions occurred at Campi Flegrei caldera and Vesuvius volcanoes in the last 4ka, and their possible effects on the environment. In the investigated cored sequences, two

superposed, separated tephra layers were found. However, glass shards from the majority of the cored sequences were deeply altered limiting any possibility to analyze and compare their chemical composition with the available literature data.

Based on i. the sedimentological features of the deposits; ii. the radiocarbon dating of organic material just below the upper tephra layer and; iii. the results of EMPA analyses of two superposed tephra layers from one of the cores (Figure 1), samples were correlated to the activity of Mt. Vesuvius (Figure 2). Specifically, the oldest tephra was attributed to the AP1-AP3 eruptions and the youngest to the 79 A.D. eruption.

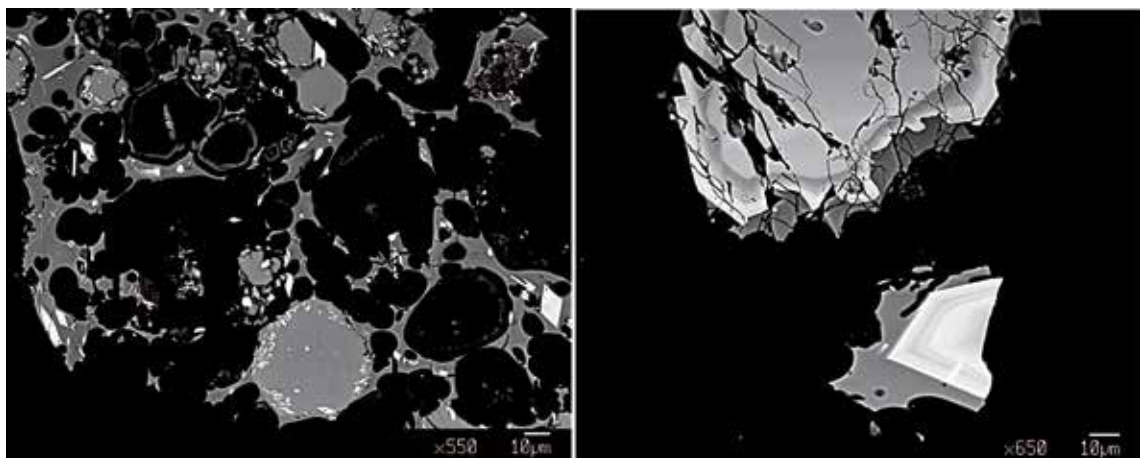


Fig. 11 Images of the analysed upper tephra layer.

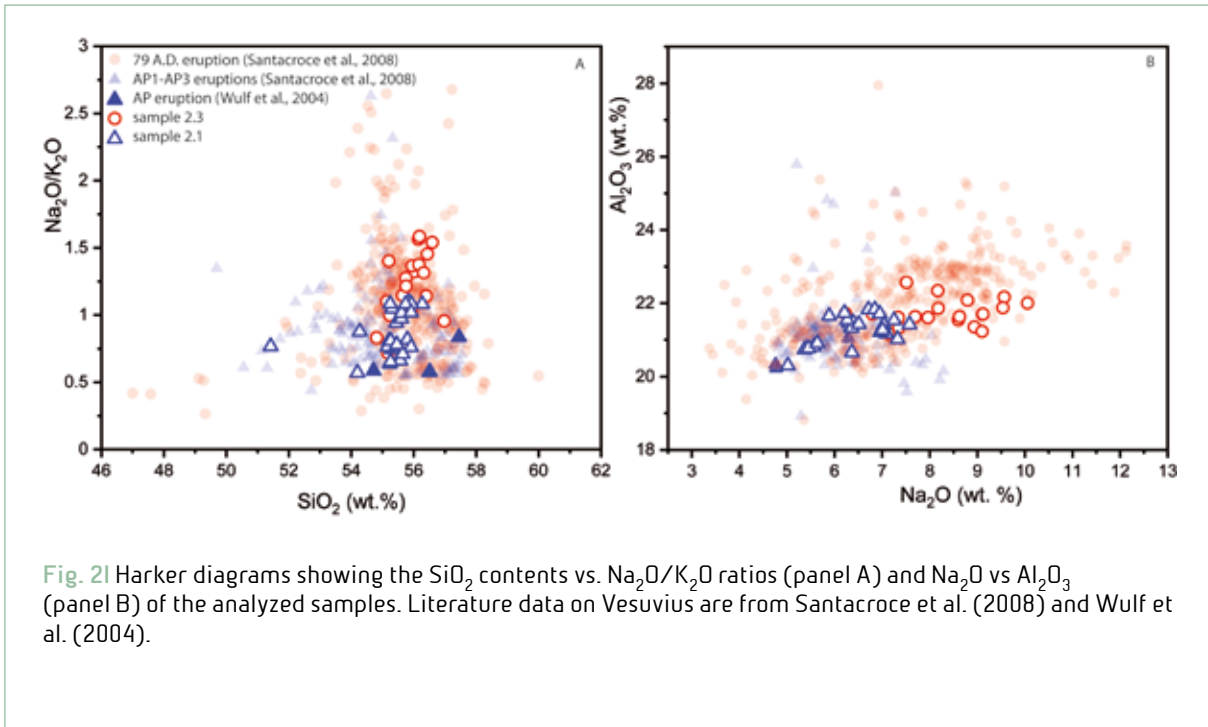


Fig. 21 Harker diagrams showing the  $\text{SiO}_2$  contents vs.  $\text{Na}_2\text{O}/\text{K}_2\text{O}$  ratios (panel A) and  $\text{Na}_2\text{O}$  vs  $\text{Al}_2\text{O}_3$  (panel B) of the analyzed samples. Literature data on Vesuvius are from Santacroce et al. (2008) and Wulf et al. (2004).



## Geochemical characterization of volcanic tephra from an archeological site of Pontecagnano (Salerno, South Italy)

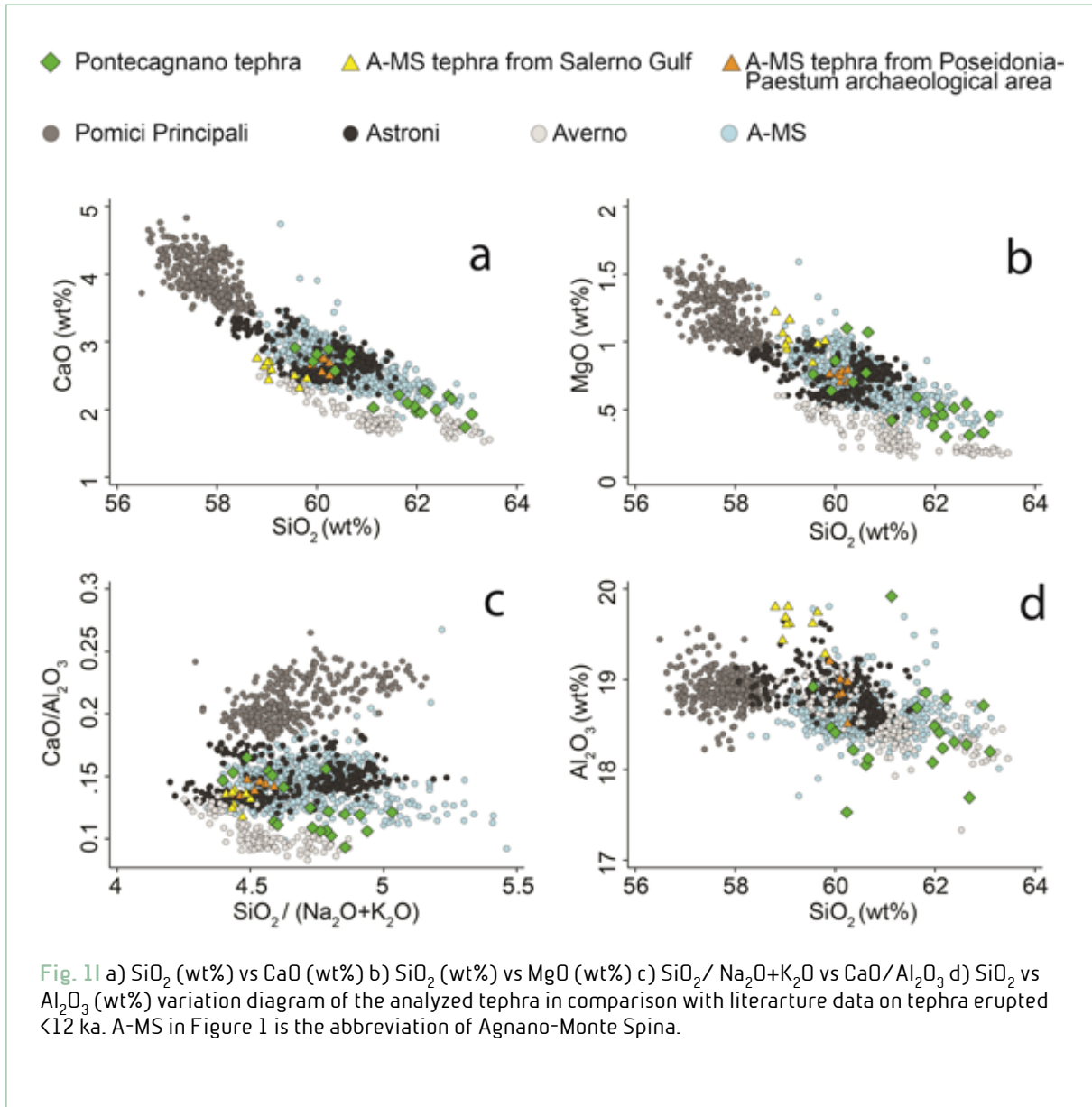
Pelullo C., Arienzo I., Di Vito M.A.

In the framework of the Pianeta Dinamico task VI project, electron microprobe analyses (EMPAs) have been performed on volcanic products recently found in an archeological site of Pontecagnano (Salerno, South Italy). Glass shards major element compositions were acquired at the HP-HT Laboratory of Experimental Volcanology and Geophysics of the Istituto Nazionale di Geofisica e Vulcanologia (INGV) in Rome (Italy), using a Jeol-JXA8200 field-emission electron microprobe equipped with five wavelength dispersive spectrometers. The samples from Pontecagnano were collected by 4 recently exposed sequences, in which 3 different tephra units have been recognized. Major element glass compositions of the ashy layer in intermediate stratigraphic position have been compared with those of volcanic products belonging to Phlegrean eruptions that occurred in the last 12,000 years (Pomici Principali, 12.1-11.9 ka; Averno, 3.75-3.65 ka; Astroni, 4.3-4.1 ka; Agnano-Monte Spina, 4.10-4.08 ka).

The analyzed glasses show a bimodality in terms of silica content, which makes it possible to distinguish a group of compositionally less evolved glasses ( $\text{SiO}_2 \approx 59$  wt%) and a group of more evolved glasses ( $\text{SiO}_2 \approx 63$  wt%). The major elements variations ( $\text{SiO}_2 = 63-59$  wt%,  $\text{TiO}_2 = 0.7-0.2$  wt%,  $\text{Al}_2\text{O}_3 = 19.9-17.5$  wt%,  $\text{FeO} = 3.8-2.4$  wt%,  $\text{MgO} = 1.1-0.3$  wt%,  $\text{CaO} =$

$2.9-1.7$  wt%,  $\text{Na}_2\text{O} = 4.9-2.8$  wt%,  $\text{K}_2\text{O} = 10.8-8.0$  wt%) suggest that the compositions of the analyzed glass samples are compatible with those of products emplaced during both the Agnano-Monte Spina and the Averno eruptions. Nevertheless, matrix-glasses from Averno show remarkable lower MgO, CaO and  $\text{CaO}/\text{Al}_2\text{O}_3$ . The products of other eruptions occurred in the last 12,000 years of volcanic activity do not well represent all the chemical variability found in the Pontecagnano glasses (see  $\text{SiO}_2$  wt%). Moreover, the chemical composition of the analyzed samples also fit that of volcanic layers from cores drilled in nearby areas, investigated in previous studies and attributed to the Agnano-Monte Spina eruption. Lastly, Sr-isotopic data of feldspar crystals picked from the Pontecagnano tephra, acquired at the Radiogenic Isotope Laboratory of the INGV, Osservatorio Vesuviano of Napoli, are compatible with ratios obtained on some mineral phases of the Agnano-Monte Spina products (Figure 1).









## Inferences on the feeding system at Stromboli volcano from the composition of the matrix glasses

Landi P., D’Orlando C., Petrelli M., Nazzari M., Andronico D.

A large set of chemical analyses (both of major and trace elements) of the glassy matrix from products erupted at Stromboli in the past two decades was performed, with the aim to improve the knowledge on the plumbing system that feed the persistent activity of the volcano. About 350 major elements analyses mostly of glass and few analyses of plagioclase, clinopyroxene and olivine were performed in the HPHT Laboratory

Samples emitted during different type of explosive activity were analyzed. In detail among the them, 8 samples are representative of mingled pumice and/or lapilli and ash erupted during 4 major explosions (23 August 1998, 8 and 24 November 2009, 19 July 2020) and 4 paroxysms (5 April 2003, 15 March 2007, 3 July 2019 and 28 August 2019), and 6 samples correspond to the scoriae and ash emitted during the normal activity of July 2019, October 2019 and October 2020.

The detailed analytical study allowed to better define the role of the different petrogenetic processes (degassing, crystallization, mineral

dissolution, magma mixing,) that occur in the present feeding system and concur to the transformation of the LP magma into the HP magma.

The compositional variations of the matrix glasses, associated with the chemistry of the minerals, have also made it possible to draw a picture of the vertical chemical zoning of the feeding system, thus providing insights into the pre-eruptive and syn-eruptive magmatic dynamics that controls the violent explosions of Stromboli.

As an additional result, the major and trace element dataset presented in this work, that involves products erupted during explosive activity with variable energy, can be used as a reference picture for evaluating possible chemical variations in the Stromboli’s feeding system. This data set can be also useful for evaluating minor chemical variations in the products erupted at Stromboli during the normal activity and their nexus with the more hazardous activity styles (Figure 1).

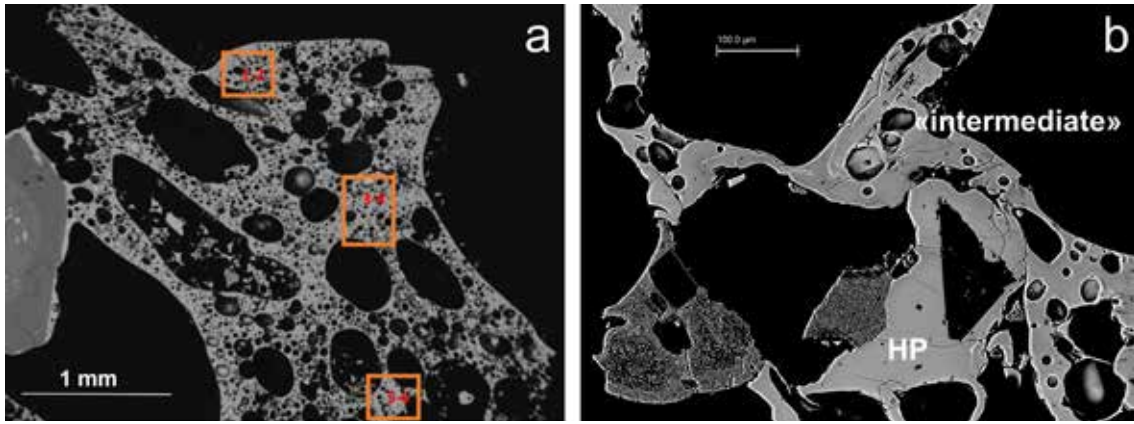


**Fig. 11** SEM images of matrix glasses selected for the major/trace elements analyses. (a) matrix glass of an LP pumice (3 Jul 2019 paroxysm); (b) contact between glasses with different composition and vesicularity (19 Jul 2020 major explosion).



## The “Camporotondo” occurrence of the volcanic-rich layer of 5.5 Ma (VRL-5.5): petrography, geochemistry and deposition

Potere D., Iezzi G., Scisciani V., Nazzari M., Piochi M., Mormone A., Pierantoni P.P.

The Messinian volcanic-rich layer cropping out along the Apennines chain has been studied in the past in the central part of the chain, from Piavola (Forli-Cesena, Emilia Romagna) to Basciano (Teramo, Abruzzo), being interpreted either like a primary fallout or as a secondary turbiditic deposit.

In this study this tephra, emerging in the well-known stratigraphic section of Camporotondo (Marche, 43°08'11" N; 13°53'29" E), is analyzed by field, mesoscopic, microscopic, crystallographic, geochemical and textural observations. The section is lithified and contain sedimentary structures, such as plane-parallel, undulate and even more complex features. The XRPD (X-ray powder diffraction) analysis unveil the presence of glass materials, with few magmatic minerals (feldspars and biotite), plus sedimentary ones like calcite, quartz, and montmorillonite. The optical and especially SEM (scanning electron microscopy) observations, coupled with 2D image analysis, allow to quantify the textures of these materials. The most part of samples are composed of very fine (<62,5 μm) glass shards, hosting very few (<5 area%) crystals. The carbonate phases occur like clasts and filling voids among volcanic shards. The micro-chemical determinations of the glass by EPMA-WDS (electron-probe microanalysis in wavelength dispersion) retrieve a rhyolitic composition for all of the analysed volcanic

materials. Their composition perfectly overlaps those of previous investigated and stratigraphically related sections cropping along the Apennines.

The 2D textures of the samples of the whole section are similar in grain-size distribution, length and width of shards, their aspect ratio, but differ in their roundness: the more rounded shards occur in conjunction with more complex sedimentary structures linked to local and limited in space remobilization of these pyroclasts after their primary deposition. By contrast, the less rounded shards are displayed by samples free of structures or displaying only plane-parallel features.

The outcomes provided here report the Camporotondo occurrence of this volcanic-rich layer of 5.5 Ma (VRL-5.5) as an example of a primary deposit, partially remobilized, of the volcanic horizon found spreading along the Apennines chain, in the NNW-SSE direction, for at least 300 kms along. The reconstruction of its depositions mechanisms could be extended further north and south to the other sections already known in the Abruzzo, Marche and Emilia-Romagna regions, helping in better understanding their deposition dynamics. The analytical protocols used in this study can be useful to investigate other ancient volcanic-rich layers, especially those that are found lithified (lithified tephra) (Figure 1).

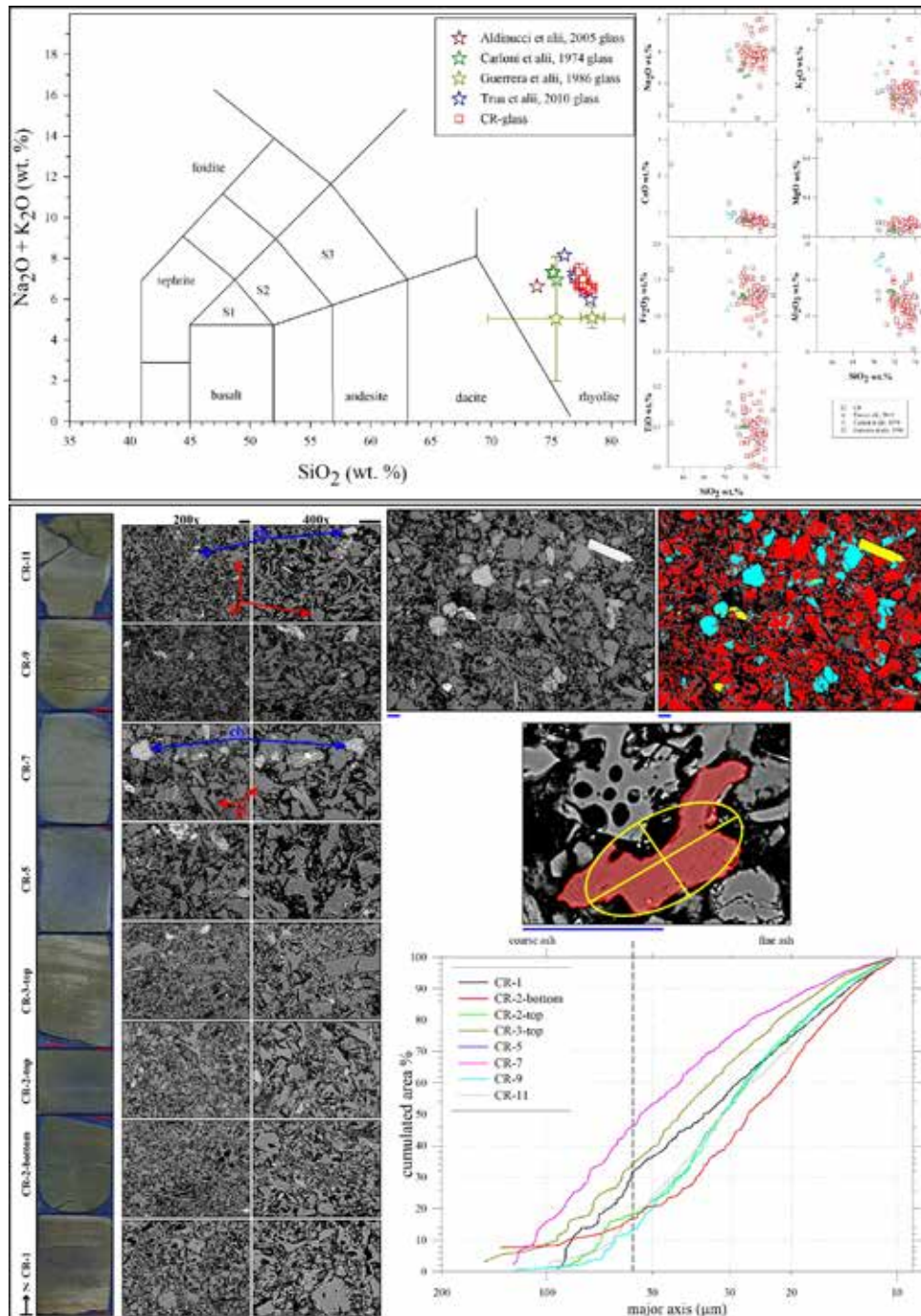


**Fig. 11** Chemical data from bulk and microchemical (on glassy phase) analyses plotted onto TAS and Harker diagrams (up); polished thin sections scans and BSE-SEM microphotographs used to perform 2D image analyses to get morphological parameters of the glass shards, such as the major axis length, reported in the GSD cumulated curve (down).



## Decoding multiple zoning patterns in clinopyroxene phenocrysts at Vulcano Island: A record of dynamic crystallization through interconnected reservoirs

Palummo F., Mollo S., Petrone C.M., Ellis B.S., De Astis G., Nazzari M., Scarlato P., Bachmann O.

Here we document how the different growth features and intracrystalline distributions of both major and trace cations in clinopyroxene phenocrysts are important recorders of the intricate magma dynamics at Vulcano Island (Aeolian Arc, Italy). The compositions of clinopyroxene phenocrysts from products erupted over the last ~54 ka cluster at different degrees of evolution, paralleling the polybaric-polythermal differentiation of mantle-derived mafic magmas into more evolved silicic melts. The hotter lower crust is the most favorable location for the storage of mafic magmas and the early crystallization of diopsidic (Mg#91) clinopyroxene ( $P_{\max} \approx 750$  MPa and  $T_{\max} \approx 1220$  °C). Diopsidic phenocrysts are depleted in both rare earth elements (REE) and high field strength elements (HFSE) but are enriched in transition elements (TE). The transfer and accumulation of primitive magmas in the colder upper crustal regions lead to the formation of an interconnected series of more differentiated magmatic reservoirs ( $P \approx 100$ –450 MPa and  $T \approx 1100$ –1180 °C) hosting discrete populations of clinopyroxene (Mg#84–85) with a broad spectrum of zonations and dissolution features. Recharge bands in clinopyroxene are markers of multiple inputs of primitive REE-HFSE-poor, TE-rich magmas from depth. Augitic phenocrysts (Mg#82) with strong negative Eu anomaly and REE + HFSE enrichments crystallizes from

highly differentiated trachytic and rhyolitic melts stored at very shallow crustal conditions ( $P \leq 50$  MPa and  $T \leq 1100$  °C). These silicic reservoirs represent residual melts trapped-extracted from crystal-dominated mush regions in the uppermost part of the plumbing system. The residence time of clinopyroxene increases from ~0.1 to ~44 years from basalt to rhyolite, together with an increasing number of recharge bands. The mineral assemblage in more silicic and viscous mush melts is sufficiently resilient to record numerous mafic injections and high degrees of magma mixing, hybridization, and crystallization before eruption. Overall, the compositional zoning pattern of clinopyroxene presents a picture of plumbing system that extends through the crust and is characterized by distributions of melts and crystals which are progressively more evolved and heterogeneous in both space and time (Figure 1).



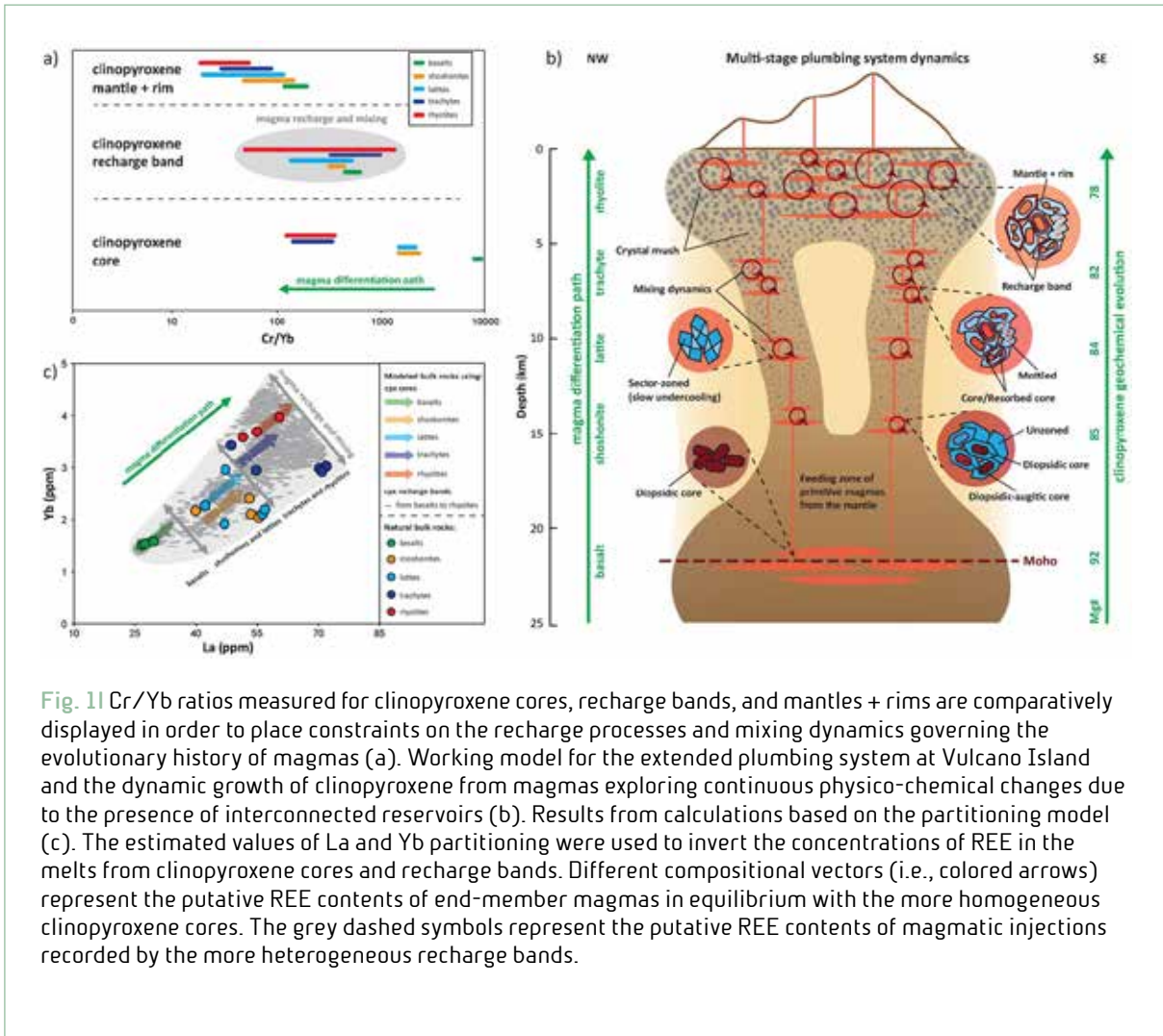


**Fig. 11** Cr/Yb ratios measured for clinopyroxene cores, recharge bands, and mantles + rims are comparatively displayed in order to place constraints on the recharge processes and mixing dynamics governing the evolutionary history of magmas (a). Working model for the extended plumbing system at Vulcano Island and the dynamic growth of clinopyroxene from magmas exploring continuous physico-chemical changes due to the presence of interconnected reservoirs (b). Results from calculations based on the partitioning model (c). The estimated values of La and Yb partitioning were used to invert the concentrations of REE in the melts from clinopyroxene cores and recharge bands. Different compositional vectors (i.e., colored arrows) represent the putative REE contents of end-member magmas in equilibrium with the more homogeneous clinopyroxene cores. The grey dashed symbols represent the putative REE contents of magmatic injections recorded by the more heterogeneous recharge bands.



## Parameterization of clinopyroxene growth kinetics via crystal size distribution (CSD) analysis: Insights into the temporal scales of magma dynamics at Mt. Etna volcano

Moschini P., Mollo S., Gaeta M., Fanara S., Nazzari M., Petrone C.M., Scarlato P.

There is increasing recognition that both textural and compositional changes of clinopyroxene crystallizing from mafic alkaline magmas are the direct expression of complex dynamic processes extending over a broad range of spatial and temporal scales. Among others, supersaturation and relaxation phenomena play a key role in controlling the final crystal cargo of variably undercooled magmas erupted from active alkaline volcanoes. Following this line of reasoning, we have carried out isothermal-isobaric, decompression, and cooling rate experiments on a basalt interpreted as the parental magma of mafic alkaline eruptions at Mt. Etna volcano (Sicily, Italy). The main purpose is to reconstruct and quantify the textural changes (i.e., length of major and minor axes, surface area per unit volume, area fraction, and maximum growth rate) of clinopyroxene at variable pressures (30–300 MPa), temperatures (1050–1100 °C), volatile contents (0–5 wt% H<sub>2</sub>O and 0–0.2 wt% CO<sub>2</sub>), and equilibration times (0.25–72 h). Melt supersaturation, corresponding to a degree of undercooling variable from 14 to 125 °C, drives the formation of clinopyroxene crystals with different textures and sizes as a function of growth rate and relaxation time. By integrating experimental data and thermodynamic modeling, the transition between interface-

controlled (euhedral morphologies) and diffusion-controlled (anhedral morphologies) growth regimes has been determined to occur at degrees of undercooling higher than 30 °C. The decrease of clinopyroxene growth rate with increasing the equilibration time is combined with the crystal size distribution (CSD) analysis of naturally undercooled clinopyroxene crystals erupted during 2011–2012 lava fountain episodes at Mt. Etna volcano. Results indicate that the crystallization of microlites and microphenocrysts is on the order of ~100–101 min (large undercooling, short equilibration time) and ~101–102 h (small undercooling, long equilibration time), respectively. This temporal information allows to better constrain the cooling-decompression paths of Etnean magmas rising and accelerating along a vertically extended, highly dynamic plumbing system. While clinopyroxene microlites develop during the fast ascent of magmas (~100–101 m s<sup>-1</sup>) within the uppermost part of the conduit or immediately before ejection from the vent, the onset of microphenocryst crystallization occurs at depth and continues within the plumbing system during the slow ascent of magmas (~10<sup>-2</sup> m s<sup>-1</sup>) that migrate through interconnected storage regions (Figure 1).



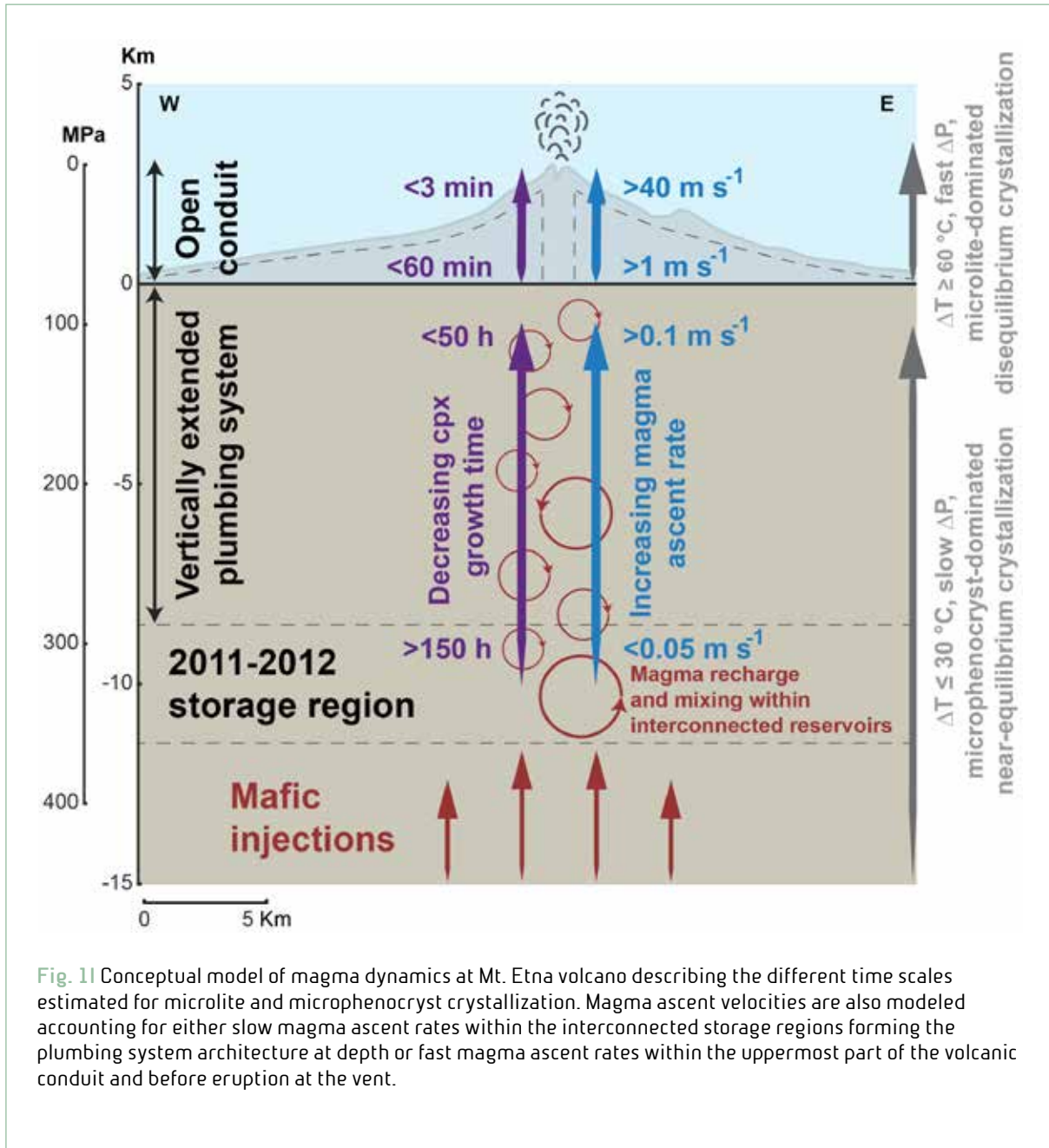


**Fig. 11** Conceptual model of magma dynamics at Mt. Etna volcano describing the different time scales estimated for microlite and microphenocryst crystallization. Magma ascent velocities are also modeled accounting for either slow magma ascent rates within the interconnected storage regions forming the plumbing system architecture at depth or fast magma ascent rates within the uppermost part of the volcanic conduit and before eruption at the vent.



## Partitioning of Ti, Al, P, and Cr between olivine and a tholeiitic basaltic melt: Insights on olivine zoning patterns and cation substitution reactions under cooling rate conditions

Lang S., Mollo S., France L., Misiti V., Nazzari M.

The mechanism governing the kinetic growth of olivine in dynamic volcanic settings has been the subject of considerable attention in recent years. Under variable cooling rate (CR) and undercooling ( $-\Delta T$ ) regimes, the textural maturation of olivine proceeds from skeletal/dendritic crystals to polyhedral morphologies by infilling of the crystal framework. Owing to the establishment of a diffusion-controlled growth regime, a sharp diffusive boundary layer develops in the melt next to the advancing olivine surface (Figure 1). In this perspective, we have quantified the apparent partitioning of Ti, Al, P, and Cr between olivine and a Hawaiian tholeiitic basaltic melt at  $P = 1$  atm,  $fO_2 = \text{QFM}-2$  buffer, and  $CR = 4, 20,$  and  $60$  °C/h over a constant  $-\Delta T = 85$  °C. Differences in charge and/or size between the substituent minor cations and the major species in the olivine crystallographic site dominate the energetics of homovalent and heterovalent cation substitutions. While the entry of Ti in the olivine lattice site accounts for the simple exchange  $[^T\text{Si}^{4+}] \leftrightarrow [^T\text{Ti}^{4+}]$ , more complex charge-balancing coupled-substitution mechanisms have been determined for the incorporation of Al, P, and Cr, i.e.,  $[^M\text{Mg}^{2+}, ^T\text{Si}^{4+}] \leftrightarrow [^M\text{Al}^{3+}, ^T\text{Al}^{3+}]$ ,  $[2 ^T\text{Si}^{4+}] \leftrightarrow [^T\text{P}^{5+}, ^T\text{Al}^{3+}]$ , and  $[^M\text{Mg}^{2+}, ^T\text{Si}^{4+}] \leftrightarrow [^M\text{Cr}^{3+}, ^T\text{Al}^{3+}]$ , respectively.

In order to maintain charge balance, the disequilibrium uptake of minor cations in rapidly growing crystals is controlled by the same substitution mechanisms observed under equilibrium crystallization.

This finding is consistent with the achievement of a local interface equilibrium at the olivine-melt interface independently of the diffusive boundary in the melt. A statistical approach based on multivariate analysis of olivine/melt compositional parameters confirms that the control of melt structure on the partitioning of Ti, Al, P, and Cr is almost entirely embodied in the crystallochemical change of olivine. Therefore, the magnitude of minor element partition coefficients is weakly dependent on diffusion kinetics in the melt but rather strongly governed by olivine zoning patterns resulting from fast crystal growth rates.

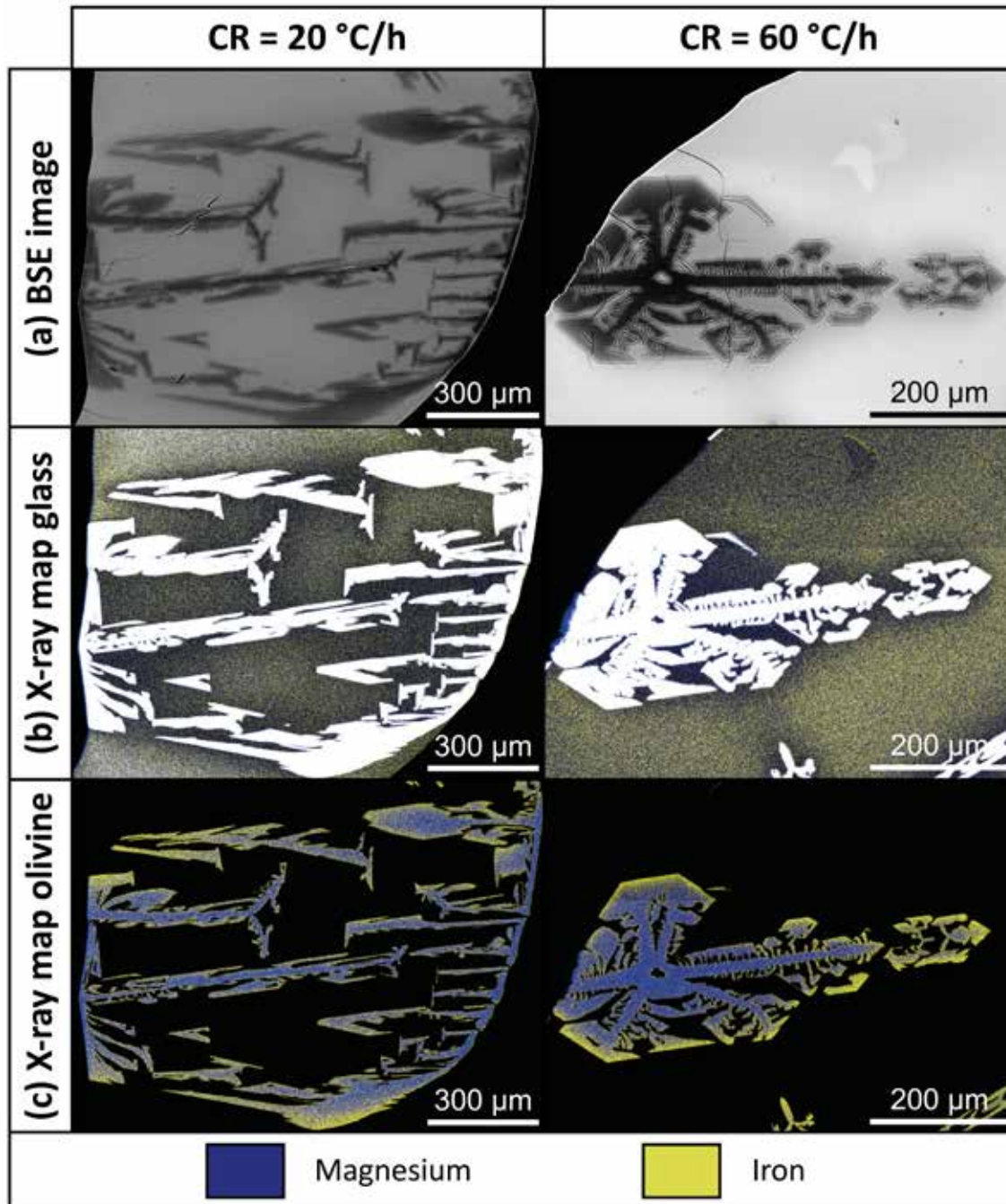


**Fig. 11** BSE (back-scattered electron) photomicrographs of experimental charges obtained at cooling rates of 20 and 60 °C. The figure shows also combined Fe-Mg X-ray maps with color scales adjusted for the glass and crystal compositions.



## Kinetic partitioning of major and trace cations between clinopyroxene and phonotephritic melt under convective stirring conditions: new insights into clinopyroxene sector zoning and concentric zoning

Di Fiore F., Mollo S., Vona A., MacDonald A., Ubide T., Nazzari M., Romano C., Scarlato P.

Within subvolcanic plumbing systems, along volcanic conduits and post-eruptive emplacement, mineral textures and compositions are governed by complex kinetic (undercooling) and dynamic (convective) processes that deviate from theoretical models and equilibrium criteria. In this perspective, we have investigated the partitioning of major and trace cations between clinopyroxene and phonotephritic melt under convective stirring conditions at high degrees of undercooling and atmospheric pressure.

We have integrated this novel data set with conventional static (no physical perturbation) clinopyroxene-melt compositions obtained under interface- and diffusion-controlled growth regimes.

Results show that clinopyroxene growth kinetics and diffusion boundary layers caused by melt supersaturation are partly mitigated by the homogenizing effects of stirring.

Because of continuous supply of fresh melt to the advancing crystal surface, the partitioning of major and trace cations is governed by local equilibrium effects, which are interpreted as the extension of equilibrium thermodynamic principles to non-equilibrium bulk systems.

Major cations are incorporated into the clinopyroxene structure via the coupled substitution  $[^{M1}Mg, ^T Si] \leftrightarrow [^{M1}Ti, ^T Al]$  and in conformity with the thermodynamic mixing

properties of  $CaMgSiO_2$ ,  $CaAl_2SiO_6$  and  $CaTiAl_2O_6$  components.

The complementary relationship between lattice strain and electrostatic energies of heterovalent substitutions is the most appropriate thermodynamic description for the accommodation of trace cations in the clinopyroxene lattice site.

The excess energy of partitioning changes principally with Al in tetrahedral coordination and determines the type and number of charge-balanced and -imbalanced configurations taking place in the structural sites of clinopyroxene (Figure 1).



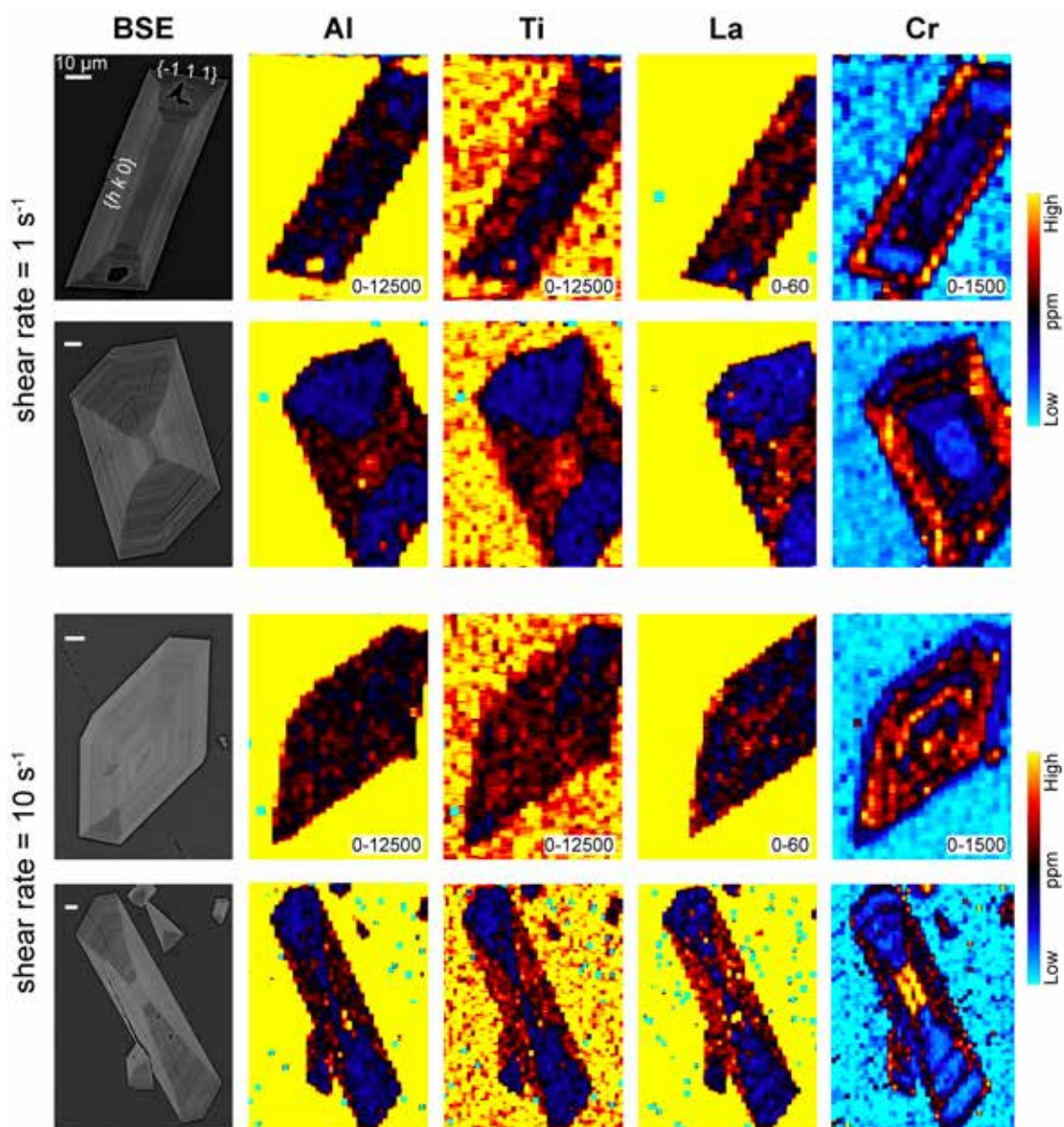


**Fig. 11** LA-ICP-MS maps selected for some key cations in clinopyroxenes. Note that Cr is the only cation that strongly concentrates in synchronous concentric zones.



## Tracking alkaline magma evolution through cumulate rocks

Pontesilli A., Mollo S., Brenna M., Masotta M., Scarlato P., Nazzari M.

The importance of amphibole-clinopyroxene assemblage during lower crustal fractionation processes in arc magmas is widely acknowledged, although the role of amphibole in intraplate settings, where hydrous input through active subduction is missing, is still poorly understood.

The formation of amphibole cumulates beneath arc-related volcanoes has been shown to have a key control on magma differentiation, as well as generation of a hydrous lower crust. This fractionation is often referred to as “cryptic” because the amphibole does not represent a common phenocryst phase in arc magmas. Lower crustal “hot-zones” have been identified on the basis of amphibole-rich cumulates produced by reaction-replacement of antecrystic clinopyroxene. Amphibole-clinopyroxene-bearing cumulates are also known to have played a major role in the older activity of active volcanoes, like Mt. Etna and Stromboli (Italy). Intraplate composite volcanoes commonly feature amphibole-rich intrusive and volcanic rocks, indicative of enhanced amphibole stability. At the long-lived Dunedin Volcano (New Zealand), coexisting amphibole and clinopyroxene often occur in mafic to intermediate magmas (alkali basalts to mugearite and phonotephrite), and are observed to form cumulate rocks, represented by gabbros, clinopyroxenites, and amphibolites. Although the two phases generally crystallize under equilibrium conditions, some cumulates

show evidence of clinopyroxene resorption and amphibole overgrowth. These cumulates are heralds of magma differentiation driven by hydrous magma batches that ascend and interact with crystalline mushes in the lower crust. Cumulates from more differentiated magmas (syenites) are instead characterized by crystal remnants which indicate resorption of Mg, Ti-rich amphibole and clinopyroxene. Overgrowth textures resulting from Fe-rich amphibole and clinopyroxene crystallization indicate fractionation from more evolved magmas (benmoreites, tephriphonolites, phonolites) at shallow crustal levels. Here major and trace element compositions from natural amphibole-clinopyroxene assemblages are compared with those obtained via temperature-gradient experiments reproducing the textural features of crystalline mushes. Results are then integrated with equilibrium melt compositions estimated by means of published partitioning schemes for amphibole and clinopyroxene. This approach allows reconstructing the original melt compositions in equilibrium with natural cumulate parageneses and the crystallization sequences resulting from crystal replacement reactions. We observe that cumulate rocks can be used to track the evolution of melts from which cumulate crystals are segregated, thus offering new physicochemical constraints on cumulate-forming processes operating in alkaline magmatic systems (Figure 1).

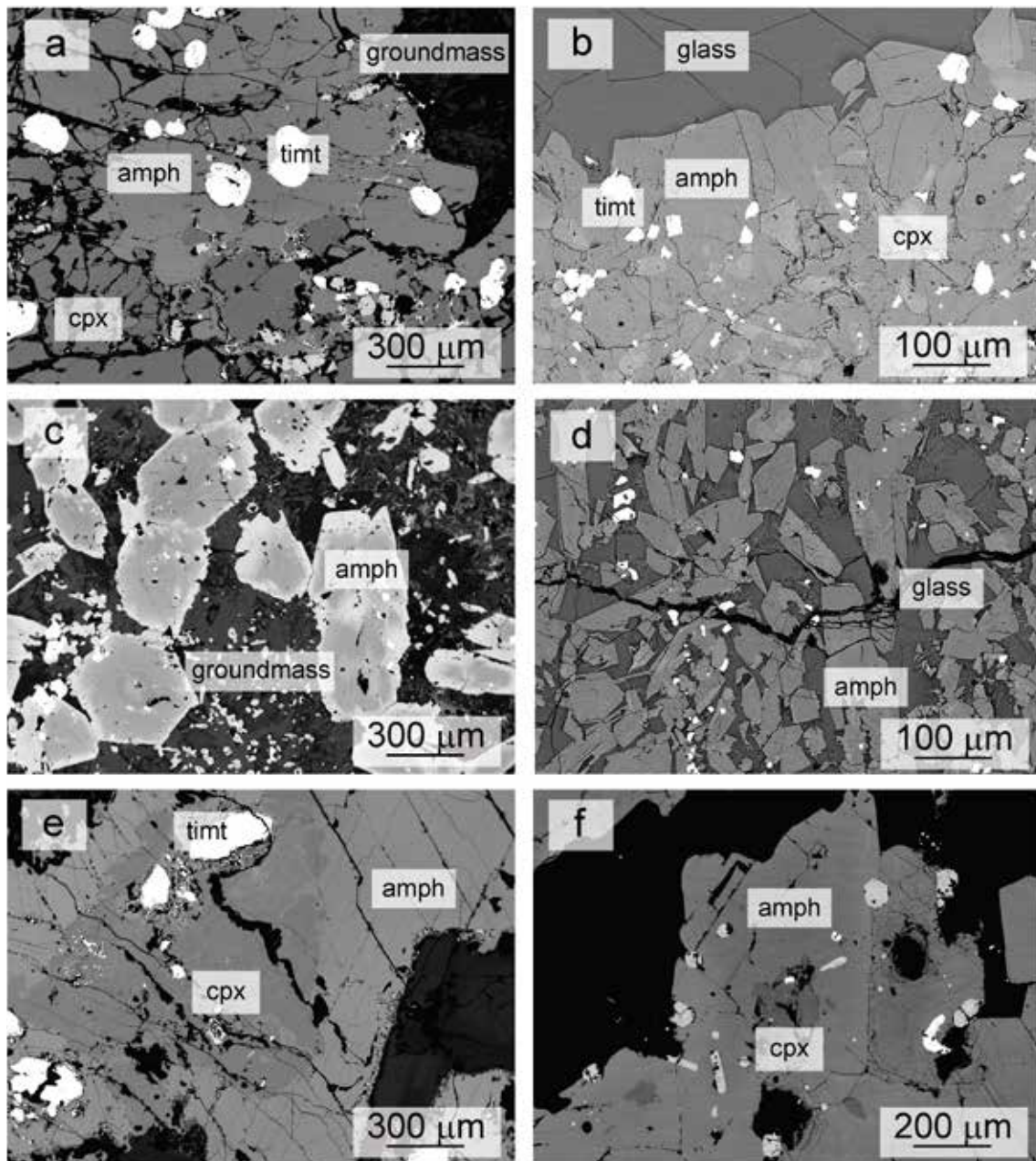


**fig. 11** Back Scattered Electron (BSE) images of amphibole-clinopyroxene bearing cumulate rocks and experimental equivalents. a) amphibole-clinopyroxene cumulate with abundant titanomagnetite inclusions; b) experimental equivalent of cumulate in (a) produced via thermal-gradient experiments, with amphibole-clinopyroxene intergrown and abundant titanomagnetite inclusions; c) amphibole-rich cumulates hosted by a microcrystalline lava; d) experimental equivalent of (c) produced in thermal-gradient experiments, and constituted by amphibole-rich cumulate and residual glass preserved in the interstices of the crystalline network; e) resorbed clinopyroxene overgrown by amphibole crystals from a gabbroic sample. f) relics of resorbed clinopyroxene crystals hosted in amphibole cores from an amphibolite.





## Integrated petrological monitoring and eruptive parameters of volcanic products: high resolution analyses of the 11<sup>th</sup> May 2019 explosive events at Stromboli volcano (Italy)

Pontesilli A., Del Bello E., Scarlato P., Mollo S., Ellis B., Andronico D., Taddeucci J.

Typically, petrological monitoring studies focus on comparing eruptive phenomena with textural and compositional features of eruptive products recovered over long term (days to years) sampling campaigns aiming at identifying major changes in the magmatic plumbing system and eruptive dynamics. However, as far as we are aware, there have been few attempts to combine whole rock, microchemical, and microtextural data with ground-based imaging of volcanic eruptions at high spatial (individual eruptive centers) and high temporal (minutes to hours) resolutions. Here, we present a high-resolution petrological investigation using as test site Stromboli volcano, one of the most active and intensely monitored open-conduit volcanoes in the world and an important benchmark in understanding the physico-chemical processes related to magma and conduit dynamics. Normal eruptive activity is dominated by frequent and intermittent low-energy explosions (6 events/hour on average), throwing jets of crystal-rich basaltic scoriae, gas and ash to heights <150 m above the summit vents. On May 11<sup>th</sup> 2019, we recorded 5 hours of explosive activity and sampled individual fresh fallout ash products from eighteen explosions. Six products were erupted from the N1 vent, whereas twelve products were erupted from the S2 vent. Analysis of high speed (50 Hz) infrared videos

revealed that explosive activity was more frequent at the S2 vent (8-10 events/hour) than at the N1 vent (3-5 events/hour). The explosion types were differently distributed at the two areas, with prevalent ejection of coarser material at the N1 vent and ash-dominated explosions being more frequent at the S2 vent. Thermometric and hygrometric calculations based on clinopyroxene-plagioclase-melt equilibria comparatively highlight that N1 eruptions were fed by a colder, more degassed, and differentiated magma relative to that feeding S2 eruptions. Diffusion modeling of Li concentration profiles in plagioclase also indicate longer timescales of magma degassing and ascent for N1 eruptions, possibly due to enhanced groundmass crystallization at conduit walls. The final emerging picture is that concurrent normal eruptions from distinct vent areas at Stromboli are heralds of distinct magma differentiation conditions within the uppermost part of the magma storage region, in close agreement with observed eruptive phenomena. This high-resolution approach has the potential to unequivocally constrain the processes driving transient, rapid, explosive eruptions in active volcanoes, thus offering new insights on the interplay between magma dynamics, ascent timescales, and eruptive behavior (Figure 1).

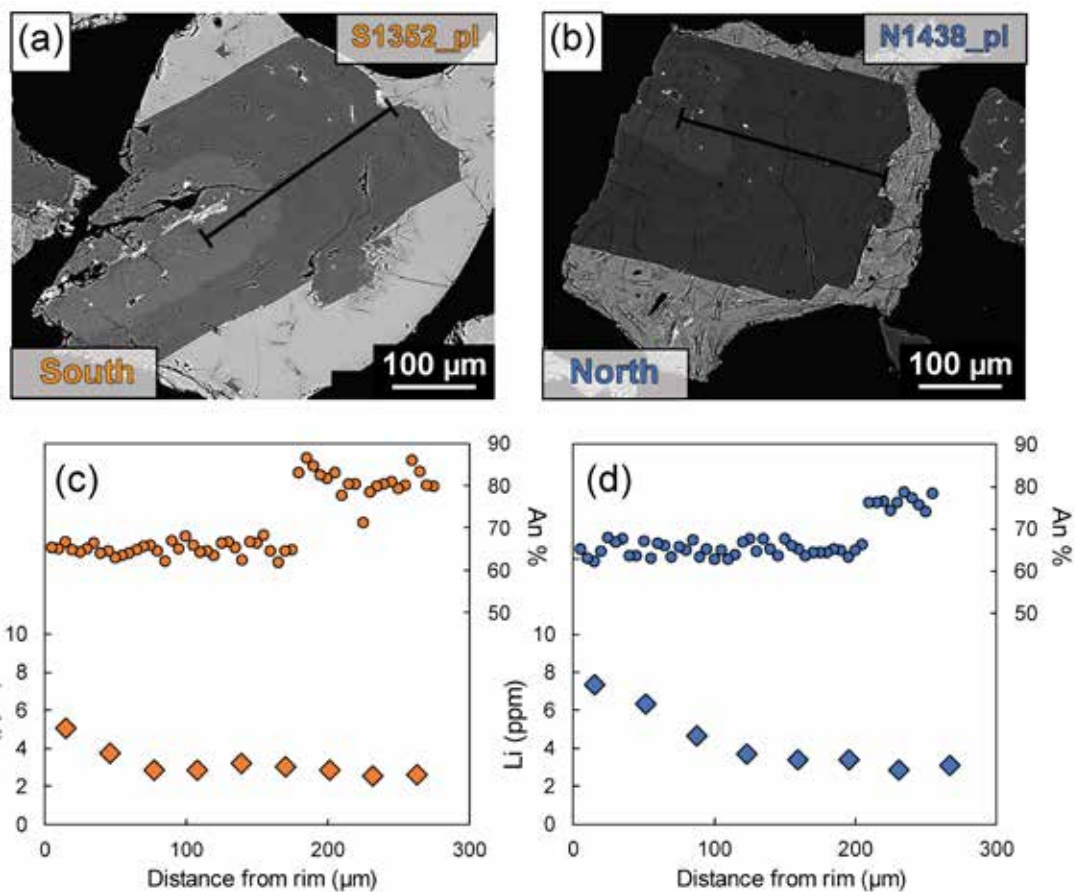


**Fig. 11** Compositional profiles of plagioclase crystals from 11th May 2019 eruptive products. Back Scattered Electron (BSE) images of representative plagioclase crystals from (a) South and (b) North craters. Plagioclase anorthite content and Lithium concentration profiles for the same crystals are represented for (c) South and (d) North craters.



## CHIMERA: Cryptotephra In Marine sEquences of the Ross Sea, Antarctica: implications and potential applications

Del Carlo P., Re G., Di Roberto A., Nazzari M.

Glaciomarine sediment sequences from the Southern Ocean surrounding the Antarctic continent contain tephra produced by explosive eruptions of Antarctic volcanoes. Tephra layers can be highly preserved in the marine environment which is often characterized by fairly continuous sedimentation and relatively small disturbance if compared to terrestrial records. Tephra have a significant potential as time-synchronous marker horizons crucial to establish independent correlations between different geological archives as marine, terrestrial, lacustrine and ice-core records providing an accuracy that is hardly achieved with other methods. Moreover, tephra layers may provide significant data for volcanological reconstructions, including intensity and magnitude of eruptions, age and recurrence, and eruptive dynamics. Tephra records can be significantly extended by examining succession for the presence of cryptotephra, e.g., non-visible tephra, identifiable by means of ad hoc measurements, in order to increase the number of eruptions recognizable of any magnitude and in distal occurrence.

This potential is especially effective in Antarctica where subaerial record of volcanism is often incomplete, because it is hidden by thick ice and snow accumulations or physically eroded by ice. In addition, some of the volcanic complex of Antarctica are extremely difficult to be studied due to the extreme climatic

conditions and distance of outcrops from Antarctic bases.

It is known that the glaciomarine sedimentary sequences of the Ross Sea contain abundant primary and volcaniclastic deposits. Despite this, only few projects were designed for tephrochronology and volcanology studies and marine sediments have not been exploited yet, except in a few cases.

This finding has widened the research possibilities of distal tephrochronology with implications for volcanological, paleoclimatic and paleoenvironmental investigations.

For these reasons, several sediment cores sampled during previous PNRA expeditions within sedimentary basin on the continental shelf along the northern Victoria Land, will be readdressed; these cores have not been studied in detail for tephrochronological purposes, and they would reasonably contain cryptotephra (Figure 1) erupted from the Victoria Land volcanoes or possibly from even more distal volcanic sources. In particular, litho-sedimentological characteristics of the deposits (e.g., grain size, concentration, clast shape, etc.), geochemical compositions on glass matrix (major and trace elements), and geochronological ages will be addressed to fingerprint a tephra deposit in order to gain stratigraphic markers for independent correlations between geological archives (e.g., marine, continental and ice -cores).



The results will be used to widen the knowledge on the volcanic history of the North Victoria Land, where at least five mid to high intensity (Plinian to Subplinian)

explosive eruptions occurred during the Late Pleistocene-Holocene period from Mt. Melbourne and Rittmann.

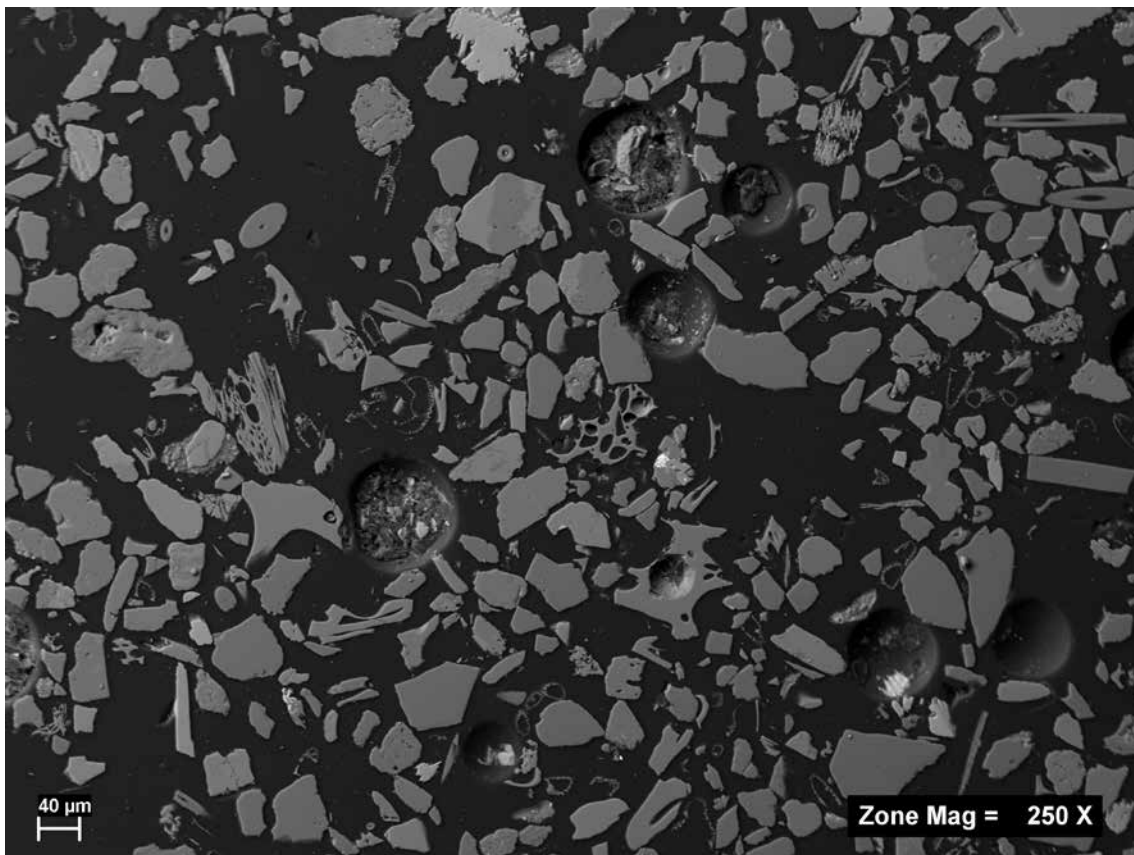


**Fig. 11** Backscattered electron (BSE) image of a cryptotephra. Small pumices and glass shards, enclosed within the marine sediment, display consistent textural features and homogeneous chemical composition, identifying an eruptive event occurred during the continuous hemipelagic deposition. Correlations with the volcanic sources will be done on the basis of geochemical fingerprinting and age constraints.



## Unravelling the early crystallization conditions of the Jersey minette lamprophyre (Channel Islands, UK): insights from Ti-zoning in phlogopite

Lucci F., Boukili B., El Moutaouakkil N., Holtz F., Nazzari M., Della Ventura G.

Dark mica is ubiquitous in a wide variety of geological environment having a chemistry covering a broad range of solid solutions. Moreover, dark micas are well known to record the pressure and temperature conditions of crystallization, thus representing a valuable tool for disentangling the genesis of the parent magma. In this work we focus on the most famous Fort Regent lamprophyre minette (Jersey Island, Channel Islands, UK) intruding the Cambrian granophyre basement and characterized by a mineral assemblage made up of phlogopite-clinopyroxene-feldspar with minor apatite and amphibole. In particular, phlogopite shows extremely Ti-rich ( $\text{TiO}_2 > 9.0 \text{ wt\%}$ ) rounded cores enveloped by high-amplitude oscillatory Ti-Mg-Ba-F-zoning patterns.

The aim of this project is to unravel the pressure-temperature genetic conditions of the Jersey minette by integrating classic mineral-melt thermobarometry modelling to the Ti-rich phlogopite and associated rock-

forming minerals. Complementary to the chemical (EMPA) work, FTIR spectroscopy is applied to address the Ti-solubility mechanism in phlogopite. The final goal of this project will be at developing a conceptual model for genesis of Ti-rich phlogopite-bearing minette lamprophyres (Figure 1).



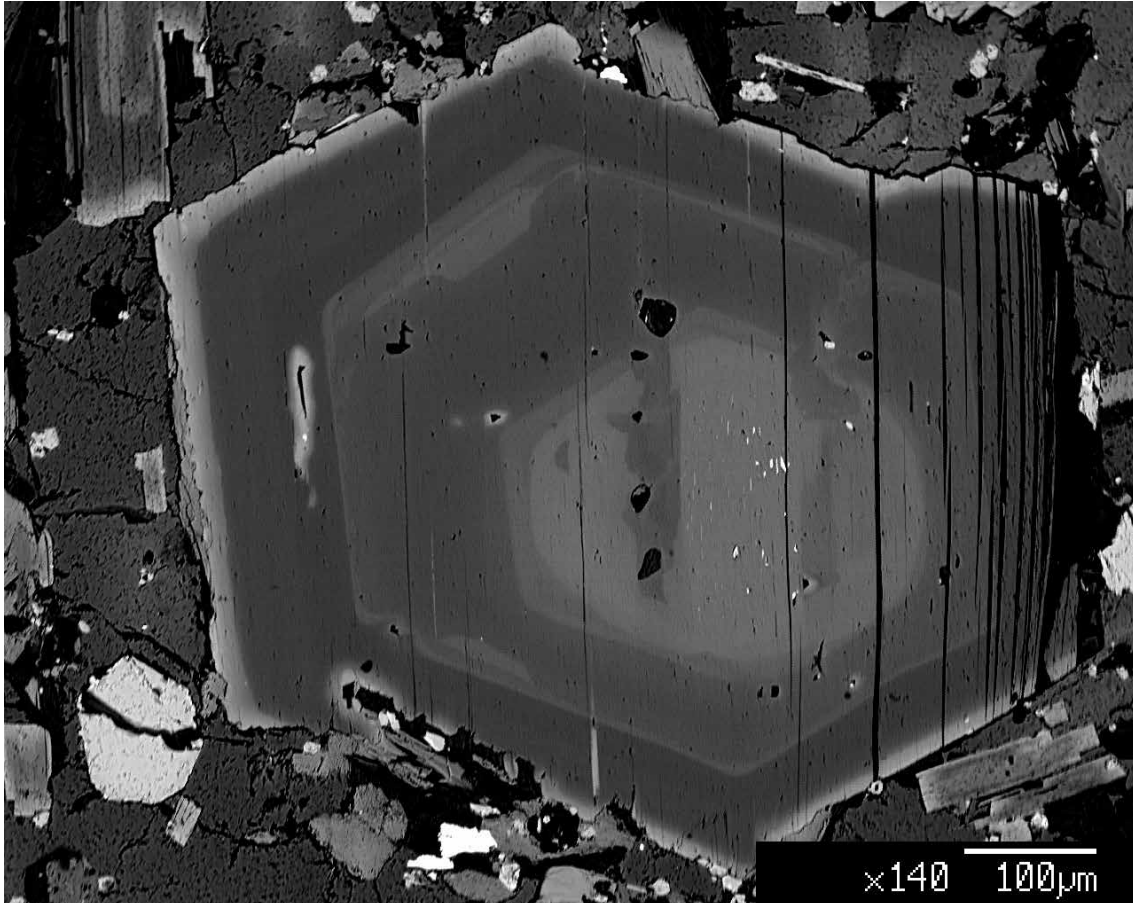


**Fig. 11** SEM-BSE image showing the typical oscillatory concentric zoning texture observed in the phlogopite from Jersey minette lamprophyre. In particular it is possible to observe the rounded Ti-rich core enveloped by a euhedral oscillatory zoning texture.



## Titanite from metacarbonate: a powerful petrological and geochronological tool, an example from Valle Strona di Omegna; Ivrea-Verbano Zone, Italy

**Bonazzi M., Langone A., Nazzari M.**

Titanite ( $\text{CaTiSiO}_5$ ) is an abundant common accessory mineral in metacarbonates. It contains several important geochemical elements, such as REE, Pb, U, Zr resulting in a useful petrological and geochronological tool. We performed a geochemical and petrological characterization of titanite from metacarbonate rocks occurring at the different levels of the Variscan continental crust exposed along the Valle Strona di Omegna, Ivrea-Verbano Zone (IVZ).

The crustal section consists mainly of middle-high grade metapelites and metabasites, with numerous lenses of metacarbonate rocks. The crustal section is characterised by a progressive increase of P-T conditions, from amphibolite to granulite facies, with increasing crustal depth (Figure 1). Metacarbonates appear as layers and lenses of variable thicknesses, from a few centimetres to several tens of metres. These lithologies range in composition from impure marble to calc-silicates and contain mostly calcite, with local occurrence of dolomite (Figure 1).

The chemical data of major mineral phases were collected at the HP-HT Laboratory of Experimental Volcanology and Geophysics of INGV in Rome (Italy), using a Jeol-JXA8200 electron microprobe. These analyses were also preliminary for trace elements characterization. Combining chemical data of major and trace elements allows

us to investigate the evolution of mineral assemblage along the Valle Strona di Omegna. The mineral assemblages are related to metamorphic grade: clinopyroxene, feldspar, amphibole and epidote are common in amphibolite facies rocks whereas scapolite, garnet and olivine appear in granulitic samples. Major and trace elements were determined for major mineral phases (calcite, clinopyroxene, scapolite) and titanite.

Generally, titanite is homogeneous among samples consisting of  $\text{SiO}_2$  (30.42-31.84 wt. %),  $\text{TiO}_2$  (36.31-34.12 wt. %),  $\text{CaO}$  (28.10-29.18 wt.%) and  $\text{Al}_2\text{O}_3$  (3.42-4.42 wt. %).

Interestingly, we noted that for a mylonitic sample (VSD012) the titanite chemistry is slightly different being characterized by lower  $\text{Al}_2\text{O}_3$  contents ( $<3$  wt. %; Figure 1).

Trace elements concentration of major mineral phases show a relation between concentration of trace elements and silicate modal abundances. In addition, the thinnest layer of metacarbonate (VSD015) embedded within metapelites is characterized by the highest concentration of REE. On the contrary, the mylonitic sample shows the lowest REE concentrations.

Titanite trace element composition is also related to different mineral assemblages along the crustal profile. The chemistry of titanite shows interesting correlations with lithologies, mineral assemblages and titanite modal





abundance. In order to constrain temperature, we adopted the Zr-in titanite thermometer by considering Pressure estimates from adjacent coexisting metapelitic and metabasic rocks. The obtained temperatures are in the range of 700-900 °C and are coherent with the high temperature conditions recorded by surrounding metapelites/metabasites at Carboniferous-Permian interval.

The titanite U concentration ranges from about 20 to 300 ppm without apparent correlation with metamorphic grade and/or mineral assemblages. U-Pb dating was only performed for titanite grains containing more than 100 ppm of U and preliminary U-Pb dates range from Middle Triassic to Lower Jurassic.

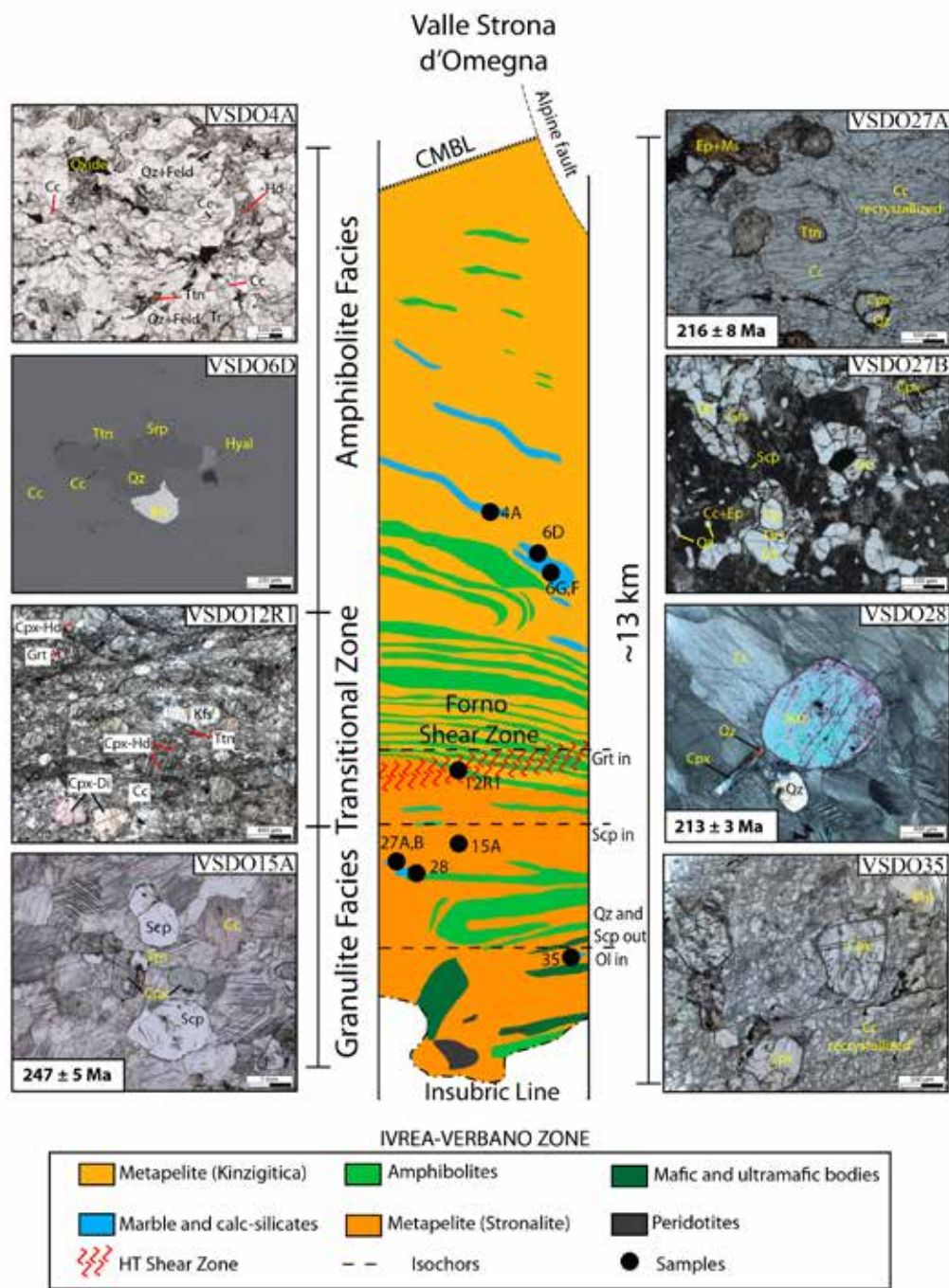


**Fig. 11** Schematic profile of the lower crustal section in the Val Strona di Omegna, with metamorphic facies and mineral isograds (dotted black lines), the metamorphic field gradients are from Redler et al. 2012. The black circles define the localities of metacarbonate samples and photographs show the mineral assemblages of samples. Mineral isograds are based on metacarbonate samples of this work.



## Cicirara lava flows from Mt. Etna

Casarin A., Nazzari M., Lanzafame G., Scarlato P., Ferlito C., Iezzi G.

The morphology of lava flows crust provides hints on their bulk composition, strain rate and rheologic behavior. Commonly, pahoehoe lavas are  $\text{SiO}_2$ -poor, erupted with a low crystal content and emplaced at moderate strain rates, whereas aa are favored by the opposite situations. At Mt. Etna, ciciraras are characterized by an apparent paradox: in fact, they display many and large plagioclase and clinopyroxene minerals (phenocryst), albeit their crusts are commonly pahoehoe. In this work we investigated different Etnean cicirara lavas, one emitted in a prehistoric event, three emplaced during the 17<sup>th</sup> century and one from the 1985 eruption, with the aim to reconstruct their solidification path(s).

Bulk chemical compositions were investigated by XRF, the textural characteristics and the quantification of both tiny and large crystals were accurately analyzed by a combination of facilities and methods, such as high-resolution scanner (HRS), transmission optical microscopy (TOM) and scanning electron microscopy in back-scattered mode (BS-SEM) at the HPHT lab (INGV-Rome), acquiring sequential microphotographs. Microchemical characterization by SEM-EDS completed the determinations of glassy and crystalline phases. The textures of these five lavas were imaged at different magnification to fully constrain their features. The abundance, size dimensions and shapes, size frequencies, numbers of crystals per surface and

orientations were measured by 2D image analysis (Figures 1a, 1b).

The quantitative textural attributes of large crystals, i.e.  $> 0,5$  mm, unveil that the 5 ciciraras are similar, with a high content of mm-sized plagioclases and clinopyroxenes both with a prismatic shape (aspect ratio 1:2/4) and a frequent development of a fabric and a limited amount of bubbles (Figures 1a, 1b). These similarities were also shown by the calculated CSD (crystal size distribution) curves for plagioclases and clinopyroxenes for each sample (Figure 1c). Large crystals  $> 1/2$  mm have a low slope, whereas relative tiny crystals ( $< 1/2$  mm) have a relatively high one (Figures 1a, 1b). The first sub-group of sizes in the CSD records low undercooling degree ( $\Delta T$ ) and kinetics conditions, the second sub-group mirrors an inverse situation of solidification (Figures 1a, 1b). The accurate textural features were used to construct hypothetical viscosity curves accounting for chemical composition (anhydrous and hydrated) of the bulk system, temperature, amount of crystals plus their shapes, as well as strain rates.

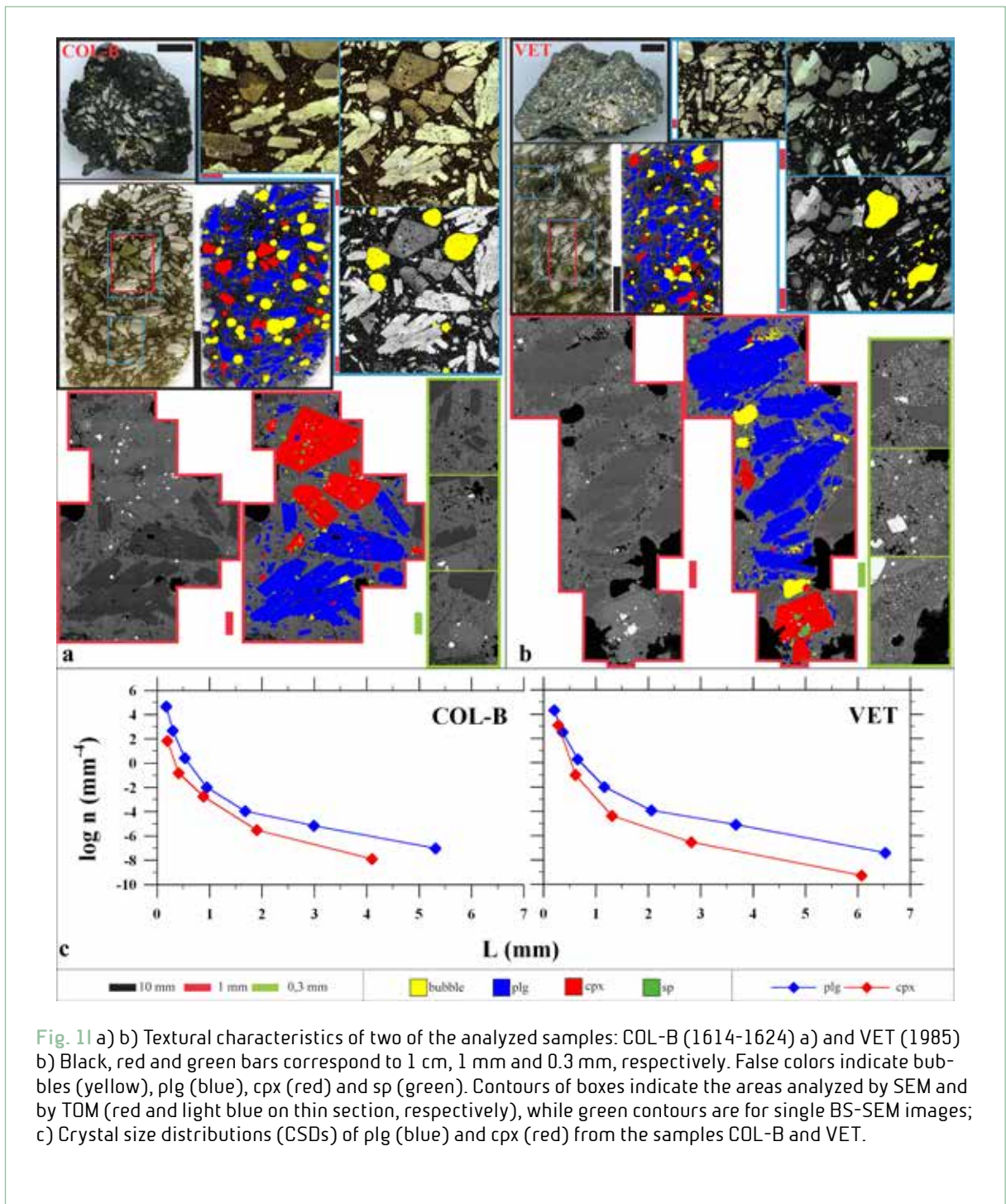
All these data and models point out that large cicirara plagioclase and clinopyroxene crystals nucleated during the residence of these magmas in reservoir(s) and ascent in conduit; however, their attained their large sizes during growing after eruption in the initial stage of flowing. Most intermediate and tiny crystals nucleated and grown after the release





of volatiles ( $H_2O$ ) and final cooling at syn- to post- eruptive conditions. Results of this work underline that the petrologic significance of large phenocrysts in volcanic rocks should be

reconsidered and caution must be given in attributing their size and shape to processes occurring exclusively at subvolcanic conditions.





## Prehistoric dyke from Mt. Somma

Scaglioso M., Piochi M., Nazzari M., Iezzi G.

The study of dykes is fundamental for understanding the solidification path and rheological behavior of magmas ascending up from magmatic reservoirs. The chemical and textural attributes and variations of phases (minerals, glasses and gases) recorded along the thickness of dykes are of paramount importance to reconstruct such dynamics of magmas at the time of emplacement. The aim of the work here summarized was to identify the chemical, mineralogical and textural variations along the thickness of a prehistoric dike of the Monte Somma-Vesuvius volcano (Southern Italy), such to reconstruct its solidification behavior. This SPA dyke is exposed along the Mt. Somma caldera wall; its thickness is of about 3 m. Five coaxial samples to the dike exposure were collected at a distances of 0 (SPA0), 20 (SPA20), 50 (SPA50), 150 (SPA150) and 200 (SPA200) cm from the host wall-rock. Textural features were observed first by i) scanning (HRS) of thin sections at 1 X, ii) optical microscopy (TOM) at 25 and 100 X, at the Chieti University, and then investigated by iii) back-scattered scanning electron microscopy (BS-SEM) at 100, 250, 500 and 1000 X at the HPHT Lab of Istituto Nazionale di Geofisica e Vulcanologia (INGV). Crystal-chemical attributes of phases were determined and quantified at the INGV by: i) X-Ray Powder Diffraction (XRPD) at the OV (Osservatorio Vesuviano) Lab and ii) Electron MicroProbe Analysis (EPMA) at the HPHT Lab.

The bulk chemical composition of major, minor and trace elements was also quantified at the Northwest external service, evidencing that SPA20, SPA50, SPA150 and SPA200 are shoshonitic, while SPA0 is phonotephritic. The XRPD outcomes straightforward evidence that the SPA dyke is made of spinel (sp), clinopyroxene (cpx), olivine (ol), leucite (lc), plagioclase (plg), alkali-feldspar (afd) and mica (mi). The abundance of phases is not constant moving from the outer margin to the inner portion of the SPA dyke. However, the micro-chemical composition of phenocrysts (ph crystals > 1000  $\mu\text{m}$ ), micro-phenocrysts (mph crystals < 1000 and > 100  $\mu\text{m}$ ) and microlites (mic crystals < 100  $\mu\text{m}$ ) of lc, plg, cpx and ol is on the whole almost constant moving from SPA0 to SPA200, especially the crystal-chemistry of their ph cores (Figure 1a). The image analysis allowed us to quantify textural attributes, i.e., the modal abundances (area%) of the lc + plg + afd, ol + cpx and sp. The tectosilicates slightly decrease between SPA0 and SPA20, increase in SPA 50 and 150 and decrease in SPA200. This trend is reversed for the cpx + ol. The amount of sp is instead constant but invariably close to few area% along the SPA thickness (Figure 1b). The sizes of the largest cpx + ol and sp linearly increase from dyke margin to its center (Figure 1c). It is accompanied by an increasing number of cpx + ol crystals per unit area ( $\#/ \text{mm}^2$ ) (Figure 1d).



All the collected results highlight that the outer margin of dyke has different bulk chemical and mineralogical compositions with textural features showing several quantitative

variations from its margin to the center; whereas, the crystal-chemical variations of lc, plg, cpx and ol are poorly variable moving along its thickness.



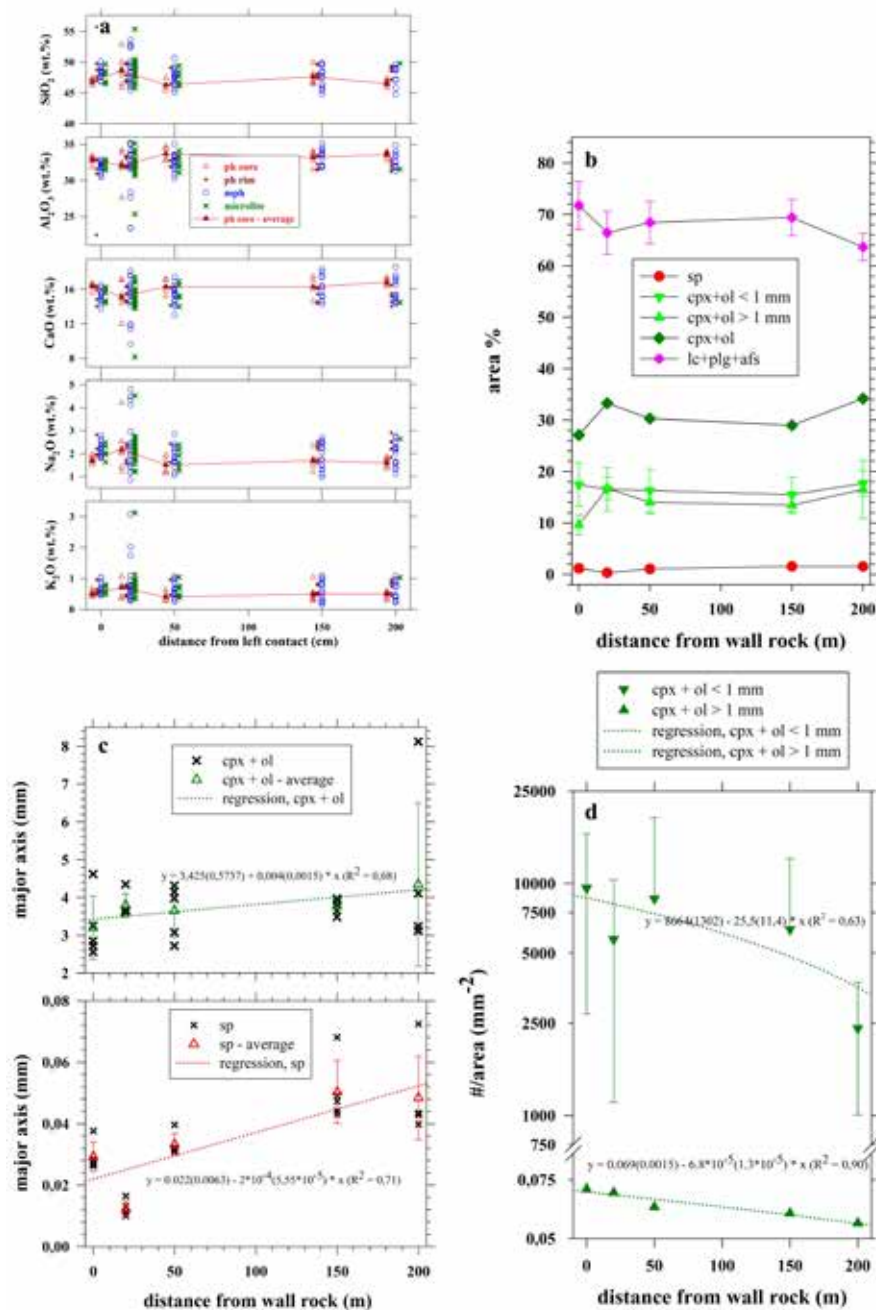


**Fig. 11** a) Major oxide composition of plagioclase phenocrysts (ph: 500-1000 $\mu$ m), microphenocrysts (100-500  $\mu$ m) and microlites (<100  $\mu$ m); b) Area % of mineralogical phases along the SPA dyke; c) Variation of the five longest equal-area ellipse axes and related average sizes as function of distance from the contact between dyke and wall-rock for cpx (top) and sp (bottom); d) Number of crystal per unit area of clinopyroxene + olivine greater than 1 mm and less of 1 mm.



## Viscosity and mobility of Ti-rich volatile-bearing melts representative of metasomatic fluids in the Earth's upper mantle

Matteoli A., Stoppioni V., Hrubciak R., Yu T., Wang Y., Pontesilli A., Stagno V.

There is evidence in nature of chemical reactions occurring between minerals both from peridotite and eclogites rocks with pervasive volatile-bearing fluids the chemical composition of which has been often referred to carbonatitic and carbonate-silicate melts generated in the Earth's upper mantle by low degrees of partial melting of carbonated mantle peridotites and representing the natural carriers of C up to shallow depths. These melts are characterized by a chemical composition which is transitional between carbonatitic and basaltic melts, having  $\text{SiO}_2$  and  $\text{CO}_2$  content of 10-35 wt% and 40-10 wt%, respectively. However, the analyses of metasomatized mantle rocks highlights an enrichment in titanium along with  $\text{CO}_2$  and  $\text{H}_2\text{O}$ . This is the case of metasomatized spinel-peridotites from Calatrava (Spain), xenoliths from Queensland, from Bultfontein Mine in South Africa, as well as the melt inclusions in preserved olivines from Mt. Erebus volcanic products in Antarctica ( $\text{TiO}_2$  up to 4 wt%). The Ti-enrichment of mantle-derived metasomatic melts is also well-supported by experimental studies on melting of carbonated eclogites at depths of about 300 km in the upper mantle producing melts with  $\text{TiO}_2$  up to 20 wt%. The aim of this project is to determine the viscosity and melt structure of a synthetic Ti-rich,  $\text{CO}_2$ - $\text{H}_2\text{O}$ -bearing liquid representative of metasomatic melts by in situ synchrotron X-ray

radiography and multi-angle energy dispersive X-ray diffraction at using the Paris-Edinburgh press at Argonne National Lab (US).

Preliminary experiments were performed using a synthetic silicate glass prepared by mixing oxides and carbonates as  $\text{SiO}_2$ ,  $\text{MgO}$ ,  $\text{Fe}_2\text{O}_3$ ,  $\text{CaCO}_3$ ,  $\text{TiO}_2$ ,  $\text{Na}_2\text{CO}_3$ ,  $\text{Al}_2\text{O}_3$  plus 4% of  $\text{CO}_2$  (added as  $\text{Ag}_2\text{C}_2\text{O}_4$ ) and 6%wt of  $\text{H}_2\text{O}$ . The glass was quenched at about 1400-1450°C and 500 MPa using the Quick Press piston cylinder installed at the HPHT laboratory of the Istituto Nazionale di Geofisica e Vulcanologia (Rome, Italy). The quenched products were analyzed using the JEOL JXA-8200 Superprobe. These glasses were, then, grinded and stored in a desiccator.

Viscosity measurements were performed with the falling sphere technique assisted by in situ X-ray radiography. Figure 1 shows the descent of the Re probing sphere through the molten Ti-rich liquid at HP-T as a function of time recorded in real time through in situ X-ray imaging in combination with the use of an ultrafast camera (250 fps). In-situ X-ray diffraction measurements were performed both by multi-angle energy dispersive X-ray diffraction (MA-EDXD) at HPCAT beamline and angle dispersive X-ray diffraction (ADX) at GSECARS beamline. In this case, monochromatic X-rays are produced with a double crystal silicon monochromator set with a maximum energy of 42 keV and 60 keV,



respectively. Figure 2 shows X-ray scattering data collected for the Ti-rich volatile-bearing melt representative of a metasomatic fluid at 1.2 GPa/1375 °C, which testify the amorphous state of the investigated sample and allow the determination of both the intermediate-range and local structure.

A total of 12 measurements were performed in a P range of 1.2 – 4.4 GPa and T of 1375-1990 °C in the case of melt structure measurements,

and P range of 1.7-3.7 GPa and T of 980 - 1460°C for viscosity measurements. Our preliminary results show low viscosities ( $10^{-1}$  Pa·s) of the corresponding magmas that is an order of magnitude higher than carbonate-silicate melts, on the basis of which metasomatic fluids are expected to slowly move by porous flow in the upper mantle experiencing, therefore, chemical interaction with the surrounding crystalline matrix.

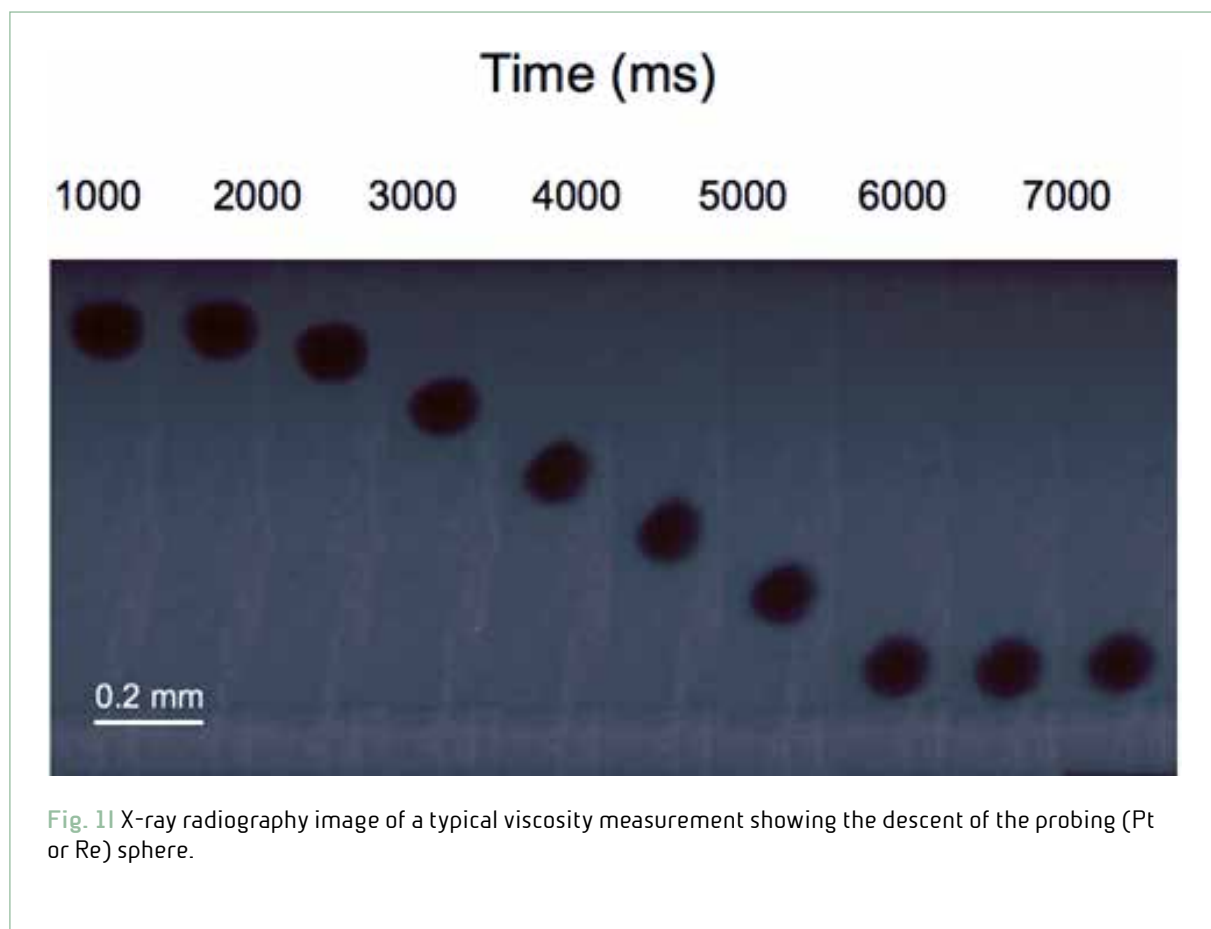


**Fig. 11** X-ray radiography image of a typical viscosity measurement showing the descent of the probing (Pt or Re) sphere.

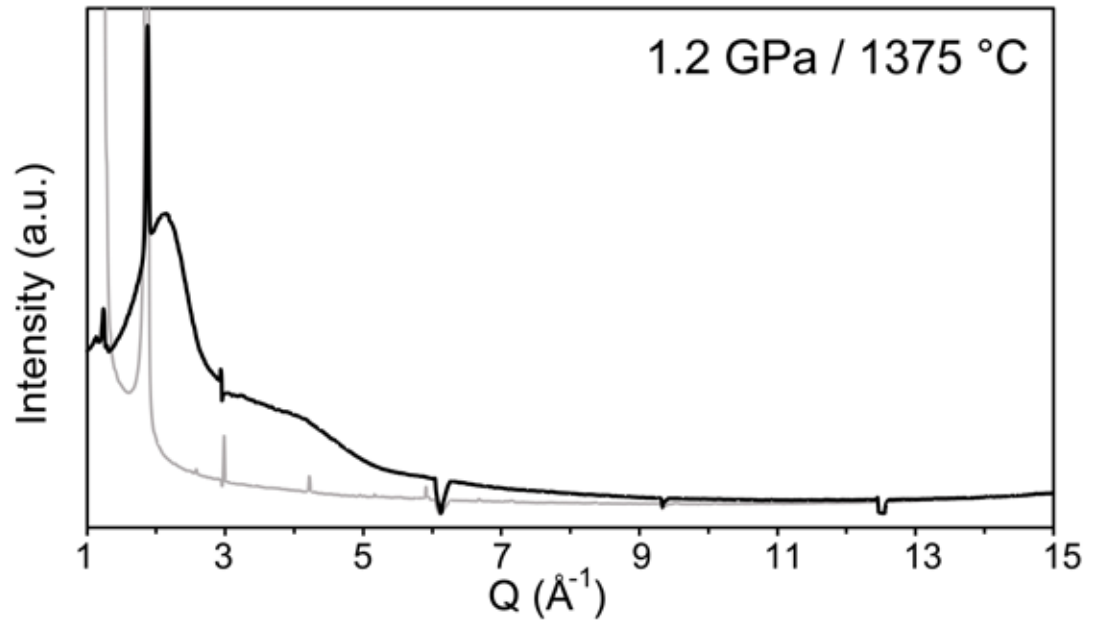


**Fig. 21** X-ray scattering data collected for the Ti-rich volatile-bearing melt (black line) representative of a metasomatic fluid at 1.2 GPa/1375 °C. The grey line is the typical pattern collected from the graphite capsule.



## Tephrochronological study of the lacustrine succession of the Castiglione maar (Central Italy) and evaluation of the possible impact on the climate of the explosive eruptions of the perithyrrenic volcanoes

Di Roberto A., Scateni B., Re G.

The research activity is part of the multidisciplinary project AMUSED: A MULTidisciplinary Study of past global climate changes from continental and marine archives in the Mediterranean region (Environment Department Project-INGV). The project has as its ultimate goal to reconstruct climate variability in the central Mediterranean region during the middle-late Quaternary, with a special focus on the Holocene.

The activity carried out concerns the tephrochronological study of a continental sediments succession sampled in the Castiglione maar (Central Italy), located 20 km east of Rome along the ancient Via Prenestina where two parallel 120 m-long cores, one 15-m long core were drilled, spanning last ~280 kyr and ~12 kyr respectively and two 12 m-long and 3 m-long cores at the edge of the basin were performed. Furthermore, the tephrochronological study of two marine cores, the 5.7 m-long NDT09 and the 3.8 m-long NDT12, spanning the last ~50 kyr and ~5 kyr respectively, recovered in the Tyrrhenian Sea during the NextData 2016 cruise.

In the last 20 years, "tephrochronology", ie the use of volcanic ash (tephra) as an isochronous (ie as a time marker), has been shown to provide high temporal and stratigraphic resolution information crucial for

the dating, correlation and synchronization of archaeological, geological, paleoecological and paleoclimatic records. In fact, the main feature of tephra is to deposit almost synchronously over large areas, forming a level that has an almost identical geological age in all the sites where it is identified (isochronous). The age of the eruption that produced the tephra can be determined in various ways, the most common of which include the dating of some minerals contained in the tephra (e.g. potassium feldspar) with methods such as  $^{40}\text{Ar} / ^{39}\text{Ar}$  and  $\text{K}/\text{Ar}$ . The age obtained is then transferred to the succession in which the tephra are interspersed. Tephrochronology, therefore, can implement or sometimes replace the classic dating methods that have time limitations (for example the  $^{14}\text{C}$  method can be used for materials no older than ~ 50,000 years). The study of tephra provides very important information also from the volcanological point of view. By studying the physical characteristics of tephra (granulometry, texture, etc.), their mineralogy and in particular the chemical composition of the volcanic glass (major elements, trace elements and isotopes) it is possible to identify the volcanic source and the eruption that produced the tephra. Tephrochronological studies therefore allow for information on the eruptive





frequency of a given volcano, on the eruptive dynamics or on the geochemical evolution of the source.

Due to its geodynamic structure and the great abundance of active volcanoes, the Mediterranean area has always been considered an ideal area for the development

and application of tephrochronology. The intense explosive activity of the perithyrrenic volcanoes and the Hellenic arc produced a large number of tephra levels that are interspersed in the continental and marine sedimentary sequences (Figure 1).

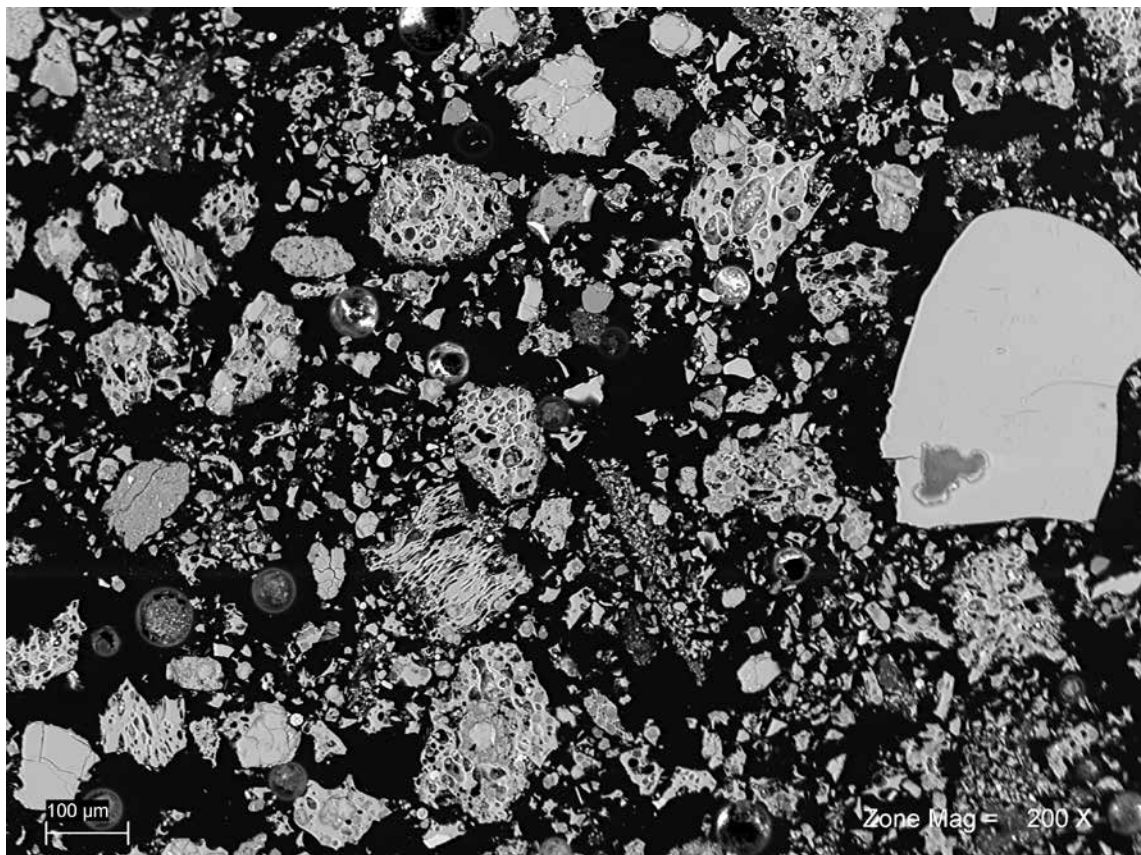


**Fig. 11** Image in back-scattered electrons (BSE) mode of tephra layer collected with a scanning electron microscope (SEM) Zeiss EVO MA at the INGV of Pisa.





## Introduction to Fractal Buster: an experimental apparatus to uncover seismo-acoustic response and jet dynamics in complex conduit geometries

Spina L., Taddeucci J., Morgavi D., Perugini D., Scarlato P.

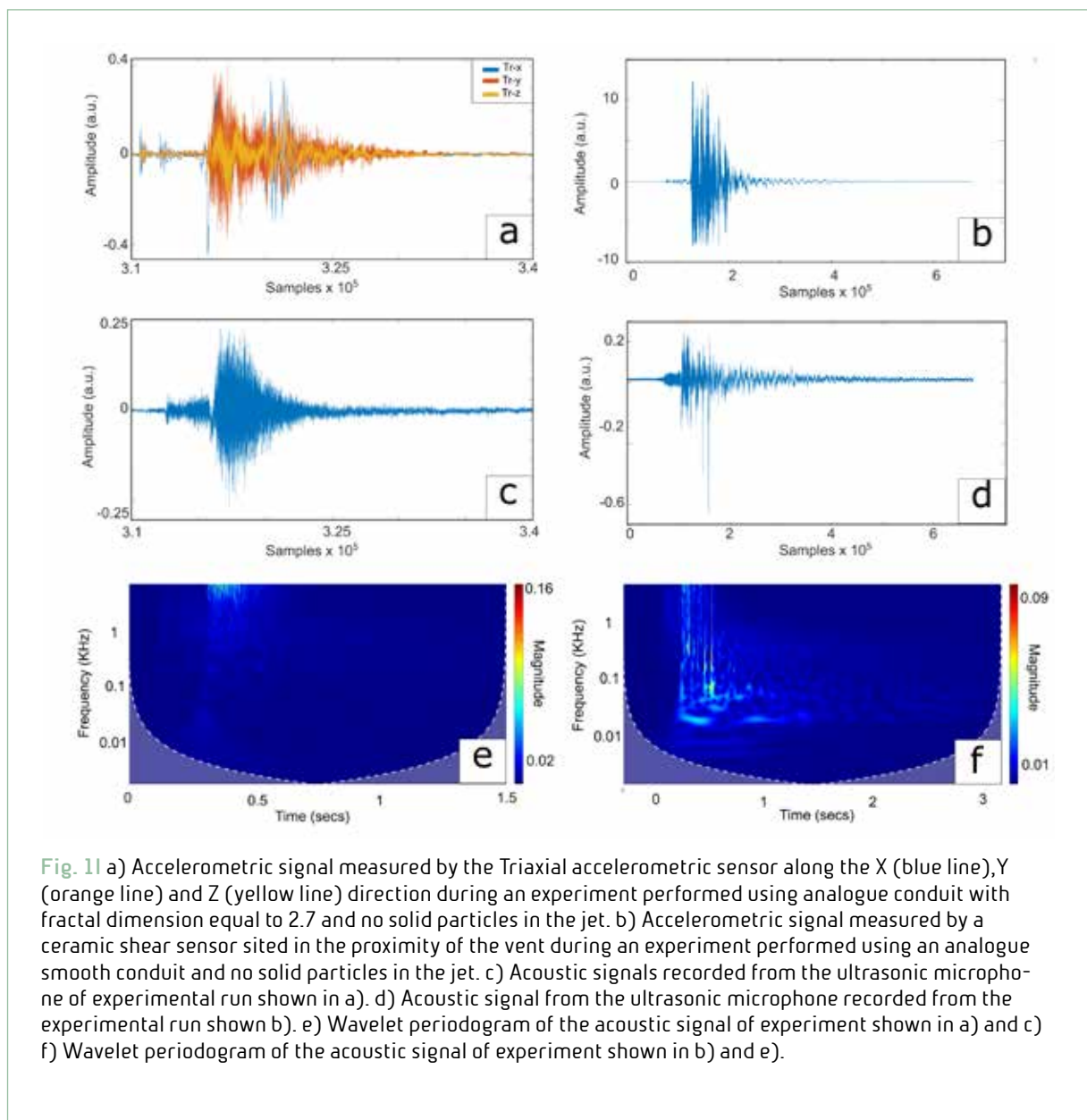
The interaction of magmas with the volcanic edifice within the plumbing system is a fundamental process that controls chemical evolution, rheology and eruptive styles of magmas. Overcoming limitations -deriving from the inaccessibility of volcanic conduit to direct observations and from the difference between the resolution offered by geophysical method and the much smaller spatial scale relevant for volcanological processes- requires indirect approaches. With the aim of addressing different aspects of the interaction between magmatic flow and conduit morphology, we developed an experimental setup, hereafter *Fractal Buster*, capable of generating scaled volcanic jet in a geometrically complex conduit and measuring the related seismic and acoustic radiation. The *Fractal Buster* is composed of three main components: i) the injection system; ii) the analogue conduit; iii) the array of sensors. The injection system is made up of an electro-valve linked to the manometer through a gas reservoir that supplies compressed air at controlled pressure in the range 1-8 bar. The controlled opening of the electro-valve allows for a sharp release of gas that interacts with the analogue conduit and reaches the exit vent. The experimental analogue conduit is realized either in Plexiglas or in epoxy with variable length and diameter. In the case of the epoxy conduit, several internal conduit geometries (i.e. various fractal dimensions of the internal surface) have

been implemented following Spina et al. (2019). Conduit interaction is monitored through a set of three high sensitivity ceramic shear ICP® accelerometers (10 mV/g; 2 to 7 kHz), and a Triaxial ICP® accelerometer (100 mV/g, 0.5 to 10k Hz). Accelerometric sensors are sited at fixed locations carved at different distances along the conduit wall. The radiation of acoustic signals in the atmosphere is monitored via an array of three microphones; two acoustic microphones with a freq. range of 20 kHz to 0.1 Hz and an ultrasonic microphone (freq. range 6.5 to 140 KHz). It is remarkable that such an acoustic array allows estimating the radiation pattern of different acoustic sources that is often difficult to discriminate during field activities (e.g. Jolly et al. 2017). A synchronized high-speed video-camera provides information on the flow dynamics at the exit vent. Preliminary observation has been performed to characterize the seismo-acoustic response and flow dynamics by changing gas pressure, particle content (with/without the addition of glass beads) and conduit roughness (i.e. smooth or rough conduit with fractal dimension of 2.7). Figure 1 shows an example of two different experimental conditions; panels on the left (Figures 1a, 1c, 1e) show results from an experiment performed with fractal conduit (fractal dimension of the internal surface equal to 2.7) and a pressure of 7.7 bar and without the addition of solid particles to the jet. The panels



on the right side of the picture (Figures 1b, 1d, 1f) depict an experimental run performed with smooth conduit, pressure of 7.7 bar and no solid particles in the jet. Both conduits have a length of 1 m and an internal diameter of 3 and 4 cm

for fractal and smooth conduit respectively. As clearly visible from Figure 1, different geometrical parameters of the analogue conduit strongly affect the spectral properties of the related elastic signal.





## 8.2 ROCK PHYSICS and EARTHQUAKES

### Determination of parameters characteristic of dynamic weakening mechanisms during seismic faulting in cohesive rocks

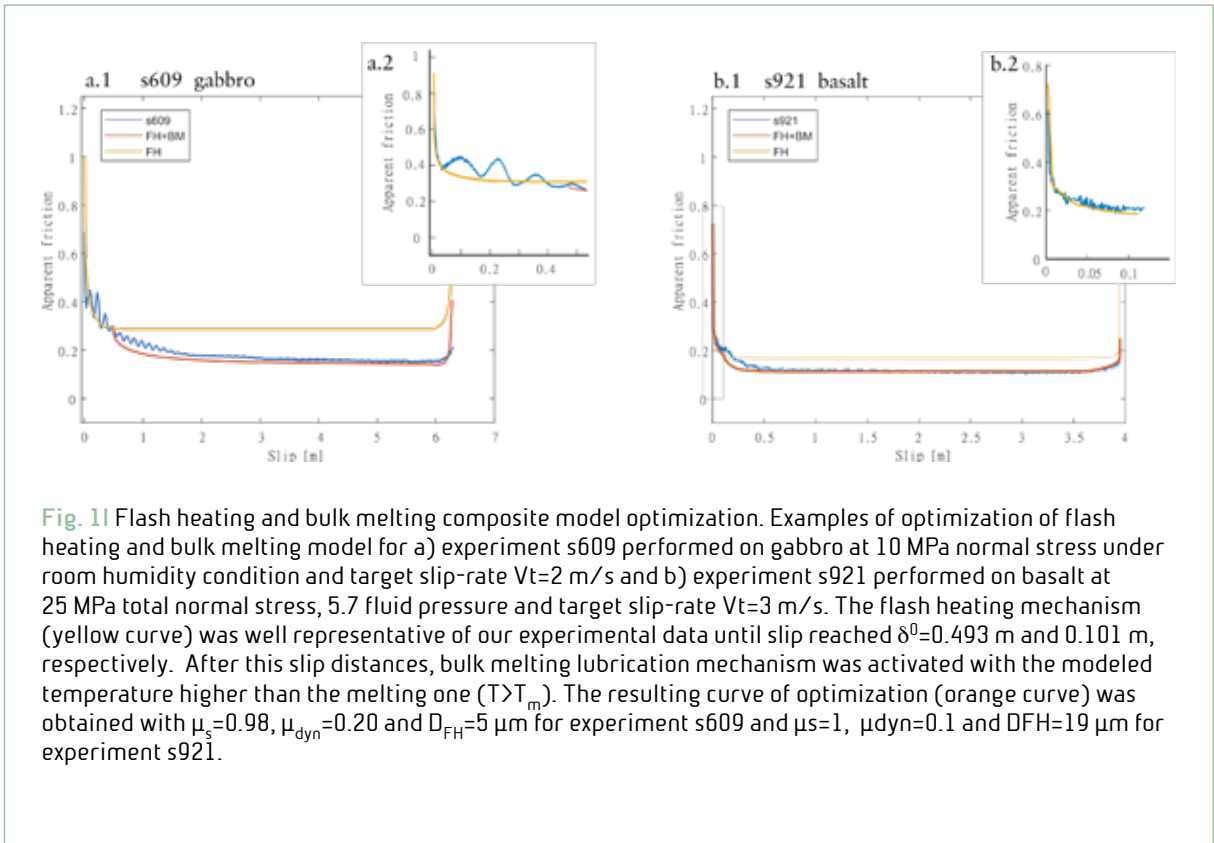
Cornelio C., Spagnuolo E., Nielsen S., Aretusini S., Passelègue F., Violay M., Cocco M., Di Toro G.

While sliding at seismic slip-rates of ca. 1 m/s, a natural fault undergoes an abrupt decrease of its stress called dynamic weakening. Asperity-scale ( $\ll$  mm) processes related to flash heating and weakening, meso-scale (mm-cm) processes involving shear across the bulk slip-zone, related to frictional melting or viscous flow of minerals, have been invoked to explain pronounced velocity-dependent weakening during seismic slip. Here we present a compilation of ca. 100 experiments performed with two rotary shear apparatuses. Cohesive rock cylinders of basalt, gabbro, granitoid rocks and calcite marble were sheared at various values of effective normal stress ( $s_n=5-40$  MPa), target slip-rate ( $V_t=0.1-6.5$  m/s) and fluid pressure (from room humidity condition RH (i.e.  $P_f=0$ ), to  $P_f=15$  MPa). We analyze the experimental results using models in which two weakening mechanisms are combined (flash heating and bulk melting, flash heating and dislocation/diffusion creep).

Moreover, we introduce a norm-based optimization routine which compares the measured shear stress during the experiments with the estimated shear stress from the models to optimize a set of model parameters. Lastly, we introduce the slip-switch distance parameter  $d_0$  defining the slip at which the

transition from asperity-scale to bulk slip-zone weakening mechanism occurs.

The decrease of  $d_0$  with fault normal stress indicates that during earthquakes, bulk mechanisms dominate over asperity scale weakening mechanisms with increasing crustal depths (Figure 1).





## Dynamic weakening in carbonate-built seismic faults: insights from laboratory experiments with fast and ultra-localized temperature measurements

Aretusini S., Nuñez Cascajero A., Cornelio C., Barrero Echevarria X., Spagnuolo E., Tapetado A., Vazquez C., Cocco M., Di Toro G.

During earthquakes, slip in faults is localized in a < 1 cm-thick Principal Slip Zone (PSZ). In the PSZ, frictional heating induces a temperature increase which activates processes and chemical reactions resulting in decrease of the fault strength (i.e., enhanced dynamic weakening). As fault strength decreases, frictional heating itself decreases in a negative feedback loop.

In the laboratory, temperature measurements in a PSZ are challenging, especially at the fast slip rates and large slip displacements typical of natural earthquakes. We recently measured the temperature evolution in the PSZ of experimental earthquakes at high acquisition rates (~ kHz) and spatial resolutions ( $\ll 1 \text{ mm}^2$ ). We used optical fibres, which convey IR radiation from the hot rubbing surfaces to a two color pyrometer, equipped with photodetectors which convert the radiation into electrical signals. The measured signals were calibrated into temperature (the calibration curves were obtained via independent experiments under controlled temperature) and then synchronized with the mechanical data measured in rotary shear experiments (e.g., slip rate, friction coefficient, shear stress). This allowed us to relate the dynamic fault strength to the temperature evolution and constrain the deformation processes and associated chemical reactions

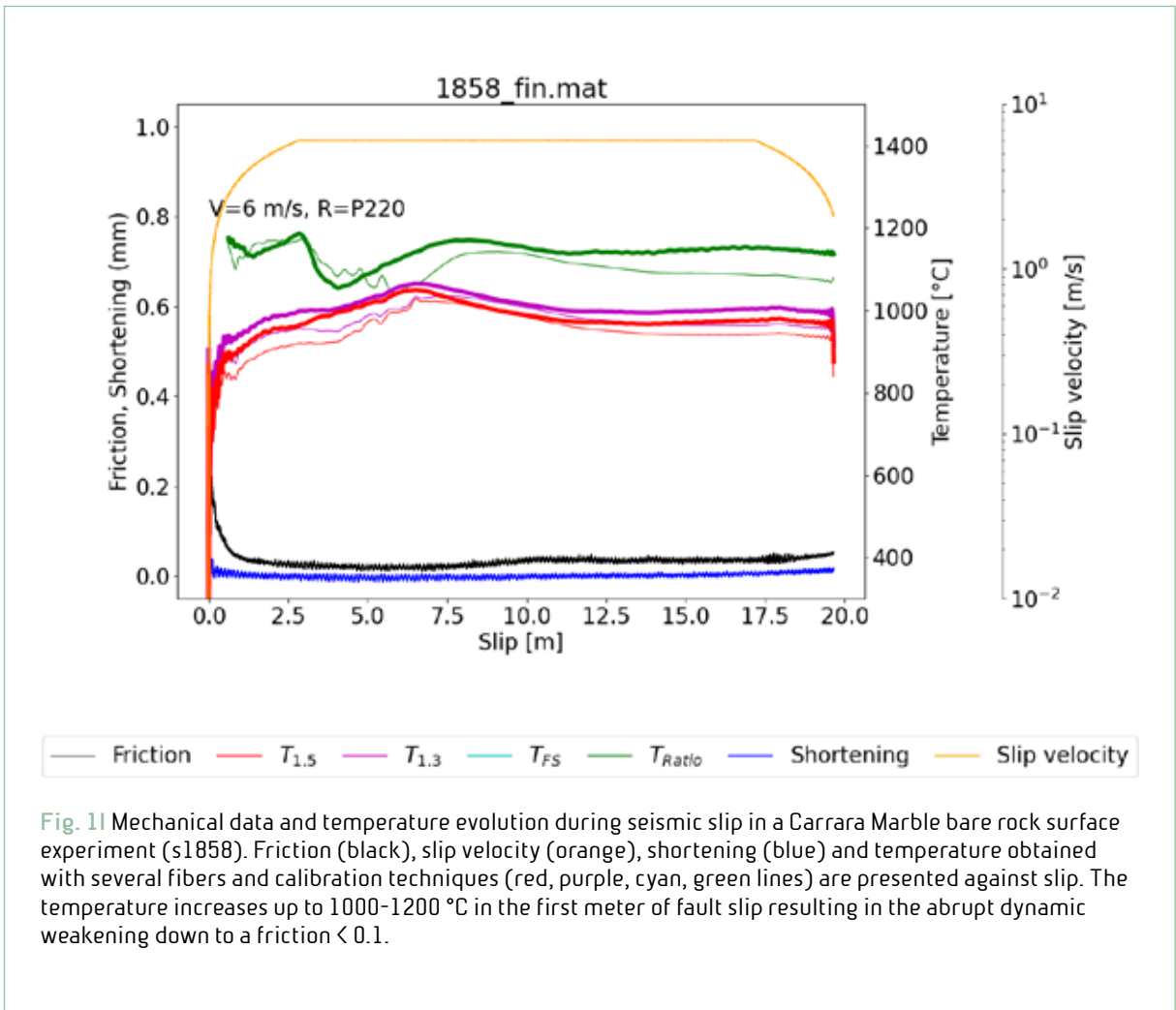
activated during seismic slip.

Here, we reproduce earthquake slip via rotary shear experiments performed on solid cylinders (= bare rock surfaces) and on gouge layers both made of 99.9% calcite using the Slow to HIgh Velocity Apparatus (SHIVA, HPHT laboratory, INGV). We applied an effective normal stress of 20 MPa. Bare rock surfaces are slid for 20 m with a trapezoidal velocity function with a target slip rate of 6 m/s. Instead, the gouge layers are sheared imposing a trapezoidal (1 m/s target slip rate for 1 m displacement) and Yoffe (3.5 m/s peak slip rate, and 1.5 m displacement) velocity function. The temperature was measured from within the PSZ. Temperature in some of the experiments increases up to 1000 °C after a few milliseconds from slip initiation. These measurements allow us to investigate the deformation mechanisms responsible for fault dynamic weakening over temporal (milliseconds) and spatial (contact areas  $\ll 1 \text{ mm}^2$ ) scales which are impossible to detect with traditional techniques (i.e., thermocouples or thermal cameras). Thanks to Finite Element numerical simulations, the in-situ temperature measurements allow us to quantify how much of the dissipated mechanical work in the PSZ is used as frictional heating (i.e., for the temperature increase), for wear processes



(e.g., to have grain comminution), and how much is actually absorbed by the energy sinks (e.g., by the endothermic decarbonation reaction, or by eventual phase changes) that would buffer the temperature increase. The generalization of our experimental data and observations, albeit being conscious

of the limitations introduced by the experiments themselves, may contribute in the future to improve the understanding on how the propagation stage of carbonate-hosted earthquakes, a main hazard in the Mediterranean and other areas worldwide (Figure 1).





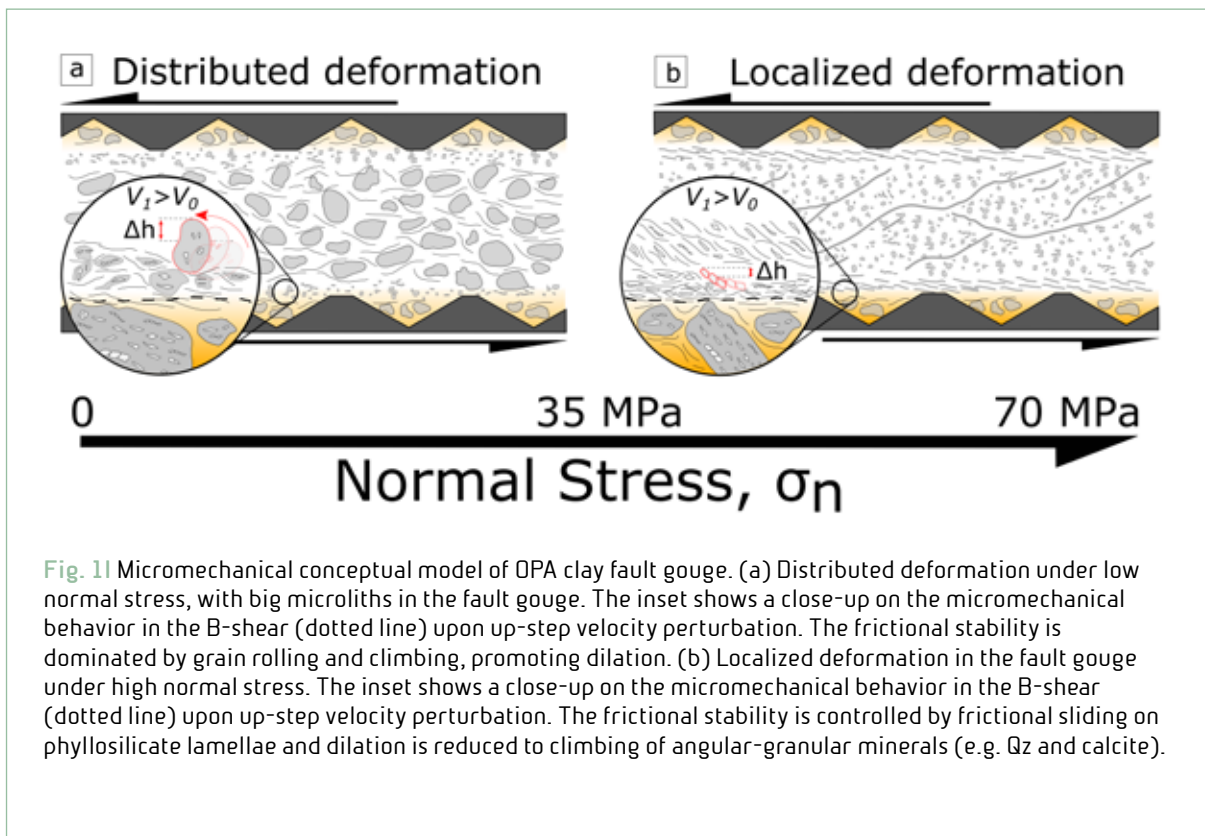


## Frictional properties of Opalinus Clay: Influence of humidity, normal stress and grain size on frictional stability

Bigaroni N., Scuderi M.M., Cappa F., Guglielmi Y., Nussbaum C., Aldega L., Pozzi G., Collettini C.

The Opalinus Clay (OPA) is an argillaceous formation that is being considered as potential host rock for repositories of radioactive waste in Switzerland. Therefore, it is of fundamental importance to study the frictional properties and frictional stability of the OPA. We designed our frictional experiments in order to characterize the effect exerted by humidity, grain size (GS) and normal stress ( $\sigma_n$ ) on frictional behavior of Opalinus clay. We explored a wide range of normal stresses, ranging from 5 to 70MPa performing velocity upsteps from 1 to 300  $\mu\text{m/s}$  and Slide-hold-slide from 1 to 3000s. Our experiments confirm that OPA clay is weak, with coefficient of friction at steady state of  $\sim 0.35$  and  $\sim 0.41$ , respectively for 100% humid and room humid experiments. The OPA clay is velocity strengthening over the entire range of  $\sigma_n$  tested. In particular we observe a direct relationship between frictional parameter a-b and slip velocity up to 35MPa where, from there on, a-b parameter seems velocity independent. We suggest that this phenomenon is caused by the progressive transition from brittle to semi-brittle behavior which reflects on the frictional stability of OPA clay. This hypothesis is supported by the microstructural data where the increase of  $\sigma_n$  promotes the transition from a distributed deformation to strain localization and GS reduction on anastomotic phyllosilicate network. The humidity does not change

deformation mechanisms, whereas decreases fault strength and increases fault stability. We hypothesize that this is a possible consequence of OPA clay swelling due to weakening of chemical bonds between phyllosilicate foliae. In the context of deep geological repositories, our results confirm that the most likely slip behavior for a fault gouge hosted in the Opalinus clay is a slow aseismic slip. However, even a small velocity perturbation can cause the fault gouge to dilate and subsequently increase in porosity, affecting the sealing capabilities of the geological barrier (Figure 1).





## Slip velocity and fault stability in serpentine-rich experimental faults

Pozzi G., Amodio A., Collettini C., Scuderi M.M., Tinti E., Tesei T., Aretusini S., Cocco M.

The rate and state framework is widely used to connect the concept of fault stability to the intrinsic frictional properties of fault rocks. Fundamental parameters are individuated in the  $a$ - $b$  parameter, the critical slip distance  $D_c$ , and the critical stiffness  $k_c$  derived by their combination. These parameters are known not to be constant even when the same fault material is used. These are in fact dependent on experimental conditions such as normal stress, temperature, and sliding velocity. Their influence is however not trivial and special interest is dedicated to the effect of sliding velocity on the rate and state parameters. No clear physical nor qualitative constraint has been proposed so far.

We explored this thematic by performing friction experiments on Elban serpentinite (composed mainly by lizardite and magnetite) powders, which show strong variation of frictional properties with sliding velocity. Serpentinite powders ( $< 125 \mu\text{m}$  grain size) were sheared at four different normal stresses (25, 50, 75 and 100 MPa) in the biaxial apparatus BRAVA. The experiments consist of an initial phase of sliding at  $10 \mu\text{m/s}$ , a slide-hold-slide test, and two series of velocity stepping (sliding velocity incremented discretely from 0.1 to  $300 \mu\text{m/s}$ ). The most interesting results appear at normal stresses from 50 to 100 MPa. The material shows friction of  $\sim 0.4$  with velocity weakening behaviour and low to negative frictional

healing. The negative  $a$ - $b$  parameter increases neatly with increasing sliding velocity while  $D_c$  slightly decreases (from 7 to  $2 \mu\text{m}$ ). At low velocities ( $< 3 \mu\text{m/s}$ ) sliding is unstable and the fault undergoes stick-slip behaviour. The slip velocity function evolves from asymmetric to symmetric towards the transition to stable sliding, which occurs at the higher sliding velocities (Figure 1a). This behaviour is explained by the increase of the critical stiffness, where  $K_c = (b-a)/D_c$ , with decreasing velocities and stick-slip instabilities arise when  $k_c$  becomes higher than the loading system stiffness. Back-scattered SEM images of the principal slip zones of recovered samples show a lizardite-rich foliated damage zone dispersed with rounded magnetite porphyroclasts (Figure 1b). From this microstructure we interpret the variation of frictional properties with the relative interaction of the strong and stiff magnetite grains, which, at low sliding velocities, interact creating force chains and promoting unstable slip. At higher velocities, dilation and separation of the strong porphyroclasts promote the activity of  $c$ -planes within the weaker phyllosilicates (lizardite) thus favouring stable slip.

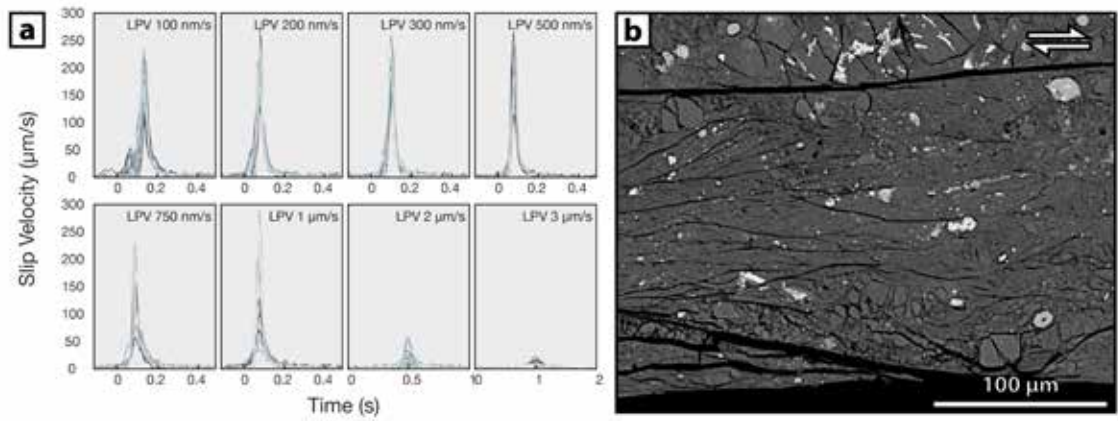


**Fig. 11** a) Slip velocity functions of stick slip events sampled at different sliding velocities. The experiment was performed at 75 MPa of normal stress. The slip velocity variation in time becomes more symmetric (gaussian) at higher sliding rates (loading point velocity, LPV) and peak velocities drop rapidly to values close to the LPV. Stable slip occurs at LPVs higher than 3  $\mu\text{m/s}$ . b) Close-up of the principal slip zone of the same experiment imaged with back-scattered electrons using a scanning electron microscope. Foliated lizardite (dark grey) hosts numerous rounded clasts of magnetite (light grey).



## Characterisation of the mineralogical and frictional properties of a selected fault in the Rotondo granite.

**Volpe G., Pozzi G., Collettini C., Cocco M.**

The Bedretto tunnel, located in the Central Swiss Alps in Northern Ticino, has been chosen to host an innovative underground laboratory for deep geothermal and geophysical research linked to the FEAR project. The aim of FEAR is to stimulate (with fluid injection) and monitor a fault cropping out in the tunnel, with the advantage of a well-controlled environment. The selection of a candidate fault is carried out with the help of field and laboratory work. The first consists of in-situ characterisation of meso-scale structures and collection of representative samples of both host rock and fault deformation products. Laboratory work consists of: characterisation of microstructures of natural rocks (optical microscope), analysis of mineralogical content (X-ray powder diffraction), and friction experiments (rate and state characterisation). The candidate fault is entirely located within a late Variscan granitic intrusion (Rotondo Granite) and it is composed of a non-pervasive damage zone and narrow principal slip zone ( $< 5$  mm), which contains fine-grained white gouge. Brittle deformation within the fault overprints a mylonitic shear zone decorated by quartz veins and chlorite foliation. The dominant phases in the gouge are quartz ( $> 60\%$ ), phyllosilicates (muscovite and minor chlorite,  $> 20\%$ ) and laumontite ( $< 3\%$ ), which indicate alteration at low temperatures (zeolite facies) of the wear products. Four shear experiments (Figure 1a)

were performed in the bi-triaxial apparatus BRAVA (INGV, Rome) using the fault gouge. Sheared samples achieve a steady state friction coefficient of  $\sim 0.49$  (Figure 1b), display a general velocity strengthening behaviour ( $a-b > 0$ , Figure 1c) and moderate healing rates ( $= 0.0058$ , Figure 1d).



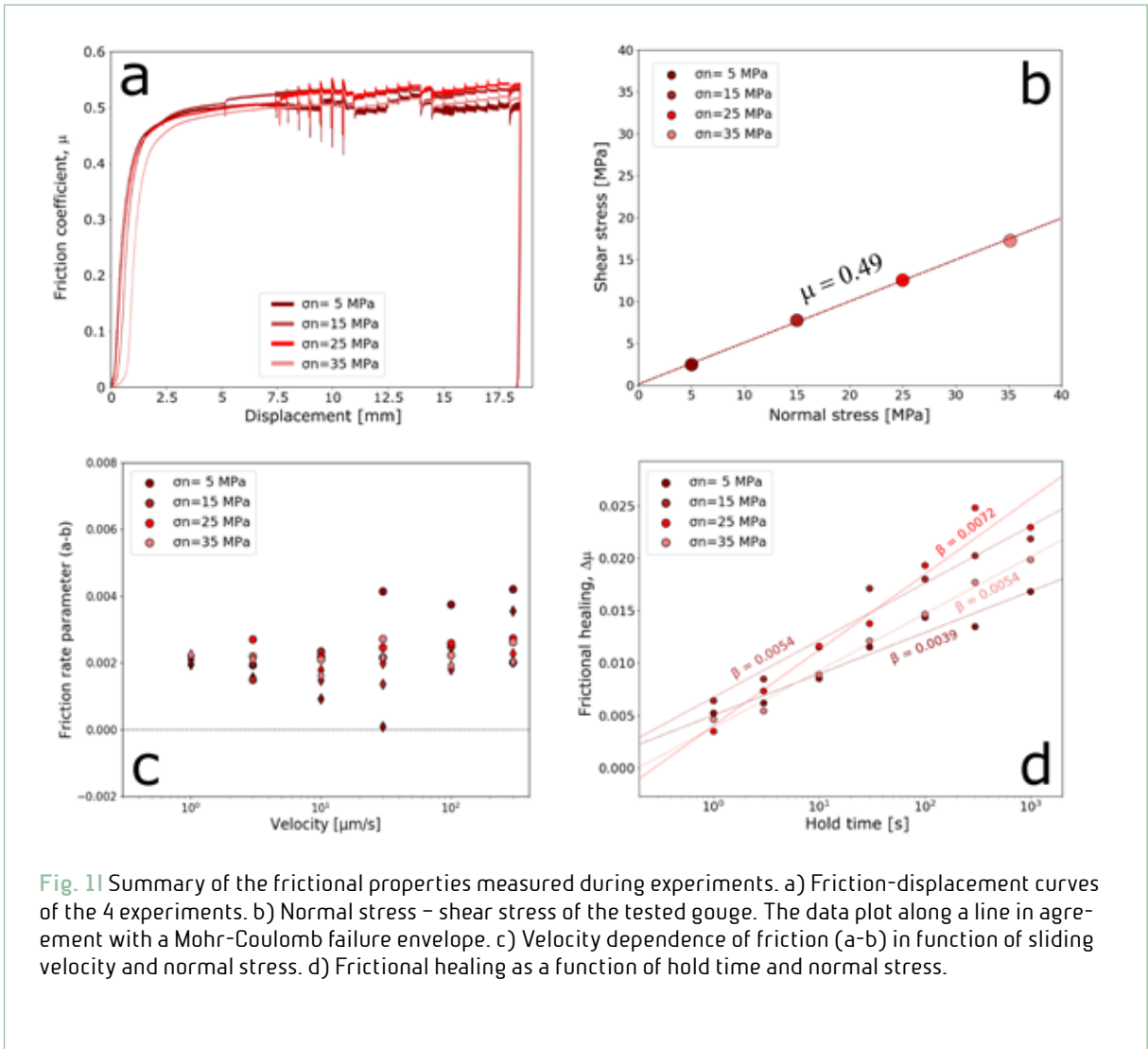


**Fig. 11** Summary of the frictional properties measured during experiments. a) Friction-displacement curves of the 4 experiments. b) Normal stress – shear stress of the tested gouge. The data plot along a line in agreement with a Mohr-Coulomb failure envelope. c) Velocity dependence of friction (a-b) in function of sliding velocity and normal stress. d) Frictional healing as a function of hold time and normal stress.



## Alpine subduction zone metamorphism in the Palaeozoic successions of the Monti Romani (Northern Apennines, Italy)

Rossetti F., Pontesilli A., Papeschi S., Romano C., Theye T.

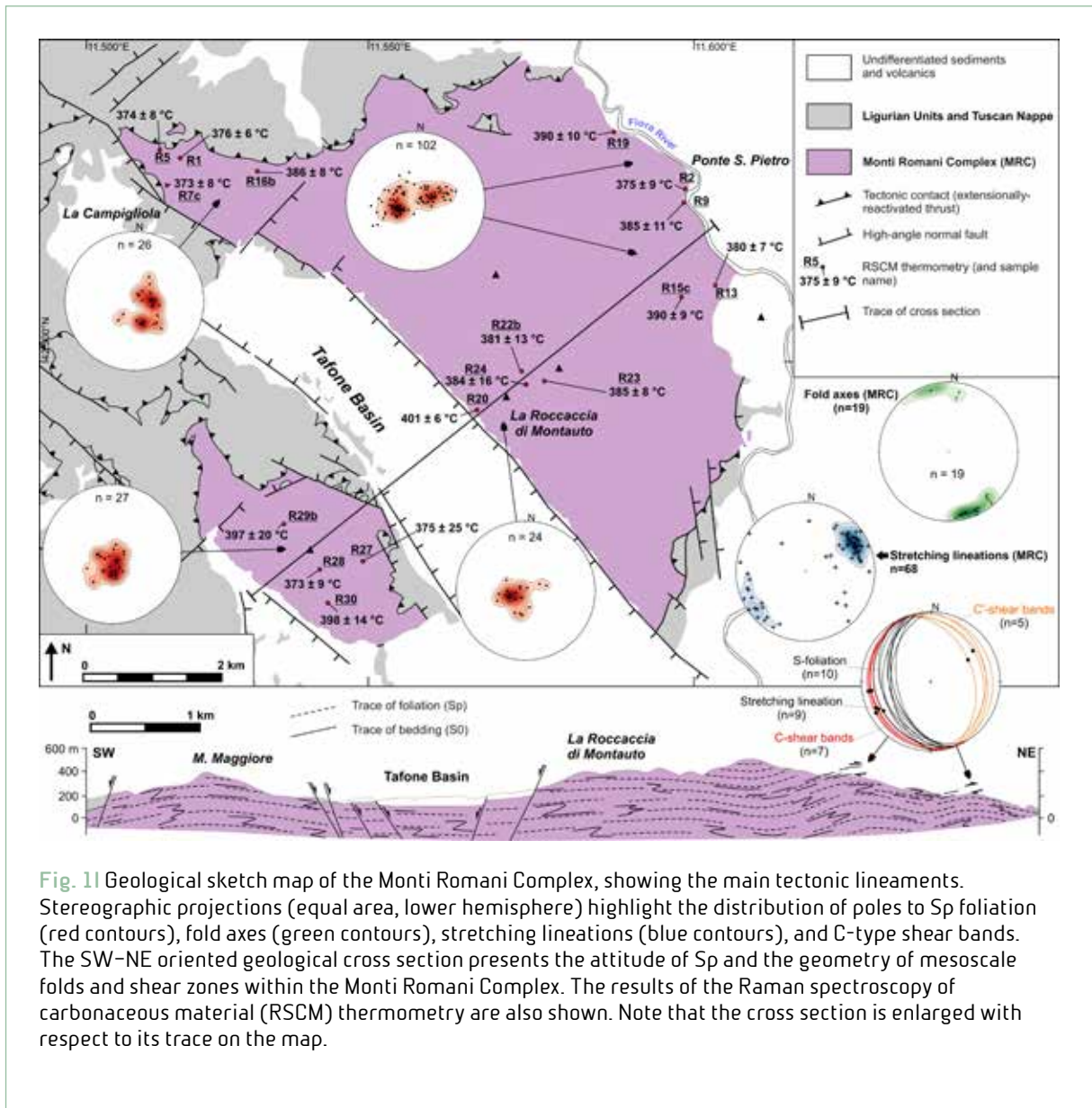
The hinterland of the Cenozoic Northern Apennines fold-and-thrust belt exposes the metamorphic roots of the chain, vestiges of the subduction-related tectono-metamorphic evolution that led to the build-up of the Alpine orogeny in the Mediterranean region. Like in other peri-Mediterranean belts, the tectono-metamorphic evolution of the Palaeozoic continental basement in the Apennines is still poorly constrained, hampering the full understanding of their Alpine orogenic evolution. In order to refine the alpine tectono-metamorphic evolution experienced by the Paleozoic sequences of the Apennines, we focused on the Monti Romani metamorphic complex, the southernmost and less studied metamorphic domain of the Northern Apennines. This work constitutes the first comprehensive tectonometamorphic study of the low-grade metasedimentary (metapsammite/metapelite) succession of the Monti Romani Complex (MRC) that formed after Palaeozoic protoliths and constitutes the southernmost exposure of the metamorphic domain of the Northern Apennines. By integrating fieldwork with microstructural studies, Raman spectroscopy on carbonaceous material and thermodynamic modelling, we show that the MRC preserves a D1/M1 Alpine tectono-metamorphic evolution developed under HP-LT conditions (1.0–1.1 GPa at  $T = 400^{\circ}\text{C}$ ) during a non-coaxial, top-to-the-NE,

crustal shortening regime. Evidence for HP-LT metamorphism is generally cryptic within the MRC, dominated by graphite-bearing assemblages with the infrequent blastesis of muscovite  $\pm$  chlorite  $\pm$  chloritoid  $\pm$  paragonite parageneses, equilibrated under cold palaeo-geothermal conditions ( $10^{\circ}\text{C}/\text{km}$ ). In detail, this represents the first report of HP-LT (Fe, Mg)-chloritoid-bearing assemblages in the region, documenting the important role played by oxidizing, structurally-controlled fluid circulation in controlling metamorphic blastesis and mineral chemistry during low-grade HP metamorphism in graphite-bearing rocks. In particular, this project aimed at expanding the microchemical dataset on the metamorphosed units, in order to refine the thermobarometric constraints on the metamorphic and fluid-rock interaction processes that controlled the blastesis of the observed parageneses. Electron Probe Micro Analysis (EPMA) on thin sections of selected samples, previously characterized through microstructural studies and Raman spectroscopy allowed a better characterization of the tectono-metamorphic evolution of the metasedimentary sequences exposed in the tectono-metamorphic units of the Northern Apennines. Results of this study allow extending to the MRC the signature of subduction zone metamorphism already documented in the hinterland of the Apennine



orogen, providing further evidence of the syn-orogenic ductile exhumation of the HP units in the Apennine belt. Finally, we discuss the possible role of fluid-mediated changes

in the reactive bulk rock composition on mineral blastesis during progress of regional deformation and metamorphism at low-grade conditions (Figure 1).





## Frictional melting in hydrothermal fluid-rich Faults: field and experimental evidence from the Bolfín Fault Zone (Chile)

Gomila R., Fondriest M., Jensen E., Spagnuolo E., Masoch S, Mitchell T.M., Magnarini G., Bistacchi A., Mitterpergher S., Faulkner D., Cembrano J., Di Toro G.

Tectonic pseudotachylytes are thought to be unique to certain water-deficient seismogenic environments and their presence is considered to be rare in the geological record.

Here, we present field and experimental evidence that frictional melting can occur in hydrothermal fluid-rich faults hosted in the continental crust.

Pseudotachylytes were found in the >40 km-long Bolfín Fault Zone of the Atacama Fault System, within two ca. 1 m-thick (ultra) cataclastic strands hosted in a damage-zone made of chlorite-epidote-rich hydrothermally altered tonalite. This alteration state indicates that hydrothermal fluids were active during the fault development. Pseudotachylytes, characterized by presenting amygdales, cut and are cut by chlorite-, epidote- and calcite-bearing veins.

In turn, crosscutting relationship with the hydrothermal veins indicates pseudotachylytes were formed during this period of fluid activity. Rotary shear experiments conducted on bare surfaces of hydrothermally altered rocks at seismic slip velocities ( $3 \text{ m s}^{-1}$ ) resulted in the production of vesiculated pseudotachylytes both at dry and water-pressurized conditions, with melt lubrication as the primary mechanism for fault dynamic weakening.

The presented evidence challenges the common hypothesis that pseudotachylytes are limited to fluid-deficient environments, and gives insights into the ancient seismic activity of the system.

Both field observations and experimental evidence, indicate that pseudotachylytes may easily be produced in hydrothermal environments, and could be a common co-seismic fault product.

Consequently, melt lubrication could be considered one of the most efficient seismic dynamic weakening mechanisms in crystalline basement rocks of the continental crust (Figure 1).



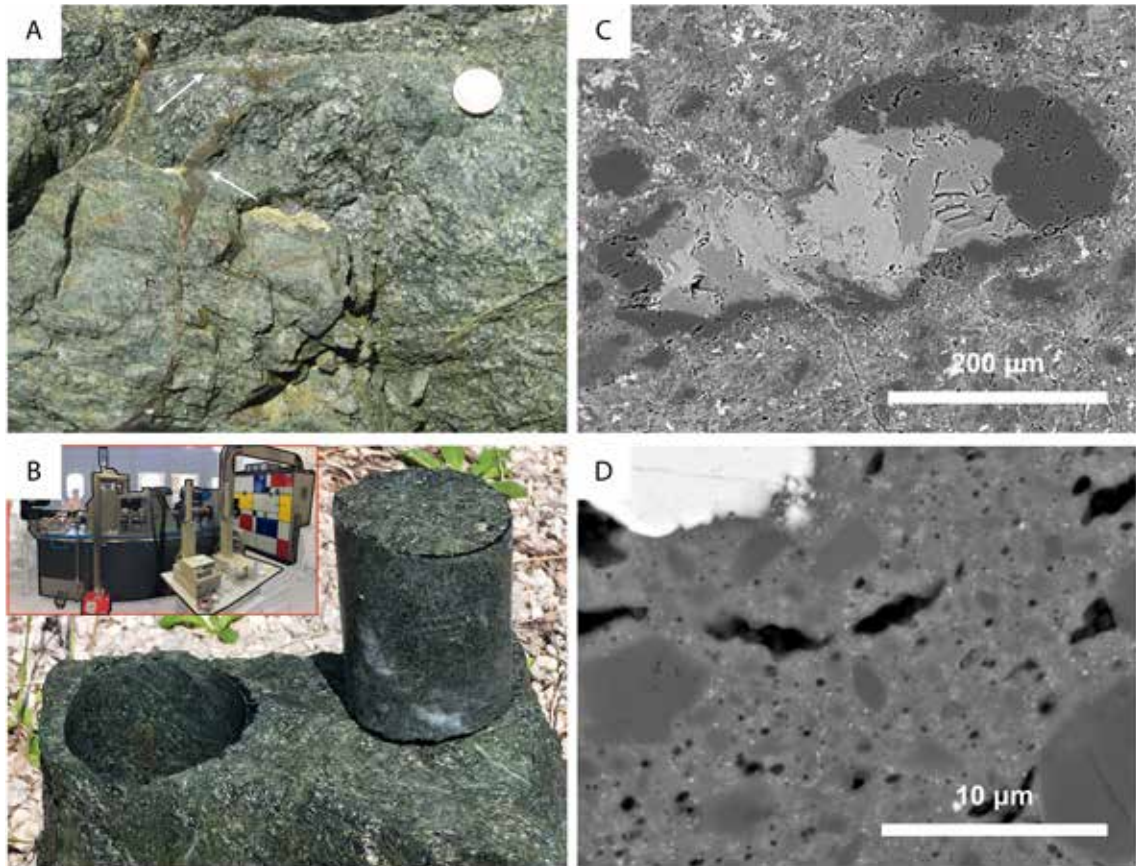


**Fig. 11** Frictional melting during earthquakes in fluid-rich faults. (A) Natural pseudotachylyte from the Bolfin Fault Zone (Atacama Desert, Chile). The pseudotachylyte cuts strongly green-schist facies altered diorites. Coin for scale. (B) Cylinders prepared to be sheared in the presence of pressurized fluids with SHIVA (in the inset). (C) Back Scattered Electron (BSE) Scanning Electron Microscope images of the natural pseudotachylyte matrix presenting amygdales filled by chlorite, epidote and calcite. (D) BSE-FESEM image of the matrix of the experimental pseudotachylyte produced with SHIVA. Note the elongated vesicles similar in shape to the amygdales found in natural pseudotachylytes.



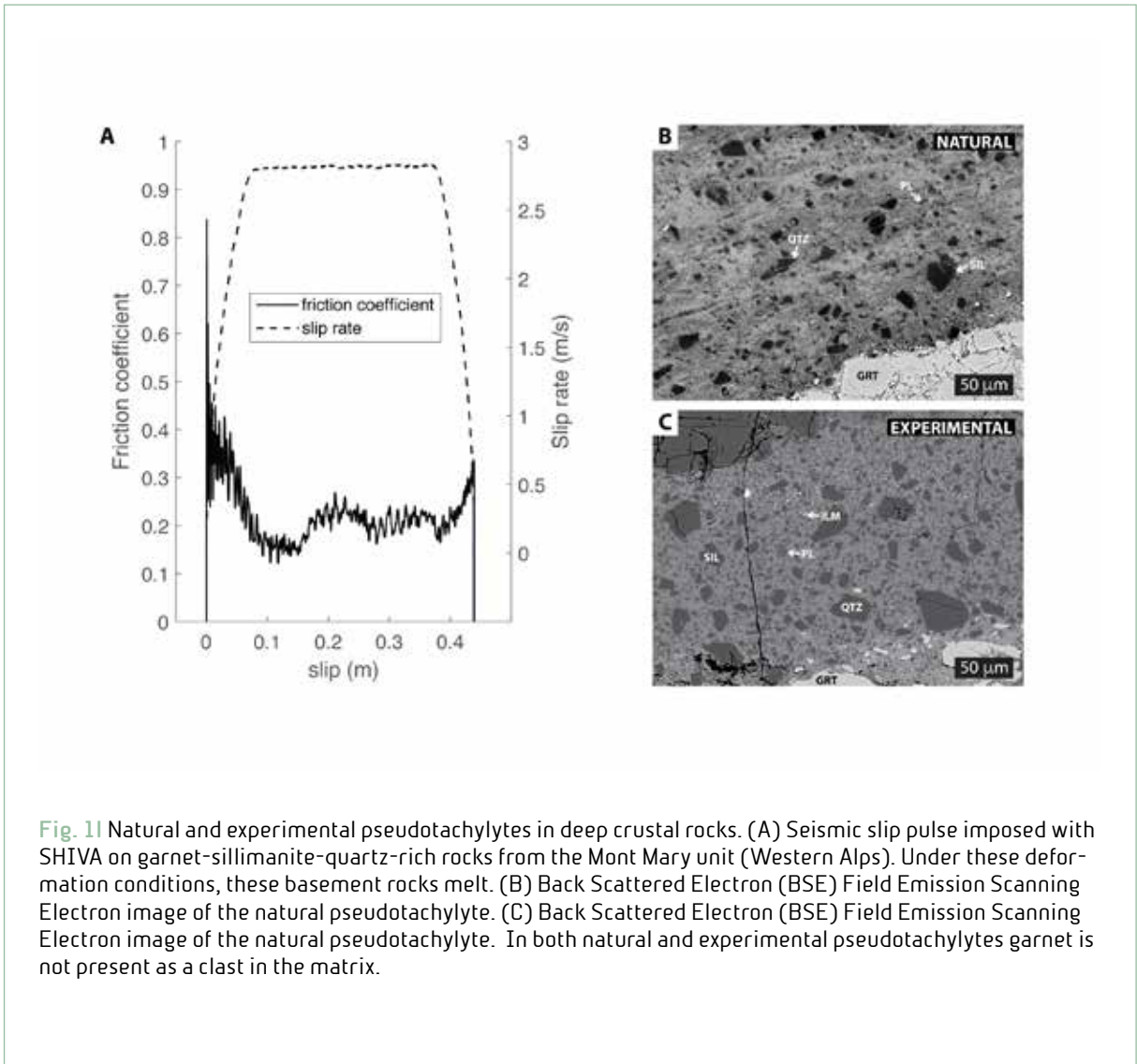


## Selective clast survival in an experimentally-produced pseudotachylyte

Papa S., Spagnuolo E., Di Toro G., Cavallo A., Favero M., Camacho A., Pennacchioni G.

On-fault processes during earthquakes contribute to seismic rupture propagation and slip. Here we investigate clast fragmentation in an experimental pseudotachylyte (solidified seismic melt) produced with a rotary shear machine. We slid for 0.44 m (corresponding to  $M_w \geq 6$  earthquakes), at slip rates  $> 1$  m/s, pre-cut samples of quartz + phyllosilicates + plagioclase + sillimanite + garnet -bearing ultramylonite, that hosts pseudotachylytes in nature. The ultramylonite minerals extensively preserved as clasts in the experimental pseudotachylyte are quartz, plagioclase, and sillimanite. Garnet is scarcely preserved, despite having a melting temperature similar to plagioclase, probably due to having low thermal shock resistance. This selective clast survival is identical to the one found in the natural pseudotachylytes.

Based on these experimental observations and assuming non-equilibrium melting, the preservation of a mineral, as a clast, in the melt appears to be controlled by its thermal shock properties as well as by its melting temperature. Since the mechanical effects of rupture propagation in these experiments were negligible, we conclude that, for  $M_w \geq 6$  earthquakes, (i) frictional slip and heating of the slipping zone plus (ii) thermomechanical properties of minerals, rather than fault rupture processes, control mineral comminution and clast survival in frictional melts (Figure 1).





## 8.3 TECHNOLOGY

### Automatic volcanic ash sampler

Di Stefano G., Mari M., Andronico D.

The project consists of a program for the development and construction of volcanic ash samplers, to be installed on active volcanoes, such as Stromboli and Etna, for the collection and subsequent analysis of volcanic ash during volcanic activities, as part of the UNO (Departmental Project) and HEAVEN Theme (Dynamic Planet Project).

The instrument is designed not only to sample the ashes emitted by volcanic activities in the fallout phase, but also to be subsequently equipped with sensors, data loggers and transmitters such as to make it a smart instrument, capable of acquiring multi-parameter information in the vicinity of crater areas.

A device is proposed that can provide the following principle objectives:

- Automatic collecting ash samples
- Measuring the accumulation rate
- Reducing maintenance on site
- Use traditional and experimental techniques

The program starts proposing the realization of a first "initial" version, as shown in Figure 1, in which the basic functions of an ash sampler are developed, but at the same time prepare the instrument to be able to insert other higher "level" functions. For this reason, during the development phase of the instrument, in

the construction phase, some solutions are prepared so as to be able to introduce other devices for future updates.

The Figure 2 shows the control block diagram projected for the current model in its general form. At the moment only the dashed red boxes are implemented to create a first basic version. Once the instrument was defined, the detailed mechanical drawings and the electronic diagrams were started. In addition, a market investigation was launched on the components and the purchase order was initiated.

The Figure 3 shows some parts of the ash sampler; other parts, which complete the frame, were made as well as the trolley with the hopper. The ordered components are awaited to complete the assembly of the sampler structure and the construction of the control system.

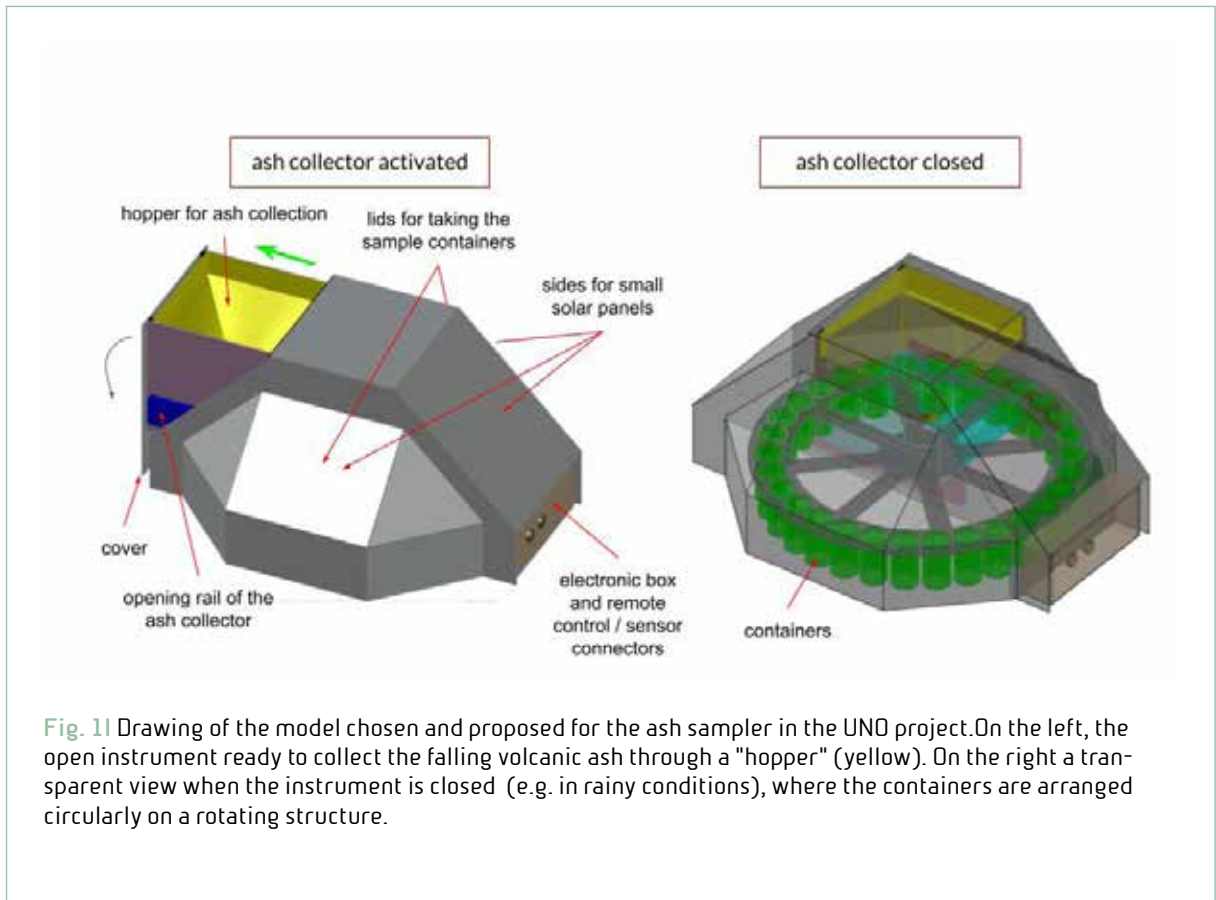
Technical improvements under study to carry out new experimental features to obtain a smart multi parameters instrument:

- Provide initial information on the particle size of the ash
- Provide first real-time parametric information via a radio link.
- Use traditional or experimental techniques based on weight measurement, electrostatic or electromagnetic phenomena, scanning techniques, images.



•Equip the system with a bidirectional radio transmitter (Wi-Fi) in order to receive, through a Master-Slave architecture, the

information acquired remotely with a view to covering the volcano with an array of devices.



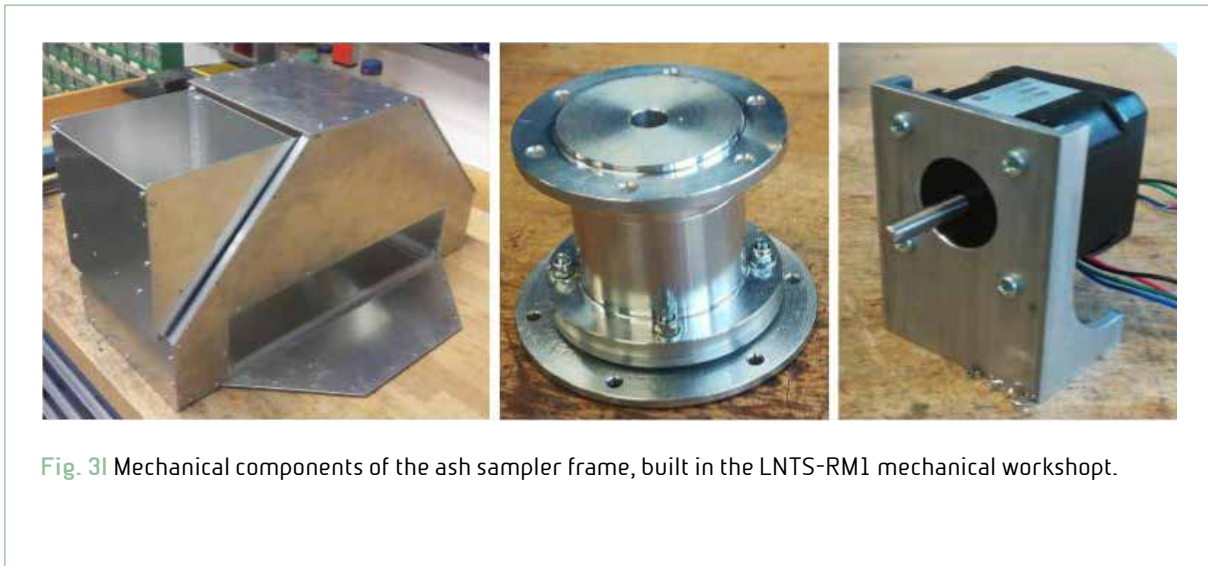
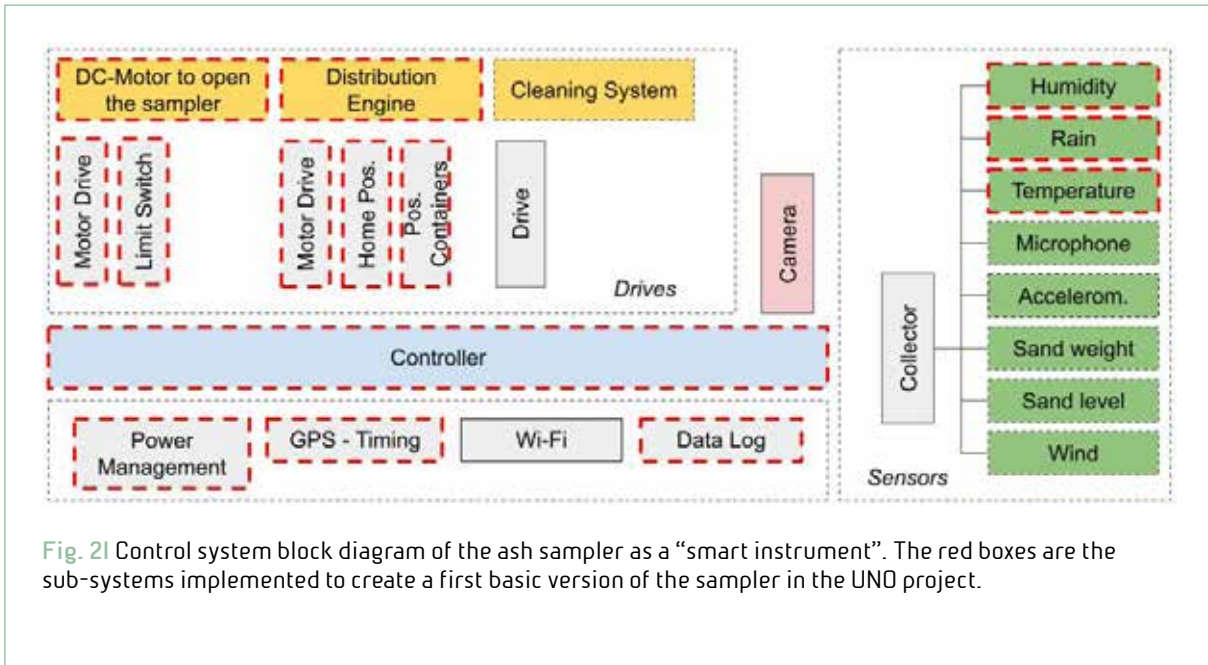


**Fig. 31** Mechanical components of the ash sampler frame, built in the LNTS-RM1 mechanical workshop.





## BRAVA2: Brittle Rock InvestigAtion Versatile Apparatus V.2 - Development of a plant for the control of new apparatus

Di Stefano G., Collettini C., Scuderi M.M., Bigaroni N., Volpe G., Pozzi G., Leeman J., Marone C., Mari M., Trippetta F.

The New Technologies and Instruments Laboratory (LNTS-INGV) collaborates with the new Laboratory of Excellent of the Department of Geology of "La Sapienza" University for the development of a new mechanical-hydraulic apparatus BRAVA2 (Brittle Rock InvestigAtion Versatile Apparatus 2).

BRAVA2 is a "tri-axial" press, used to reproduce stress conditions on brittle rock samples (5cmx5cm) necessary for the study of the mechanical behavior of fault rocks during the inter-seismic vs seismic phase, and subjected to mechanical stress even if a different one saturation condition.

BRAVA2 is developed on the experience of BRAVA1, currently in successful use at the HPHT-INGV laboratory.

The principle scheme of both apparatus is shown in the Figure 1, where you can see five hydraulic pistons (HP, HV, Pc, PPa and PPb) and a pressurized circular steel chamber, inside which the experiment takes place. The new apparatus generates stress conditions on the rock sample in double shear configuration (yellow parts), characterized by a normal stress ( $F_n$ ) and a shear stress ( $F_s$ ) and, also, creates a confining isotropic pressure around the rock through a hydraulic intensifier for the quasi-realistic behavior of the experiment. A hydraulic "tandem" system, realized by a couple of intensifier hydraulic pistons, allows

to maintain a "pore pressure" by injecting water into the sample or to induce a flow inside the rock to check the permeability during the stress.

BRAVA2 provides for heating of the sample holder to keep the rock samples hot during the rock experiment. This process takes place using three glow plugs inserted in the sample holder. The Figure 2 shows the draft of the block diagram of the plant for the operation of the apparatus. The hydraulic unit supplies pressurized oil to the hydraulic circuit for the movement of two hydraulic loading pistons (HP, VP) of normal and shear load and the three intensifier hydraulic pistons (PPa, PPb, Pc). The unit includes a master oil pump, driven by an electric motor M1, an oil tank, oil filter, a stabilization accumulator, a clogged filter and level sensor and finally a solenoid valve which opens the pump pressure towards the hydraulic circuit. A recirculation electric pump M2 transfers the hot oil in the tank to the chiller for cooling.

After setting up the experiment inside the chamber and closing the doors, a third pump installed in the apparatus allows you to fill the chamber with natural oil for the confining action, then pressurized by the PC during the experiment

All hydraulic pistons are controlled by five two stage and differential voltage signal



controlled servovalve (MOOG D765), mounted on each piston. The pistons are equipped of the Linear Voltage Differential Transformer (LVDT) voltage output ( $\pm 10V$ ) displacement transducers, provide by the Ametek/Solartron, with stroke 15 (HP), 50 (VP) and 150mm (PPa, PPb, Pc). The normal and shared load are measured thanks to two home-made load cells. Confining pressure is measured by an 1000bar voltage output (0-10V) transducers, with accuracy 0.1%; pore fluid pressure is measured by two 700bar output voltage (0-10V) pressure transducers, accuracy 0.1%.

For the acquisition and control system a modular and compact Reconfigurable I/O system (NI cRIO-9049, by National Instruments) has been chosen. The cRIO has a 1.6 GHz, Real Time (RT) Quad-Core controller and an 8-Slot chassis that can house up to 8 S-series modules, installed to the controller through a backplane containing a 325T FPGA of the Xilinx.

The system can therefore be programmed to execute processes on two levels: a low-level one within the FPGA, where you can implement those parallel processes that operate in the background and employ processing times with hardware-type timings with a clock frequency of 40MHz. A second upper level operates in the RT Controller. Thanks to the controller without operating system, in this level can be implemented processes that require deterministic cycle times, around 10-20ms, like post elaboration and characterization of the data record and data target preparation, PID regulators and windup algorithms. Five ADC S-series modules NI-9239, each with four @ 24bit input channels at simultaneous

sampling and a speeds up to 50KS/s/ch, are used to acquire all the parameters that characterize the status of the apparatus and the experiments (loads, displacements, pressures, temperature and other optional parameters).

An S-Series DAC module with 16 single-ended channels @16bit and an aggregate update rate of 100KS/s was chosen to generate the output analog signals, coming from the control processes and used to drive the five servovalves and heaters. To drive the D765 servovalves in a differential way, five differential amplifier/converters have been inserted downstream of the DACs channels.

Finally, an NI9304 module with 32 TTL digital channels was used for reading safety devices, switch-type sensors, indicator lights and drives, such as the control unit valve. Two power supplies are used, one for the cRIO, sensors and servovalve, and a second for the command and control devices.

All modules interface with the FPGA.

The cRIO can be configured to operate both in Scan Engine and FPGA mode. In the FPGA programming mode the module is controlled directly by the low level parallel processes, through code implemented and runned in the FPGA device: data acquisition, the data vector and FIFO organization, IIR filtering, safety switches for emergency and the activation of the main electrovalves of the hydraulic unit. Digital I/O and five ADC modules are configured in this mode.

In the Scan Engine mode the controller takes the control directly of the modules, bypassing the FPGA that will be only one device interface.

In this mode the modules are controlled by



the RT process implemented in the upper level program: closed loop control processes, PID and windup algorithm. The DAC module is controlled in this mode.

The horizontal piston can be controlled both in velocity and load mode thanks to a versatile closed-loop control, as well as the two-pore fluid pressure intensifiers can be controlled in velocity and pressure mode. The confining oil pressure intensifier can be controlled automatically in pressure mode but also in positioning mode for oil filling in the piston and in the chamber before the experiments.

The vertical piston is controlled by a dedicated motion controller, which is controlled by the real-time IO Controller, allowing very short regulation times. The piston can be controlled in position, velocity and force mode thanks to closed-loop servo control.

The control and data management software is developed in a LabVIEW graphic environment and is in progress. The new program strategy provides a modular architecture easily scalable and adaptable to other similar bi-axial or tri-axial apparatus. This is important to standardize the management of the devices that operate in different laboratories, as well as to have devices that are easily usable by students.

BRAVA2 represents an evolution of the BRAVA1 and is developed by gathering both the mechanical and electronic experience of the BRAVA1 and his control system. Any improvement solutions will subsequently be implemented on BRAVA1 through an "Upgrade" plan.

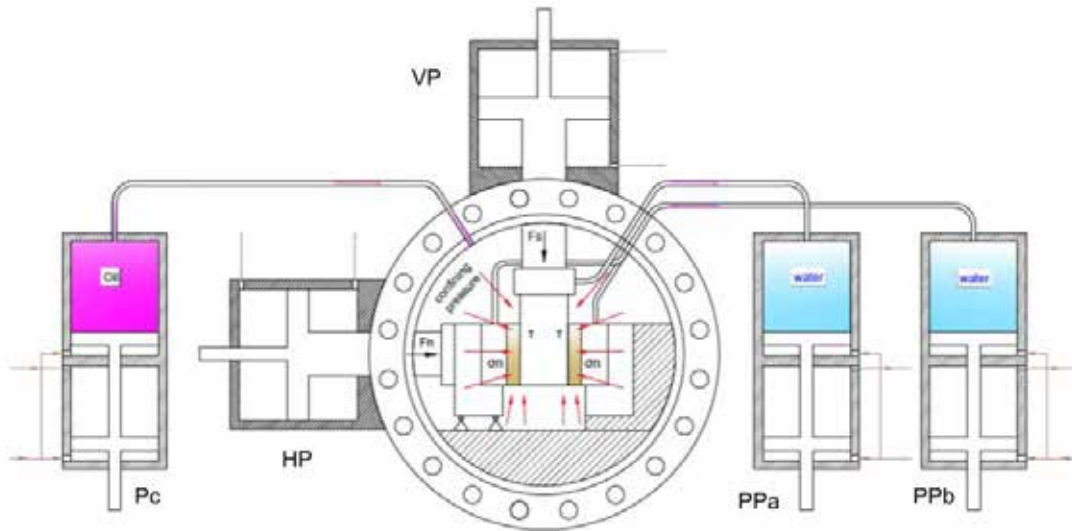
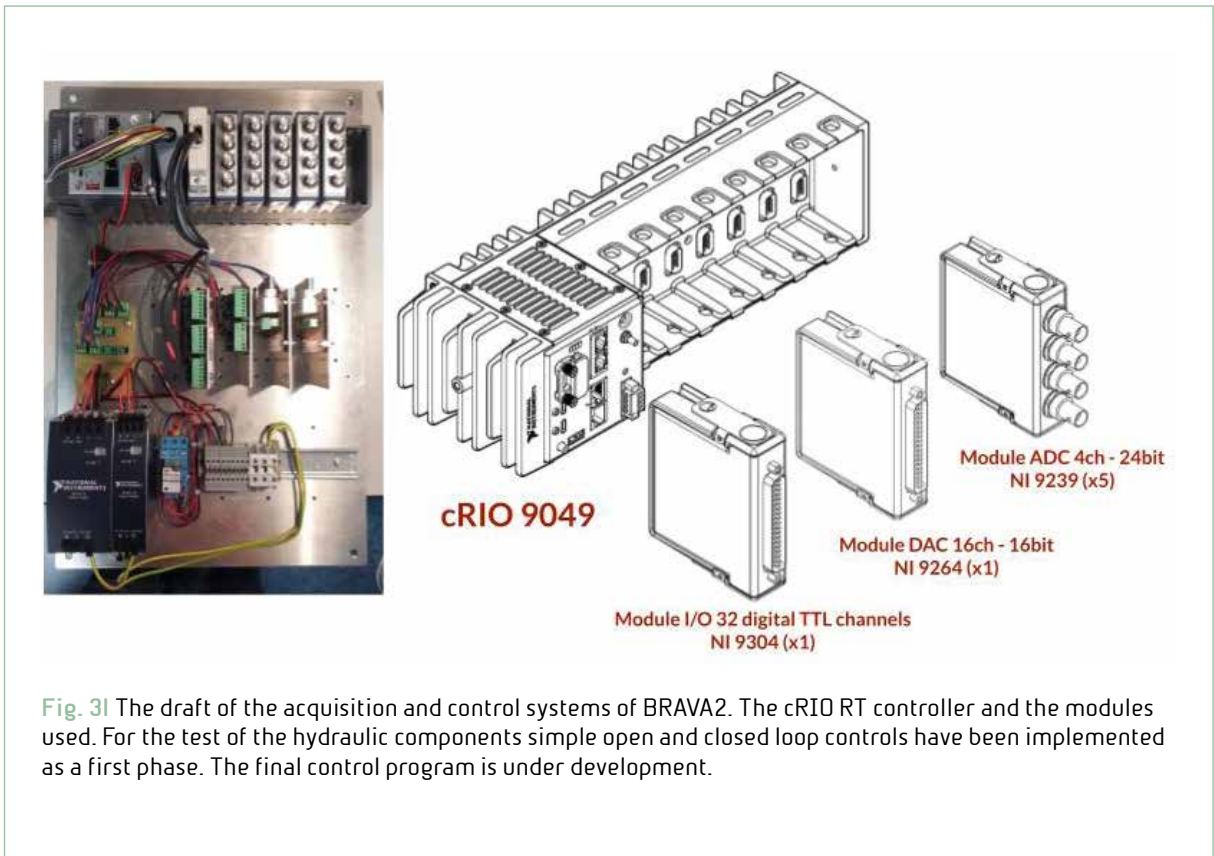
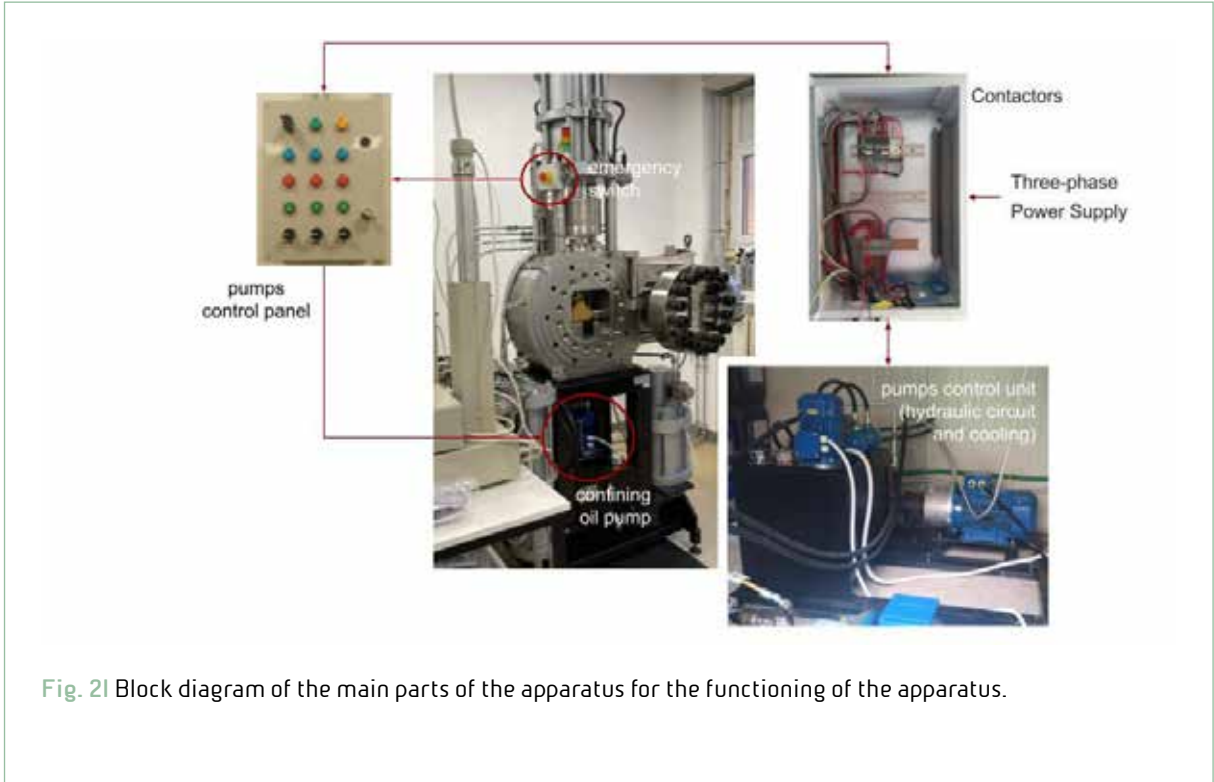


**Fig. 11** Principle diagram of a tri-axial apparatus. Two hydraulic pistons (HP, HV) exert a combination stress, normal and shear, on the rock sample in double shear configuration. The Pc, PPa and PPb pistons are pressure intensifiers and needed for raising the initial control unit pressure to a confining pressure (up to 800bar) and to pore pressure inside the brittle rock. A circular pressurized steel chamber, inside which the experiment takes place.







## A novel apparatus to study earthquake dynamics on extended experimental faults

Spagnuolo E., Di Stefano G., Aretusini S., Cornelio C., Pozzi G.

Our understanding of earthquake dynamics is challenged by limitations in obtaining observational constraints. Indeed most earthquakes occur at depths down to 5 km and far behind which are not accessible for direct observation. Therefore the dynamics of earthquakes and the mechanisms leading to all the events associated with deformation of the Earth's Crust remains largely debated. Hypotheses have been tested in the laboratory (e.g. determining constitute and governing equations of fault motion) but still a number of key questions remain and more are to come with the advent of the era of big data. In October 2021 we installed MEERA, a novel apparatus designed to simulate the stress field in a prescribed tectonic regime, to observe the evolution of the deformation and its associated signals during the loading stage and testing the hypothesis that earthquakes obey the same fundamental laws on several scales, from the laboratory scale - mm. to the natural fault scale - km. Experiments performed with MEERA are expected to provide important insights into the mechanics of earthquakes.

MEERA (Figure 1) is a biaxial type apparatus in horizontal configuration consisting of a piston for the tangential force and 5 thrust pistons for the modulation of the normal force. With a maximum of 100 kN per piston, the maximum operating pressure is approximately 30-60 MPa on samples of 300 x 80 x 5 mm and 300 x 80 x 2.5 mm respectively. The tangential

thrust piston can be controlled in force and speed, with maximum speeds of 4 cm / s. The speed control allows to simulate the passage of a rupture front that moves at low speeds up to speeds considered seismic (approx. > 10 mm / s). Furthermore, the apparatus is equipped with an environmental chamber with a Plexiglas lid for the confinement of fluids at a maximum pressure of 6 MPa. The plexiglass lid has been designed to allow the monitoring of sample deformation and temperature from the outside with high-speed cameras and thermal cameras. In anticipation, it will be possible to implement the environmental cell for a tightness of up to 20MPa. The environmental cell is also designed for the circulation of fluids at temperatures up to 150 °C. The experimental apparatus was created thanks to a loan from the Civil Protection, Fund for the prevention of seismic risk for the year 2016, pursuant to art. 2, paragraph 1, of the law 5 January 2017, n. 4.



**Fig. 11** The novel biaxial apparatus MEERA, MEchanics of Earthquake and Extended Rupture Apparatus recently installed in the HPHT laboratory of the INGV.



## Anti-aliasing filter

Romeo G., Iarocci A., Spinelli G.

In electronics aliasing is the phenomenon whereby two different analog signals can become indistinguishable once they have been sampled: this constitutes a serious problem that directly affects the output of the system in question, altering its veracity. In collaboration with the Roma Tre University we have created an anti-aliasing filter for acquisition from an accelerometer using an oscilloscope. The anti-alias filter is an analog filter used before sampling a signal, in order to narrow the band of the signal itself and approximately satisfy the Nyquist-Shannon sampling theorem. The filter designed, in addition to providing the necessary cut in frequency, removes the DC component (necessary for the use of mems accelerometers) and adapts the level and the offset of the signal for use with an ADC with a range of 0-5 V.

The features are:

Low Pass 7th order Butterworth Bessel

Gain: 15

Bandpass: -20dB at 40Hz

Band stop: -70dB at 100Hz

A first experimental assembly, in a metal box to eliminate disturbances (Figure 1), shows a perfect agreement between the theoretical response (Figure 2) and the measurement on the prototype (Figure 3).

Originally the filter, designed for a 30 Hz cutoff, provided the step response showed in Figure 3.

Subsequently, in anticipation of a change in the sampling frequency of the data, the cutoff frequency of the circuit was doubled (60 Hz cutoff) through the removal of 5 jumpers (experimental result visible in Figure 4). In the final version, the circuit will be made up of Eurocard cards, each containing 3 filters (one card for each 3-component accelerometer) from which panel will be accessible the control settings for gain and offset for each individual channel, in addition to the accelerometer input connector, while the filtered data will be taken from the backplane of the basket that will house the system.



Fig. 1| Filter inside the metallic Box.

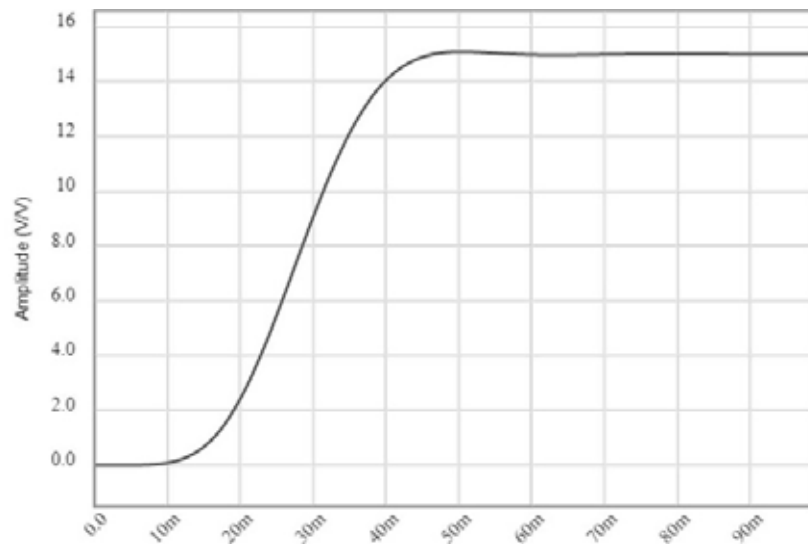


Fig. 2| Theoretical response.

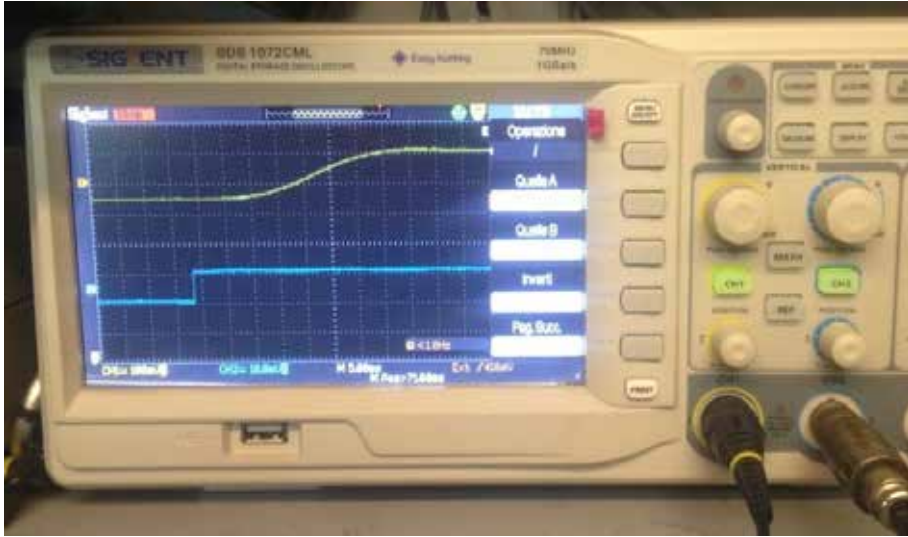


Fig. 3I Filter step response.

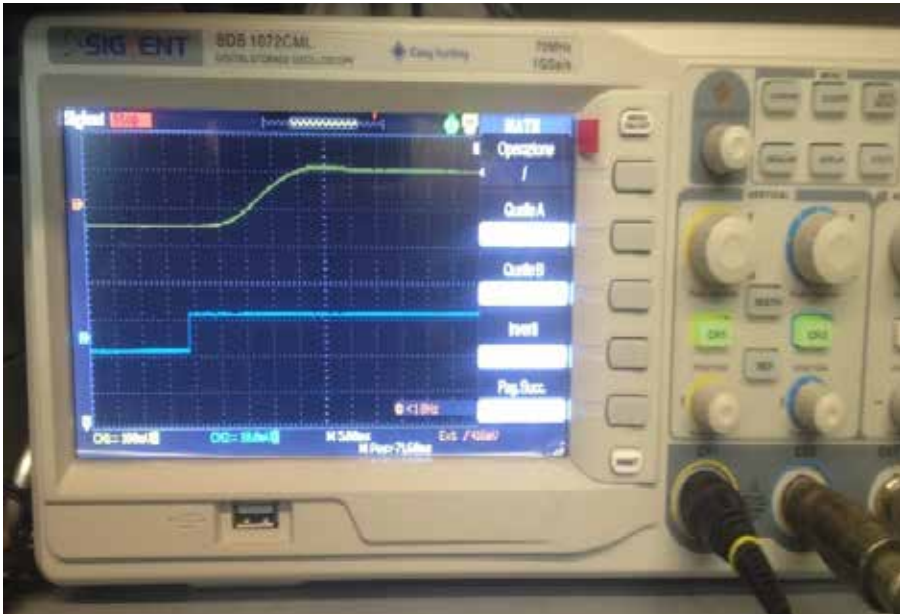


Fig. 4I New filter step response.





## Automation of a Radon Chamber and measurements (Electronic Radon Chamber)

**Pongetti F., Galli G.**

Commercial radon-in-air measuring devices (DUT: Device Under Test) are calibrated at our Radionuclide Lab. facility using an original set of equipment (radon-chamber, detector, etc.), and a procedure developed at INGV. Relative humidity (RH) and temperature of the air (T) are parameters to be varied to calibrate radon (Rn) measuring devices that use a semiconductor diode as a detector.

An electronically managed radon-chamber (RnC) can save an operator's time, set operating parameters, record sensor data, and can be programmed to automate the calibration process through software.

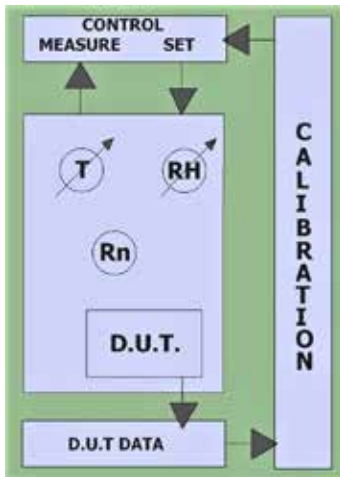
The RnC is essentially a sealed metal box which hosts the DUT during the calibration. Climatic condition inside the RnC is changed using a system that enriches or extracts water from air, composed of a pump, pipes, valves,

exchangers etc, which are arranged in an hydraulic circuit. The pump and valves are electrically actuated and are managed by the application software.

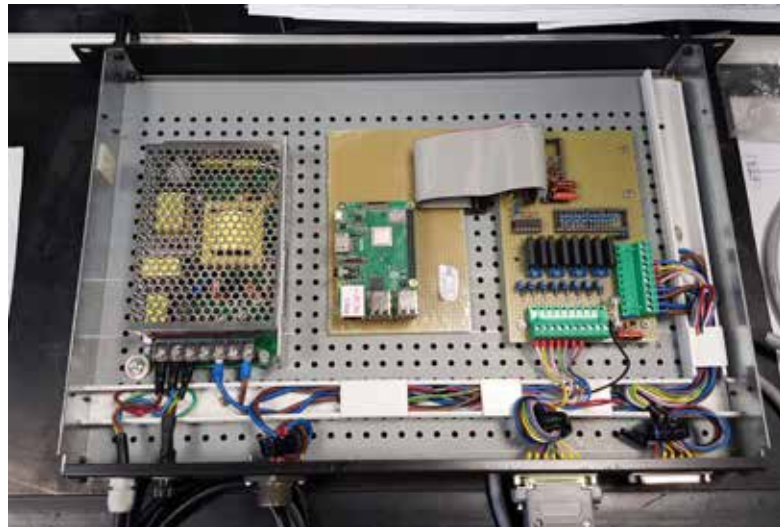
The software implements a graphical user interface (GUI), whose main features are the 'manual mode control' form, used generally for debug purposes and the 'sequencer mode control' form used to manage the tasks of calibration process versus time.

The electronic hardware is composed of a mini computer Raspberry-pi and a custom isolated-digital-in/out interface board, for driving the actuators.

For additional reliability, an array of manual switches can bypass the electronic driver and give the operator full manual control capability over the actuators (Figures 1, 2 and 3).



a



b

Fig. 11 a) Process schematic; b) Hardware/software control circuit (partial).

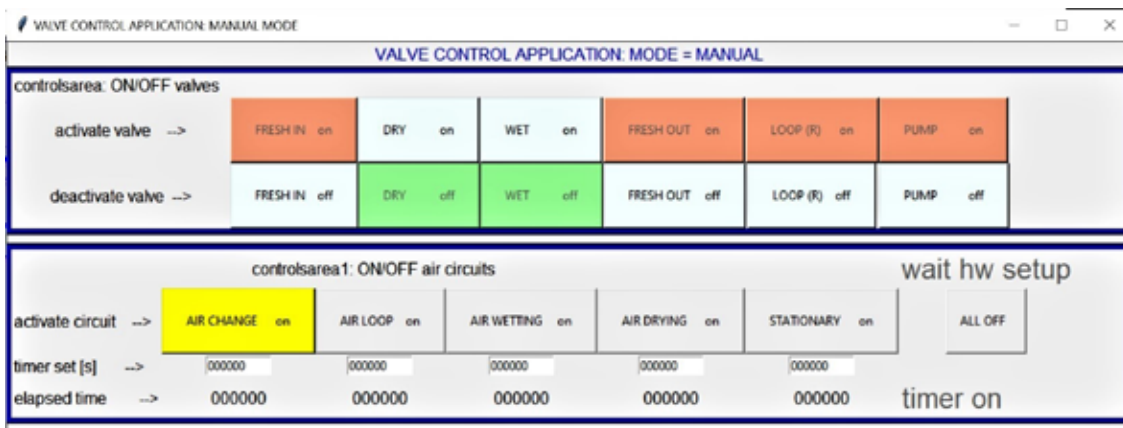


Fig. 21 Example of application GUI: 'manual control' form.



Fig. 3I Hydraulic connections and manual switches.



## Developments and upgrades of the HERMES project

Iarocci A., Addobato P., Di Stefano G., Lepore A., Romeo G., Spinelli G., Vallocchia M.

In the context of the HERMES project, in June 2021 an experimental flight, with a latex balloon, was carried out on the Etna volcano. This place was chosen with a view to making a flight in the future that would allow the glider to glide over the Etna volcano to carry out measurements. By equipping the glider with gas sensors (Cl, SO<sub>2</sub>) suitable for use in the stratosphere, the goal could be to attempt to measure the concentration of volcanic gases within the volcano plume.

Figure 1 shows the phases before launch, while Figure 2 shows the log of the Etna experimental flight.

At about 16.000 meters of altitude, the aircraft sets up and begins to glide, while at about 4.000 m the glider's battery suddenly discharged, not allowing its recovery.

In order to increase the modularity of the project, the Position & IMU module has been revised.

It is now composed of four mechanically separate modules:

- CAN I/F
- Controller
- IMU (Inertial Measurement Unit);
- GPS + Altimeter & temp

The task of the module is to acquire the gondola attitude data, coming from the sensors of the inertial platform, the altimeter and the geo-localization (GPS) data, and then transmit it to the on-board computer through a CAN bus.

Figure 3 shows the finished and assembled module, while in Figure 4 there is the module block diagram.



a



b

Fig. 11 (a) The glider ready for the flight over Etna volcano; (b) launch phase.

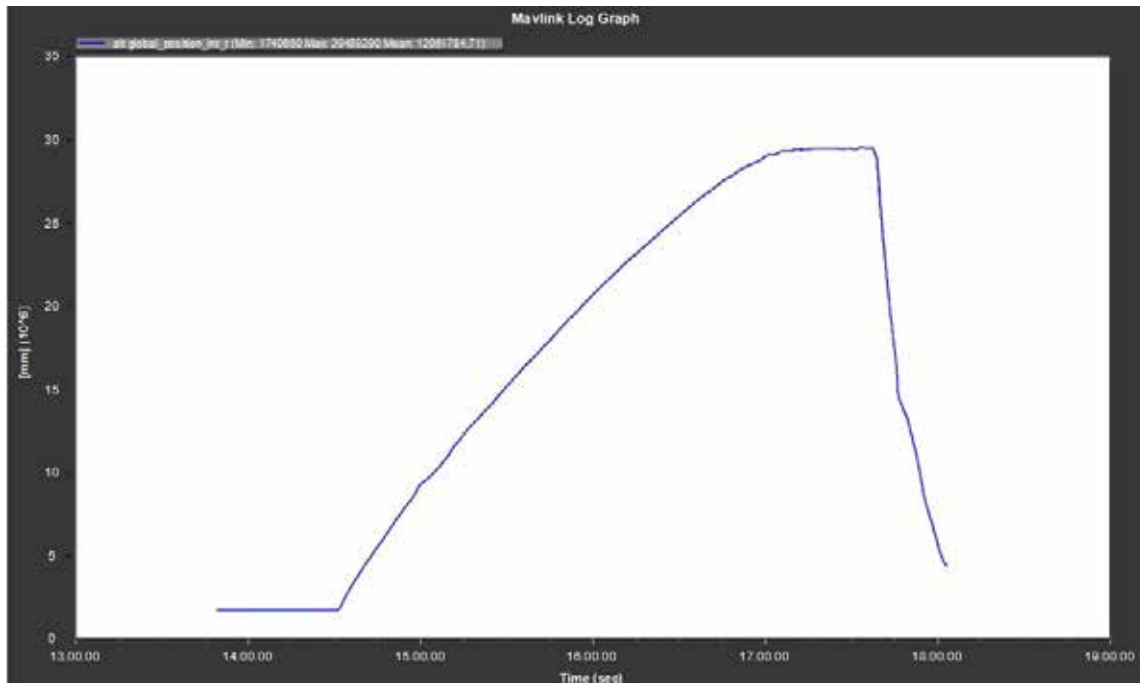


Fig. 2| Etna experimental flight log.



Fig. 3| The assembled module.

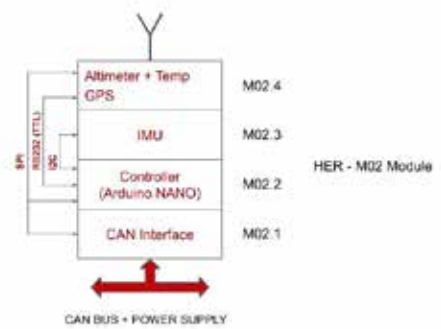


Fig. 4| Block diagram of the Position & IMU module.





## 91 SEMINARS and TEACHING

### Seminars

**Di Toro G.** | **Nascita, vita e morte di un terremoto: scegli con noi il tuo domani** | Presentazione per le Scuole sul Web, 25 Febbraio 2021

**Di Toro G.** | **Il motore dei terremoti visto da vicino** | Distinguished Lectures della Società Geologica Italiana ai tempi del COVID, Ciclo di seminari 2021, 30 Marzo 2021 (Webinar)

**Di Toro G.** | **ERC projects: hints for a successful proposal** | Dipartimento di Scienze della Terra. Università degli Studi di Firenze, Florence, Italy, 30 April 2021 (Webinar)

**Di Toro G.** | **Pseudotachylytes and earthquakes** | GFZ German Research Centre for Geosciences, Potsdam (Germany) 16 June 2021 (Webinar)

**Di Toro G.** | **Fault, friction and earthquakes** | Chemical, Geological and Environmental Sciences PhD Day, Università di Milano-Bicocca, Milano 4 October 2021

**Spina L.** | **Il vulcano in laboratorio: introduzione alla vulcanologia sperimentale e casi studio** | Università degli Studi di Catania (CT), 7 Dicembre 2021

### Teaching

**De Astis G.** | **Corso semestrale di “Inglese per Scienze della Terra”** | Laurea triennale A.A. 2020-2021  
Università di Roma La Sapienza

**Misiti V.** | **Corso semestrale di “Petrografia per Scienze Naturali”** | Laurea triennale A.A. 2020-2021  
Università di Roma La Sapienza

### Training

**1. Cantonetti M.** | **Stage | Analisi di video ad alta velocità dell'attività esplosiva di tipo stromboliano**  
Supervisors: Taddeucci J. - INGV Roma | Palladino D.M. - Sapienza University of Rome

**2. Pennacchia F.** | **Stage | High speed cameras and field deployment at Stromboli volcano**  
Supervisors: Del Bello E. - INGV Roma | Vona A. - University of Roma Tre



**3. Schiavon B.** | Stage | Applicazione di tecniche di preparazione campioni e microanalitiche per l'analisi tessiturale e microchimica di prodotti dell'attività vulcanica

Supervisors: Del Bello E. - INGV - Roma1, I Mollo S. - Sapienza University of Rome

**4. Valentini F.** | Stage | Analisi video ad alta velocità dell'attività esplosiva di tipo stromboliano

Supervisors: Taddeucci J. - INGV Roma1 | Palladino D.M. - Sapienza University of Rome

## Thesis

**1. Amodio A.** | Master Thesis | Caratterizzazione delle proprietà dell'attrito delle serpentiniti ricche in Antigorite

Supervisors: Collettini C. - Sapienza University of Rome | Pozzi G. - INGV Roma1

**2. Cantonetti M.** | Master Thesis | Studio sperimentale dei getti supersonici e loro implicazioni per le eruzioni vulcaniche Stromboliane

Supervisors: Taddeucci J. - INGV Roma1 | Palladino D.M. - Sapienza University of Rome

**3. Chiesurin. A.** | Master Thesis | Mineralogical, geochemical and microstructural characterization of fault rocks from the Koyna deep drilling project (India).

Supervisors: Di Toro G. - University of Padua | Spagnuolo E. - INGV

**4. Lombardi F.** | Thesis | Analisi micro-tessiturale delle fontane dell'Etna: Implicazioni per la stima delle velocità di risalita del magma nel condotto vulcanico

Supervisors: Mollo S. and Moschini P. - Sapienza University of Rome

**5. Moltoni R.** | Master Thesis | Caratterizzazione di rocce di faglia sperimentali

Supervisors: Collettini C. and Ruggieri R. - Sapienza University of Rome

**6. Panunzi S.** | Master Thesis | Studio sperimentale dei getti supersonici e loro emissioni acustiche nelle eruzioni Vulcaniche Stromboliane

Supervisors: Taddeucci J. - INGV Roma1 | Palladino D.M. - Sapienza University of Rome

**7. Pilotti S.** | Master Thesis | Caratterizzazione delle eruzioni Stromboliane attraverso l'analisi di video ad alta velocità

Supervisors: Taddeucci J. - INGV Roma1 | Palladino D. - Sapienza University of Rome



**8. Schiavon B.** | Master Thesis | Textural and chemical variation of Stromboli volcano magmas from high frequency sampling of recent eruptive products

Supervisors: Del Bello E. and Pontesilli A., INGV Roma1 | Mollo S., Sapienza University of Rome

**9. Valentini F.** | Master Thesis | Dinamiche delle eruzioni dello Stromboli dell'estate 2019 sulla base dei prodotti dei social media

Supervisors: Taddeucci J.- INGV Roma1 | Palladino D.M. - Sapienza University of Rome

## PhD

**1. Benà E.** | PhD | Tectonic control on enhanced geogenic radon as a first order factor in radon hazard assessment | Padua University

Supervisors: Ciotoli G., Sassi R. - CNR | Spagnuolo E., INGV Roma1

**2. Bigaroni N.** | PhD | Riprodurre il ciclo sismico di una faglia complessa in laboratorio e predire l'andamento con il machine learning

Supervisor: Scuderi M. - Sapienza University of Rome

**3. Chinello M.** | PhD | Formation of polished surfaces in natural rocks: experimental and field constraints

Supervisors: Di Toro G. - University of Padua | Spagnuolo E. - INGV Roma1 | Oliver Plumper - Utrecht University

**4. Del Rio L.** | PhD | Mechanism of formation of slip surfaces in carbonate-built rocks: seismic faulting vs. Deep Seated Gravitational Slope Deformation

Supervisor: Di Toro G. - University of Padua | co-supervisor Fondriest M., Gori S., Falcucci E., Moro M. - INGV Roma1 | Saroli M., Cassino University

**5. Lang S. D.** | PhD | Kinetic aspects of major and trace element partitioning between olivines and melt during solidification of terrestrial basaltic materials

Supervisors: Mollo S. - Sapienza University of Rome | Lyderic L. - CRPG-CNRS Nancy

**6. Masoch S.** | PhD | Structure, evolution and deformation mechanisms of large displacement seismogenic faults in the continental crust

Supervisor: Di Toro G. and Pennacchioni G. - University of Padua | Cembrano J. - Universidad Ponteficia de Chile.



**7. Moschini P.** | PhD | **Volcanic hazard assessment at Mt. Etna: a time-integrated, polybaric and polythermal perspective**

Supervisors: Gaeta M. - Sapienza University of Rome | Scarlato P. - INGV Roma1

**8. Palumbo F.** | PhD | **Reconstruction of the intensive variables and magmatic architecture of Vulcano island (Aeolian Arc, Italy)**

Supervisors: Mollo S. - Sapienza University of Rome | De Astis G. - INGV Roma1

**9. Schiavon B.** | PhD | **Petrological monitoring of magma-mush dynamics at Stromboli: Insights on the transition from mild to violent eruptive styles**

Supervisors: Mollo S. - Sapienza University of Rome | Del Bello E. and Pontesilli A. - INGV Roma1

**10. Volpe G.** | PhD | **Proprietà dell'attrito e permeabilità di faglie in basamento per una migliore caratterizzazione del loro potenziale sismogenico**

Supervisors: Collettini C. - Sapienza University of Rome | Pozzi G. - INGV Roma1

**11. Wei F.** | PhD | **Investigation of seismic slip in experimental faults under hydrothermal conditions. Chinese Government Scholarship**

Supervisor: Di Toro G. - University of Padua



## 101 VISITING SCIENTISTS

Núñez-Cascajero A., Barrero Echevarria X. | [University Carlos III](#) | Madrid | *June*  
Ohl M. | [Utrecht University](#) | [Utrecht University](#) | Netherlands | *September*

## 111 MEETINGS, WORKSHOP and SYMPOSIA

### Meetings and sessions organization

#### [vEGU21: Gather Online](#)

Wien, Austria | 19-30 April

**Demurtas M., Aretusini S., Fondriest M., Passelegue F.**

[The Mechanics of Earthquake Faulting: a multiscale approach](#)

#### [AGU 2021: Gather Online](#)

San Francisco, USA | 13-17 Decemberr

**Tisato N., Carpenter B., Spagnuolo E., Paglialunga F.**

[Fault-Slip Acceleration: From Slow to Fast, From the Lab to the Field, and In Between](#)

### Meetings and sessions attendance

#### [4a Conferenza “A. Rittmann” Giovani Ricercatori](#)

Virtual conference | 6-9 April

**Spina L., Del Bello E., Ricci T., Taddeucci J., Scarlato P.**

[Multi-parametric characterization of intermediate-size ash/gas-rich explosive activity at Batu Tara Volcano \(Flores Sea, Indonesia\)](#)





## vEGU21: Gather Online

Wien, Austria | 19–30 April

**Amoroso S., Barbača J., Belić N., Kordić B., Brčić V., Budić M., Civico R., De Martini P.M., Hećej N., Kurečić T., Minarelli L., Novosel T., Palenik D., Pantosti D., Pucci S., Filjak R., Ricci T., Špelić M., Vukovski M.**

Liquefaction field reconnaissance following the 29th December 2020 Mw 6.4 Petrinja earthquake (Croatia)

**Aretusini S., Meneghini F., Spagnuolo E., Harbord C., Di Toro G.**

Fluid pressurisation and earthquake propagation in the Hikurangi subduction zone

**Chinello M., Fondriest M., Di Toro G.**

Structural characterization of fault damage zones in carbonates (Central Apennines, Italy)

**Di Toro G., Aretusini S., Núñez-Cascajero A., Spagnuolo E., Tapetado A., Vasquez Garcia M.C.**

Fast and localized temperature measurements during simulated earthquakes in carbonate rocks

**Kordić B., Vukovski M., Budić M., Špelić M., Barbača J., Belić N., Brčić V., Filjak R., Kurečić T., Palenik D., Bočić N., Atanackov J., Bavec M., Brajković R., Celarc B., Novak A., Novak M., Jamšek Rupnik P., Amoroso S., Civico R., Pucci S., Ricci T., Boncio P., Iezzi F., Pace B., Testa A., Benedetti L., Henriquet M., Moulin A., Baize S., Métois M., Markusic S.**

Geodetic benchmark displacement measurements following the 2020 Petrinja earthquake in Croatia

**Lazari F., Castagna A., Nielsen S., Griffith A.W., Resor P., Gomila R., Di Toro G.**

Estimate of earthquake power dissipation from exhumed ancient faults (Gole Larghe fault zone, Italy)

**Masoch S., Gomila R., Fondriest M., Jensen E., Mitchell T., Pennacchioni G., Cembrano J. and Di Toro G.**

Structural evolution of a crustal-scale seismogenic fault in a magmatic arc: The Bolfin Fault Zone (Atacama Fault System)

**Misiti V., Riposati R., Di Laura F., Battelli P., Crescimbene M.**

GEOVISUAL: if you can draw it, you can learn it

**Passelegue F., Di Toro G., Schubnel A.**

INVITED. The dynamics of earthquakes rupture: A view from the laboratory



**Peres S., Griffiths T., Masotta M., Pontesilli A.**

The effect of melt water content and isothermal annealing time on the formation and evolution of clinopyroxene-titanomagnetite clusters

**Tamburello G., Marotta E., Belviso P., G. Avvisati G., Ricci T., Caliro S., Avino R., Rouwet D.**

Gas-sensors-equipped drone measurements of volcanic plume gas composition and flux at Pisciarelli, Campi Flegrei, Italy

**Vukovski M., Budić M., Špelić M., Barbača J., Belić N., Brčić V., Filjak R., Korbar T., Kordić B., Tomislav Kurečić T., Palenik D., Bočić N., Atanackov J., Bavec M., Brajkovič R., Celarc B., Novak A., Novak M., Jamšek Rupnik P., Amoroso S., Cinti F.R., Civico R., Pantosti D., Pucci S., Ricci T., Boncio P., Lezzi F., Pace B., Testa A., Blumetti A.M., Di Manna P., Benedetti L., Henriquet M., Moulin A., Baize S.**

A database of the environmental effects associated to the December 29<sup>th</sup>, 2020 Mw 6.4 Petrinja earthquake (Croatia)

## Goldschmidt 2021 Conference

Lyon, France | 4-9 July

**MacDonald A., Ubide T., Masotta M., Mollo S., Pontesilli A., Magee R., Zhao J.X.**

Tracking Thermal Pathways of Magma Ascent and Eruption Using Trace Element Partitioning in Sector Zoned

**Petrone C.M., Mollo S., Del Bello E., Scarlato P., Andronico D., Gertisser R.**

Where has the mush gone? A tale of a rejuvenated system.

## Congresso Società Geologica Italiana

Trieste, Italy | 16 Settembre

**Aretusini S., Spagnuolo E., Meneghini F., Vannucchi P., Murphy S., Harbord C., Di Toro G.**

INVITED. High velocity friction experiments on IODP materials: insights on earthquake propagation in the subduction zone

**Di Toro G., Aretusini S., Cornelio C., Nielsen S., Spagnuolo E.**

KEYNOTE. Friction during earthquakes: 25 years of experimental studies, Webinar

## ARMS11 -THE 11th ASIAN ROCK MECHANICS SYMPOSIUM, abstract

Beijing, China | October 24

**Di Toro G., Aretusini S., Cornelio C., Nielsen S., Spagnuolo E.**

KEYNOTE. Friction during earthquakes: 25 years of experimental studies



## EGEO 2021, 1° Congresso Nazionale dei Giovani Geoscientisti

Naples, Italy | 25-26 October

Masoch S., Fondriest M., Gomila R., Jensen E., Magnarini G., Mitchell T., Cembrano J.,  
Pennacchioni G., Di Toro G.

Internal structure of a crustal-scale seismogenic source: The Bolfin Fault Zone (Atacama Fault System)

## II Conferencia Internacional: Aportes de la Investigación y Monitoreo para la Gestión del Riesgo Volcánico

Arequipa, Perú | 17-19 November

Finizola A., Pedragosa J., Biteau T., Allard P., Berthezene J-M., Bertil A., Bonnardot F., Cloppet E.,  
Gusset R., Jumaux G., Martel-Asselin F., Narbaud S., Pauvret A., Peltier A., Perrier L., Poirot C.,  
Ricci T., Villeneuve N.

Eventos desastrosos ocurridos en Abril 2021 en el piton de la Fournaise, Isla de La Reunion  
(Francia)

## AGU 2021: Gather Online

San Francisco, USA | 13-17 December

Magnarini G., Aretusini S, Mitchell T.M., Di Toro G.

Friction Experiments on Anorthosite-bearing Gouges and Implications for the Hypermobility of the  
Light Mantle Landslide at the Apollo 17 Landing Site on the Moon

Resor P., Yang D., Griffith A., Shervais K., Di Toro G.

Microscale imaging of pseudotachylyte-bearing fault surface topography

Rosenblatt B., Johnson J. B., Kueppers U., Rossavik K., Ricci T., Andronico D.

A seismo-acoustic investigation of a localized crater terrace collapse at Stromboli volcano

Tisato N., Di Toro G.

Flash Heating and Weakening inferred from Thermal Imaging of High-Speed Rotary Shear  
Experiments.

Vossen C., Cimarelli C., Bennett A., Schmid M., Kueppers U., Ricci T., Taddeucci J., Dingwell D. B.

Electrical Monitoring of Basaltic Explosions at Stromboli Volcano, Italy



## 121 PUBLICATIONS

**Alfonsi L. , Macri P., Nazzari M.**

**Rock magnetic and micro-morphological analysis on snowdeposits: recognition of anthropogenic origin of particulate matter in urban and wilderness area (Central Italy)**

Annals of Geophysics, Vol. 64 No. 2 (2021) <https://doi.org/10.4401/ag-8515>

**Andronico D., Del Bello E., D’Orlando C., Landi P., Pardini F., Scarlato P., Taddeucci J., Cristald A., Ciancitto F., Pennacchia F., Ricci T., Valentini F.**

**Uncovering the eruptive patterns of the 2019 double paroxysm eruption crisis of Stromboli volcano**

Nature Communications, 12 (1), 1-14, <https://doi.org/10.1038/s41467-021-24420-1>

**Aretusini S., Meneghini F., Spagnuolo E., Harbord C. W., Di Toro G.**

**Fluid pressurisation and earthquake propagation in the Hikurangi subduction zone**

Nature Communications, 12(1), 1-8, <https://doi.org/10.1038/s41467-021-22805-w>

**Aretusini S., Núñez-Cascajero A., Spagnuolo E., Tapetado A., Vázquez C., Di Toro G.**

**Fast and localized temperature measurements during simulated earthquakes in carbonate rocks**

Geophysical Research Letters, 48(9), <https://doi.org/10.1029/2020GL091856>

**Boncio P., Amoroso S., Galadini F., Galderisi A., Iezzi G., Liberi F.**

**Earthquake-induced liquefaction features in a late Quaternary fine-grained lacustrine succession (Fucino Lake, Italy): implications for microzonation studies**

Engineering Geology, [doi.org/10.1016/j.enggeo.2020.105621](https://doi.org/10.1016/j.enggeo.2020.105621)

**Bonechi B., Perinelli C., Gaeta M., Stagno V., Fabrizio A., Mollo S., Hrubciak R.**

**High pressure experimental investigation of clinopyroxene dissolution in a K-basaltic melt.**

Chemical Geology, 584, 120533. <https://doi.org/10.1016/j.chemgeo.2021.120533>.

**Brenna M., Ubide T., Nichols A.R.L., Mollo S., Pontesilli A.**

**Anatomy of Intraplate Monogenetic Alkaline Basaltic Magmatism: Clues From Magma, Crystals, and Glass.**

Crustal Magmatic System Evolution: Anatomy, Architecture, and Physico-Chemical Processes, Geophysical Monograph Series, <https://doi.org/10.1002/9781119564485.ch4>

**Civico R., Ricci T., Scarlato P., Andronico D., Cantarero M., Carr B., De Beni E., Del Bello E., Johnson J., Kueppers U., Pizzimenti L., Schmid M., Strehlow K., Taddeucci J.**

**Unoccupied Aircraft Systems (UASs) Reveal the Morphological Changes at Stromboli Volcano (Italy) before, between, and after the 3 July and 28 August 2019 Paroxysmal Eruptions**

Remote Sensing, 13 (15), 2870, <https://doi.org/10.3390/rs13152870>



**Coppola M., Correale A., Barberio M.D., Billi A., Cavallo A., Fondriest M., Nazzari M., Paonita A., Romano C., Stagno V., Viti C., Vona A.**

**Meso-to nano-scale evidence of fluid-assisted co-seismic slip along the normal Mt. Morrone Fault, Italy: Implications for earthquake hydrogeochemical precursors**

Earth and Planetary Science Letters, 568 2021. <https://doi.org/10.1016/j.epsl.2021.117010>

**Demurtas M., Smith S.A.F., Spagnuolo E., Di Toro G.**

**Frictional properties and microstructural evolution of dry and wet calcite-dolomite gouges**

Solid Earth, vol. 12, pp. 595–612, <https://doi.org/10.5194/se-12-595-2021> (open access)

**Del Bello E., Taddeucci J., Merrison J., Rasmussen K., Andronico D., Ricci T., Scarlato P., Iversen J.J.**

**Field-based measurements of volcanic ash resuspension by wind**

Earth and Planetary Science Letters, 554, 116684, <https://doi.org/10.1016/j.epsl.2020.116684>

**Del Rio L., Moro M., Fondriest M., Saroli M., Gori S., Falcucci E., Cavallo A., Doumaz F., Di Toro G.**

**Active faulting and deep-seated gravitational slope deformation in carbonate rocks (central Apennines, Italy): a new “close-up” view.**

Tectonics, vol. 40, pp. 1–28, e2021TC006698. <https://doi.org/10.1029/2021TC006698> (open access)

**Di Fiore F., Mollo S., Vona A., MacDonald A., Ubide T., Nazzari M., Romano C., Scarlato P.**

**Kinetic partitioning of major and trace cations between clinopyroxene and phonotephritic melt under convective stirring conditions: New insights into clinopyroxene sector zoning and concentric zoning.**

Chemical Geology, 584, 120531. <https://doi.org/10.1016/j.chemgeo.2021.120531>

**Di Fiore F., Vona A., Kolzenburg S., Mollo S., Romano C.**

**An extended rheological map of pāhoehoe—‘a‘ā transition.**

Journal of Geophysical Research: Solid Earth, 126, e2021JB022035.

<https://doi.org/10.1029/2021JB022035>.

**Di Toro G., Aretusini S., Cornelio C., Nielsen S., Spagnuolo E. Núñez-Cascajero, A., Tapetado, A., Vázquez, C.**

**Friction during earthquakes: 25 years of experimental studies**

IOP Conference Series: Earth and Environmental Science, 861 052032

<https://iopscience.iop.org/article/10.1088/1755-1315/861/5/052032/meta> pp. 1–7





**Ebrahimi P., Guarino A., Allocca V., Caliro S., Avino R., Bagnato E., Capecchiacci F., Carandente A., Minopoli C., Santi A., Albanese, S.**

**Hierarchical clustering and compositional data analysis for interpreting groundwater hydrogeochemistry: The application to Campi Flegrei volcanic aquifer (south Italy).**

Journal of Geochemical Exploration, 233.

<https://www.sciencedirect.com/science/article/pii/S0375674221002016>

**Giacomet P., Ruggieri R., Scuderi M., Spagnuolo E., Di Toro G., Collettini C.**

**Frictional properties of basalt experimental faults and implications for volcano-tectonic settings and geo-energy sites**

Tectonophysics, vol. 811, pp.1-16, 10.1016/j.tecto.2021.228883

**Giudicepietro F., Chiodini G., Avino R., Brandi G., Caliro S., De Cesare W., Galluzzo D., Esposito A., La Rocca A., Lo Bascio D., Obrizzo F., Pinto S., Ricci T., Ricciolino P., Siniscalchi A., Tramelli A., Vandemeulebrouck J., Macedonio G.**

**Tracking episodes of seismicity and gas transport in Campi Flegrei caldera through seismic, geophysical and geochemical measurements**

Seismological Research Letters, doi:10.1785/0220200223

**Giudicepietro F., Esposito A.M., Spina L., Cannata A., Morgavi D., Layer L. and Macedonio G. (2021)**

**Clustering of experimental seismo-acoustic events using Self-Organizing Map (SOM)**

Front. Earth Sci., 8:581742. doi: 10.3389/feart.2020.581742

**Gomila R., Fondriest M., Jensen E., Spagnuolo E., Masoch S., Mitchell T.M., Magnarini G., Bistacchi A., Mittempergher S., Faulkner D., Cembrano J., Di Toro G.**

**Frictional melting in hydrothermal fluid-rich faults: Field and experimental evidence from the Bolfín Fault Zone (Chile)**

Geochemistry, Geophysics, Geosystems 22, e2021GC009743, 10.1029/2021GC009743 pp. 1-17 (open access)

**Harbord C., Brantut N., Spagnuolo E., Di Toro G.**

**Fault friction during simulated seismic slip pulses.**

Journal of Geophysical Research - Solid Earth, 126, e2021JB022149.

<https://doi.org/10.1029/2021JB022149> (open access)

**Hosseinzadehsabeti E., Ferré E.C., Andersen T.B., Geissman J.W., Billardello D., Di Toro, G.**

**Focal mechanisms of intraslab earthquakes: insights from pseudotachylytes in mantle units**

Journal of Geophysical Research: Solid Earth, vol. 126, pp. 1-25,

<https://doi.org/10.1029/2020JB021479>



**Lang S., Mollo S., Lyderic F., Misiti V., Nazzari M.**

**Kinetic partitioning of major- minor cations between olivine and Hawaiian tholeiitic basalt under variable undercooling and cooling rate conditions**

Chemical Geology, 584, 120485. <https://doi.org/10.1016/j.chemgeo.2021.120485>.

**Masoch S., Gomila R., Fondriest M., Jensen E., Mitchell T., Pennacchioni G., Cembrano J., Di Toro G.**  
**Structural evolution of a crustal-scale seismogenic fault in a magmatic arc: The Bolfin Fault Zone (Atacama Fault System).**

Tectonics, vol. 40, pp. 1-29, 10.1029/2021TC006818 (open access).

**Mintz B.G., Houghton B.F., Llewellyn E.W., Orr T.R., Taddeucci J., Carey R.J., Kueppers U., Gaudin D., Patrick M.R., Burton M., Scarlato P., and La Spina A.**

**Patterns of bubble bursting and weak explosive activity in an active lava lake–Halema‘uma‘u, Kīlauea, 2015, chap. E of Patrick, M., Orr, T., Swanson, D., and Houghton, B., eds., The 2008–2018 summit lava lake at Kīlauea Volcano, Hawai‘i**

U.S. Geological Survey Professional Paper, 1867, 16 p., <https://doi.org/10.3133/pp1867E>

**Mollo S., Di Stefano F., Forni F.**

**Editorial for the Special Issue “Mineral Textural and Compositional Variations as a Tool for Understanding Magmatic Processes”**

Minerals, 11:102. <https://doi.org/10.3390/min11020102>

**Mollo S., Moschini P., Galli, G., Tuccimei P., Lucchetti C., Iezzi G., Scarlato P.**

**Carrier and dilution effects of CO<sub>2</sub> on thoron emissions from a zeolitized tuff exposed to subvolcanic temperatures**

R. Soc. Open Sci., 8:201539. <https://doi.org/10.1098/rsos.201539>

**Moschini P., Mollo S., Gaeta M., Fanara S., Nazzari M., Petrone C.M., Scarlato P.**

**Parameterization of clinopyroxene growth kinetics via crystal size distribution (CSD) analysis: Insights into the temporal scales of magma dynamics at Mt. Etna volcano.**

Lithos, 396–397, 106225. <https://doi.org/10.1016/j.lithos.2021.106225>.

**Nielsen S., Spagnuolo E., Violay M., Di Toro G.**

**Thermal weakening friction during seismic slip: experiments and models with heat sources and sinks**

Journal of Geophysical Research: Solid Earth, vol. 126, e2020JB020652

<https://doi.org/10.1029/2020JB020652> (open access)



Palummo F., Mollo S., Petrone C. M., Ellis B. S., De Astis G., Nazzari M., Scarlato P., Bachmann O.  
**Decoding multiple zoning patterns in clinopyroxene phenocrysts at Vulcano Island: A record of dynamic crystallization through interconnected reservoirs.**

Lithos, 406, 106517. <https://doi.org/10.1016/j.lithos.2021.106517>

Papa S., Spagnuolo E., Di Toro G., Cavallo A., Favero M., Camacho A., Pennacchioni G.  
**Selective clast survival in an experimentally-produced pseudotachylyte**

Journal of Structural Geology, vol. 147, pp. 1-11, [doi.org/10.1016/j.jsg.2021.104328](https://doi.org/10.1016/j.jsg.2021.104328)

Passèlegue F., Tielke J., Mecklenburgh J., Violay M., Deldicque D., Di Toro G.

**Experimental plastic reactivation of pseudotachylyte-filled shear zones**

Geophysical Research Letters vol. 48, pp. 1-9, e2020GL091538 [10.1029/2020GL091538](https://doi.org/10.1029/2020GL091538)

Pontesilli A., Brenna M., Ubide T., Mollo S., Masotta M., Caulfield J., Le Roux P., Nazzari M., Scott J.M., Scarlato P.

**Intraplate Basalt Alkalinity Modulated by a Lithospheric Mantle Filter at the Dunedin Volcano (New Zealand)**

Journal of Petrology, 62, 1-36. <https://doi.org/10.1093/petrology/egab062>.

Rouwet D., Tamburello G., Chiodini G., Pecoraino G., Procesi M., Ricci T., Venturi S., Santi A., Cabassi J., Vaselli O., Tassi F., Costa A.

**New insights into the degassing dynamics of Lago Albano (Colli Albani volcano, Rome, Italy) during the last three decades (1989-2019)**

Italian Journal of Geosciences, doi:10.3301/IJG.2020.19

Sapia V., Villani F., Fischanger F., Lupi M., Baccheschi P., Pantosti D., Pucci S., Civico R., Sciarra A., Smedile A., Romano V., De Martini P.M., Murgia F., Materni V., Giannattasio F., Pizzimenti L., Ricci T., Brunori C.A., Coco I., Improta L.

**3-D deep electrical resistivity tomography of the major basin related to the 2016 Mw 6.5 central Italy earthquake fault**

Tectonics, doi:10.1029/2020TC006628

Scarlato P., Mollo S., Petrone C.M., Ubide T., Di Stefano F.

**Interpreting magma dynamics through a statistically refined thermometer: Implications for clinopyroxene Fe-Mg diffusion modeling and sector zoning at Stromboli**

Crustal Magmatic System Evolution: Anatomy, Architecture, and Physico-Chemical Processes, Geophysical Monograph Series, <https://doi.org/10.1002/9781119564485.ch9>



**Spina L., Del Bello E., Ricci T., Taddeucci J., Scarlato P.**

**Multi-parametric characterization of explosive activity at Batu Tara Volcano (Flores Sea, Indonesia)**

Journal of Volcanology and Geothermal Research, 413, 107199,

<https://doi.org/10.1016/j.jvolgeores.2021.107199>

**Schmid M., Kueppers U., Civico R., Ricci T., Taddeucci J., Dingwell D.B.**

**Characterising vent and crater shape changes at Stromboli: implications for risk areas**

Volcanica, doi: 10.30909/vol.04.01.87105

**Taddeucci J., Cimarelli C., Alatorre-Ibargüengoitia M.A., Delgado-Granados H., Andronico D, Del Bello E., Scarlato P., Di Stefano F.**

**Fracturing and healing of basaltic magmas during explosive volcanic eruptions**

Nature Geoscience, <https://doi.org/10.1038/s41561-021-00708-1>

**Taddeucci J., Peña Fernández J. J., Cigala V. , Kueppers U., Scarlato P., Del Bello E., Ricci T., Sesterhenn J., Panunzi S.**

**Volcanic vortex rings: Axial dynamics, acoustic features, and their link to vent diameter and supersonic jet flow**

Geophysical research letters, 48 (15), e2021GL092899, <https://doi.org/10.1029/2021GL092899>







Design by Laboratorio Grafica e Immagini INGV

Editing by Valeria Misiti

**Rome, March 2022**

### **Disclaimer clause**

This report contains data and information property of Istituto Nazionale di Geofisica e Vulcanologia in Rome (Italy). The information contained in this report don't imply the responsibility of the Istituto Nazionale di Geofisica e Vulcanologia.

Our purpose is to supply reliable scientific information to the members of the national and international scientific community and to whoever could be interested in them. Istituto Nazionale di Geofisica e Vulcanologia does not engage any responsibility for the content. This material is constituted by information of general character, result of specific researches, or data coming from the laboratory activity. Copy and the dissemination of this report are authorized only under licence of HP-HT Laboratory people.